Karelle Hinot

Catalytic soot oxidation by platinum on sintered metal filters

Influence of the platinum quantity, particle size and location, and investigation of the platinum-soot contact

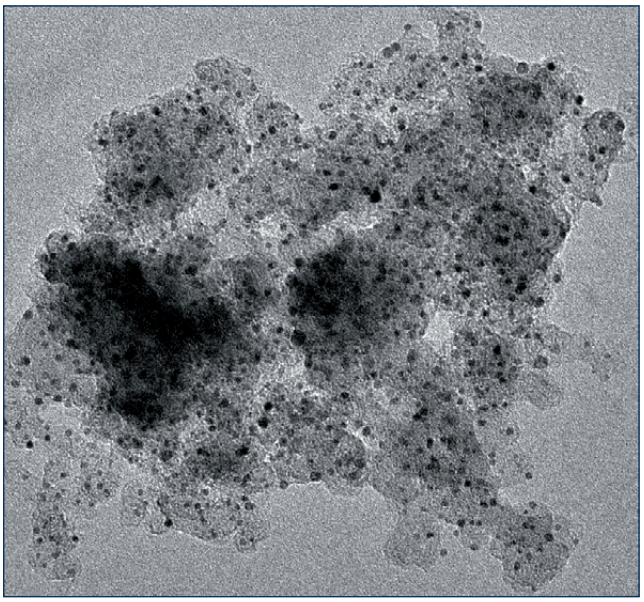

universitätsverlag karlsruhe

Karelle Hinot

Catalytic soot oxidation by platinum on sintered metal filters

Influence of the platinum quantity, particle size and location, and investigation of the platinum-soot contact

Catalytic soot oxidation by platinum on sintered metal filters

Influence of the platinum quantity, particle size and location, and investigation of the platinum-soot contact

von
Karelle Hinot

universitätsverlag karlsruhe

Dissertation, Universität Karlsruhe (TH)
Fakultät für Chemieingenieurwesen und Verfahrenstechnik, 2006

Impressum

Universitätsverlag Karlsruhe
c/o Universitätsbibliothek
Straße am Forum 2
D-76131 Karlsruhe
www.uvka.de

Universitätsverlag Karlsruhe 2007
Print on Demand

ISBN: 978-3-86644-103-3

Catalytic soot oxidation by platinum on sintered metal filters: Influence of the platinum quantity, particle size and location, and investigation of the platinum-soot contact

von der Fakultät für Chemieingenieurwesen und Verfahrenstechnik der
Universität Fridericiana zu Karlsruhe (Technische Hochschule)
zur Erlangung des akademischen Grades eines

Doktors der Ingenieurwissenschaften

genehmigte Dissertation

von

Dipl.-Ing. Karelle Hinot

aus Angers (Frankreich)

Referent:	Prof. Dr. phil. G. Kasper
Korreferenten:	Prof. Dr. sc. tech. H. Burtscher
	Prof. Dr. rer. nat. habil. O. Deutschmann

Tag der mündlichen Prüfung: 10. Juli 2006

To Krain', Yvette and Marie-Hedwige

"La vie n'est pas un problème à résoudre,
mais une réalité à expérimenter"
BOUDDHA

Acknowledgements

This work has been carried out at the Robert Bosch GmbH research center in Stuttgart in Germany, under the direction of Prof. Dr. G. Kasper from the Institut für Mechanische Verfahrenstechnik und Mechanik (IMVM) of the Universität Karlsruhe in Germany. I wish to thank him for enabling this joint research project. I greatly appreciated his cooperation and his guidance during the entire course of the thesis.

I would like to express my gratitude to Prof. Dr. H. Burtscher from the institute for aerosol and sensor technology (IAST) of the university of applied sciences, Aargau in northwestern Switzerland, for the friendly acceptance of the co-assessment of this thesis and the helpful advice regarding the experimental analysis. I spent a profitable week at the IAST in Aargau in an excellent research environment and I would like to thank particularly T. Baumgartner for his help carrying out the experiments.

To Prof. Dr. O. Deutschmann from the Institut für Technische Chemie und Polymerchemie of the Universität Karlsruhe in Germany, I wish to express my appreciativeness for the acceptance of the co-assessment, and the valuable suggestions regarding the theoretical part.

I would like also to thank Prof. Dr. A. P. Weber responsible for the nanoparticle research at the IMVM during my thesis time for his fruitful discussions and helpful criticisms. I am thankful to the staff of the IMVM for the pleasant working atmosphere during my stay there, and especially Dipl.-Ing. P. Davoodi for her kind help during the performing of aerosol experiments, and T. Lebe for carrying out the TEM measurements.

I am very grateful to Prof. Dr. K. Köhler from the Fakultät Chemie - anorganische Chemie of the Technische Universität München in Germany and his team, who received me with conviviality two weeks in their laboratory. Special thanks to Dipl.-Chem. A. Bentele for his help preparing the numerous samples. I wish to thank Dr. M. Makkee as well, from the section of industrial catalysis of the Delft university of technology in the Netherlands, for his benefit help in samples prepara-

tion. I would also like to thank Dr. V. Slovák from the department of chemistry of the university of Ostrava in Czech Republic, who kindly carried out computational calculations. And last but not least, thanks to Dr. R. Fricke from the Institut für Angewandte Chemie Berlin-Adlershof e.V. for his helpful advice for surface area measurements.

I also wish to express my gratitude to Dr. D. Steiner, who gave me the opportunity to perform this research work at the Robert Bosch GmbH company. I thank him for his thoughtful advice and knowledge, and his constant support and availability.

Thanks to all the colleagues of the Applied Chemistry and Energy Research department at Robert Bosch GmbH. In particularly my sincere thanks to M. Sänger and F. Dech for their invaluable assistance during the planing and construction of the test bench. I would like also to thank C. Houle for his contribution within the frame of his internship.

Finally, I would like to thank my parents and my brothers for their love, support and encouragement. I wish also to thanks Damien for his love and understanding throughout these years in Germany. I dedicate this thesis to the three women I lost during these three years: Krain', Yvette and Marie-Hedwige.

Contents

Abstract

The great challenge for next years concerning the emission of diesel engines is to develop diesel particle filters (DPF) with catalytic regeneration systems. This thesis is focused on the global understanding of the diesel soot oxidation on sintered metal filters (SMF). Platinum is studied as reference catalyst. The first objective is to determine which of platinum quantity, platinum particle size, or platinum location exhibits the preponderant influence on the catalytic soot oxidation in the case of a model fuel borne catalyst (FBC) system. The second objective is to determine if it is possible to achieve the same catalytic effect on a platinum coated filter as the one obtained by using a FBC. The answers to these objectives should help to analyze the improvement potential of coated filters and FBCs in future.

To answer these objectives, a method was developed to calculate the kinetic parameters of the thermal and the catalytic soot oxidation from temperature ramp experiments. The global activation energy of the catalytic soot oxidation does not differ from the one of the thermal soot oxidation. The catalytic effect was thus defined as the pre-exponential factor ratio between the catalytic and the thermal soot oxidation with the other kinetic parameters being kept constant, following an oxygen transfer mechanism.

Temperature ramp experiments were performed in a thermogravimetric analysis (TGA) device for platinum-soot powder samples. A reactor was also designed and built to investigate the catalytic soot oxidation on sintered metal filters. Conversion curves obtained from reactor experiments do not allow to calculate kinetic parameters. For this case the catalytic effect was related to the temperature difference for 50% soot conversion between the thermal and the catalytic soot oxidation.

Six different soot sources were used along this thesis. The kinetic parameters of each soot source were first investigated in the TGA device. Soot produced by pyrolyzing toluene exhibits the closest structure and composition to the reference diesel soot. Its oxidation behavior is also the closest to the reference diesel soot. But all soot sources were found to have reasonably similar composition, structure and thermal behavior to diesel soot.

The catalytic soot oxidation on established DPF technologies was first investigated. Platinum-doped soot produced via FBC shows a catalytic effect, increasing with the platinum-to-soot mass ratio. But platinum coated filters do not display any catalytic effect. It was decided to deepen these results by investigating the catalytic effect of platinum on the soot oxidation with artificial platinum-doped soot samples, and with artificial platinum-soot contact scenarios on SMF.

In the case of a model FBC, the catalytic effect was observed to increase linearly with the platinum-to-soot mass ratio, and the initial platinum specific surface area. This reinforces the theory of the oxygen transfer mechanism. Platinum particles sinter during the oxidation, but as the soot was itself consumed, this did not affect the platinum surface area related to the soot mass. By investigating the influence of the initial platinum particle size for soot samples containing same platinum quantity, a size optimum was found at a mean diameter of 3 nm. Quantum size effect or geometric size effect theories could explain this optimum. However, this size effect is low compared to the influence of the platinum quantity. The platinum location, embedded in the soot agglomerate or present on the soot surface does not influence the catalytic effect.

The catalytic effect of three configurations modeling three contact possibilities on SMF was investigated. Filtering platinum and soot aerosol consecutively does only exhibit a marginal catalytic effect. But filtering platinum and soot aerosol simultaneously exhibits the same catalytic effect as filtering a platinum-doped soot aerosol. It suggests that it is possible to enhance the catalytic effect of coated filters by increasing uniformly the platinum particle density in the soot cake.

The results of this thesis suggest that the use of platinum as FBC is limited by the cost of platinum, as the catalytic effect was found to be linear with the platinum-to-soot mass ratio. The only possibility to improve the performances of a platinum FBC for a fixed platinum quantity is to optimize the platinum particle size in the obtained platinum-doped soot, however with low influence on the catalytic effect. The cost problems of platinum FBC could principally be avoided by attaching a fixed platinum quantity on a coated SMF. The contact between filtered soot and platinum is today too low to establish a catalytic effect on a coated filter. However, it has been shown that if all platinum particles are uniformly distributed in the soot cake (simultaneously filtration), the catalytic effect is the same as for a platinum FBC. The enhancing of the platinum density in the soot on a coated filter is thus a great research challenge for next years.

Nomenclature

Latin Letters

A	-	Catalytic effect: pre-exponential factor ratio
D	nm	Agglomerate diameter
d	nm	Primary particle diameter
E_a	kJ/mol	Activation energy
f	-	Stoichiometric factor
h	J.s	Planck constant
K	-	Equilibrium constant
k	1/s	Reaction rate constant related to r_s
k_B	J/K	Boltzmann constant
k_i	kg/s.m^2	Reaction rate constant related to r_i
k_0	1/s	Arrhenius pre-exponential factor related to r_s
k_0'	1/s	Pseudo Arrhenius pre-exponential factor
$k_{0,i}$	kg/s.m^2	Arrhenius pre-exponential factor related to r_i
M	g/mol	Molar mass
m	-	Parameter in the PRO or PG model
m_c	kg	Remaining mass of carbon
$m_{c,d}$	kg	Mass of dissipated carbon
$m_{c,0}$	kg	Initial mass of carbon
N	atom/mol	Avogadro's number
n	1/cm^3	Particle number
n_{O_2}	-	Reaction order of oxygen
P	-	Relative pressure
p_{CO}	-	Partial pressure in carbon monoxide
p_{CO_2}	-	Partial pressure in carbon dioxide
p_{O_2}	-	Partial pressure in oxygen
Q	l/min	Volumetric flow rate
q	mol/g	Quantity
R	J/mol.K	Gas constant
r	kg/s	Global reaction rate
r_i	kg/s.m^2	Interfacial reaction rate

r_s	1/s	Conversion rate
S	m^2/g	Specific surface area
S_i	m^2	Interfacial surface
$S_{i,0}$	m^2	Initial interfacial surface
s	atom/m^2	Surface density
T	K	Temperature
t	s	Time
X	-	Conversion

Greek Letters

α	-	Absorptivity
ΔG	kJ/mol	Free enthalpy
$\Delta^{\neq} G$	kJ/mol	Free activation enthalpy
$\Delta_r G$	kJ/mol	Free enthalpy of the reaction
$\Delta_r G^0$	kJ/mol	Standard free enthalpy of the reaction
$\Delta_f G^0$	kJ/mol	Standard free enthalpy of formation
$\Delta^{\neq} H$	kJ/mol	Activation enthalpy
$\Delta_r H^0$	kJ/mol	Standard enthalpy of the reaction
$\Delta^{\neq} S$	kJ/mol.K	Activation entropy
ΔT_{50}	K	Temperature difference at conversion X = 0.5
$\delta\lambda$	m	Wavelength range
ϵ	-	Emissivity
λ	m	Wavelength
ρ	g/cm^3	Soot bulk density
ρ	-	Reflexivity
σ	nm	Standard deviation
τ	-	Transmissivity
Φ	W/m^2	Radiation

Subscripts

av	Average
BET	Measured with BET
cat	Catalytic soot oxidation
f	Related to the filter surface
r	Related to the reactor chamber
$SMPS$	Measured with SMPS

TEM	Measured with TEM
th	Thermal soot oxidation
w	Related to the reactor window

Abbreviations

BET	Brunauer, Emmett and Teller
CPA	Chloroplatinic Acid
CRT	Continuously Regenerating Trap
DPF	Diesel Particle Filter
EA	Elemental Analysis
EG	Ethylene Glycol
FBC	Fuel Borne Catalyst
HC	Hydrocarbons
IMVM	Institut für Mechanische Verfahrenstechnik und Mechanik
IAST	Institute for Aerosol and Sensor Technology
LPW3	Lister Petter Engine
MFC	Mass Flow Controller
MFM	Mass Flow Meter
NDIR	Non Dispersive Infrared
OSC	Oxygen Storage Capacity
PG	Pore Growth
PM	Particulate Matter
PN	Platinum Nitrate
PRO	Pseudo Reaction Order
SDG	Spark Discharge Generator
SEM	Scanning Electron Microscope
SMF	Sintered Metal Filter
SMPS	Scanning Mobility Particle Sizer
SOF	Soluble Organic Fraction
SF	Solid Fraction
TAPN	Tetraamine Platinum Nitrate
TEM	Transmission Electron Microscopy
TGA	Thermogravimetric Analysis
THF	Tetrahydrofuran
TOF	Turn Over of Frequency
TON	Turn Over of Number
TPO	Temperature Programmed Oxidation
TWC	Three Way Catalyst

Chapter 1

Introduction and objectives

1.1 Emissions from internal combustion engines

Automotive pollution is associated with the emission of carbon dioxide CO_2, which is depending on the fuel composition and proportional to the fuel consumption. Carbon dioxide is a non-toxic gas, but it contributes to the green house effect [1]. Internal combustion engines also emit four basic pollutants: carbon monoxide CO, unburned hydrocarbons HC, oxides of nitrogen NO_x and particulate matter PM [2]. Local high concentrations of CO and NO_x are detrimental to health and could be fatal [3], [4]. HC are composed of hundreds of compounds, which are mostly toxic for the health and the environment. PM are ultra fine particles which are composed of a solid fraction SF (elemental carbon and ash), a soluble organic fraction SOF (HC particles and adsorbed HC), and sulfate particulates SO_4 (sulfuric acid and water). The chemical complexity of PM makes its impact on health and environment difficult to assess, but adverse health effects of ultrafine particles have been widely discussed [5–7].

Standards for automobiles have been applied worldwide to reduce the emissions of these four pollutants. Emission standards for passenger cars in the European Union (EU) are presented in Table 1.1. The majority of gasoline engines are operated with a stoichiometric air-fuel ratio, but imperfect combustion leads to the formation of CO, HC and NO_x. Three way catalysts (TWC) transform nearly all of these species into carbon dioxide CO_2, water H_2O and nitrogen N_2 [8]. Noble metals such as platinum are mainly used as oxidation catalyst [8].

Diesel engines are operated with fuel injection at the end of the air compression stroke. Therefore, diesel engines may be designed with a higher compression ratio than gasoline engines, leading to higher combustion temperatures and higher effi-

Table 1.1: European Union emissions standards for passenger cars (g/km), [9]

Diesel	Date	CO	HC	HC + NO_x	NO_x	PM
Euro 2	1996.01	1.0	-	0.9	-	0.10
Euro 3	2000.01	0.64	-	0.56	0.50	0.05
Euro 4	2005.01	0.5	-	0.30	0.25	0.025
Euro 5	mid-2008	0.5	-	0.25	0.20	0.005
Gasoline	Date	CO	HC	HC + NO_x	NO_x	PM
Euro 2	1996.01	2.2	-	0.5	-	-
Euro 3	2000.01	2.3	0.20	-	0.15	-
Euro 4	2005.01	1.0	0.10	-	0.08	-
Euro 5	mid-2008	1.0	0.075	-	0.06	-

ciency. However these high temperatures are responsible for the thermal formation of NO_x. Besides, the mixing quality between air and fuel is worse for diesel than for gasoline engines, leading to the formation of PM. The majority of PM is however immediately reburned during combustion if the temperature is high enough [11]. Therefore, high temperatures during the combustion lead to higher efficiency of the engine, lower PM emissions but higher NO_x emissions, and vice versa. This is called the trade-off effect and illustrated in Figure 1.1. Additional aftertreatment strategies are thus necessary to reduce both NO_x and PM in diesel exhaust gas in order to fulfill Euro 4 and Euro 5 standards. For diesel trucks, where the efficiency is the economical parameter, NO_x reduction catalysts working in lean condition are used. Selective catalytic reduction (SCR) technology is now state of the art. For passenger cars, an exhaust gas recirculation is performed to lower the combustion temperature and reduce NO_x emission. Here, diesel particle filter (DPF) has to be added to reduce the PM emissions of the engine.

1.2 Diesel particle filter technology

DPFs can reduce 70 to 95 wt% of the PM mass (95 to 99.9 wt% of the solid fraction). New emission limits based on the PM number are presently discussed [12]. DPFs combine generally depth filtration (low efficiency and low pressure drop) and cake filtration process (high efficiency and high pressure drop). The mainly used filters are ceramic wall-flow monoliths (ca. 70% utilization) and ceramic fibers (ca. 25% utilization). Cordierite ($2MgO\text{-}2Al_2O_3\text{-}5SiO_2$) and silicon carbide (SiC) are the most popular ceramic substrates. Cordierite offers good thermal shock resis-

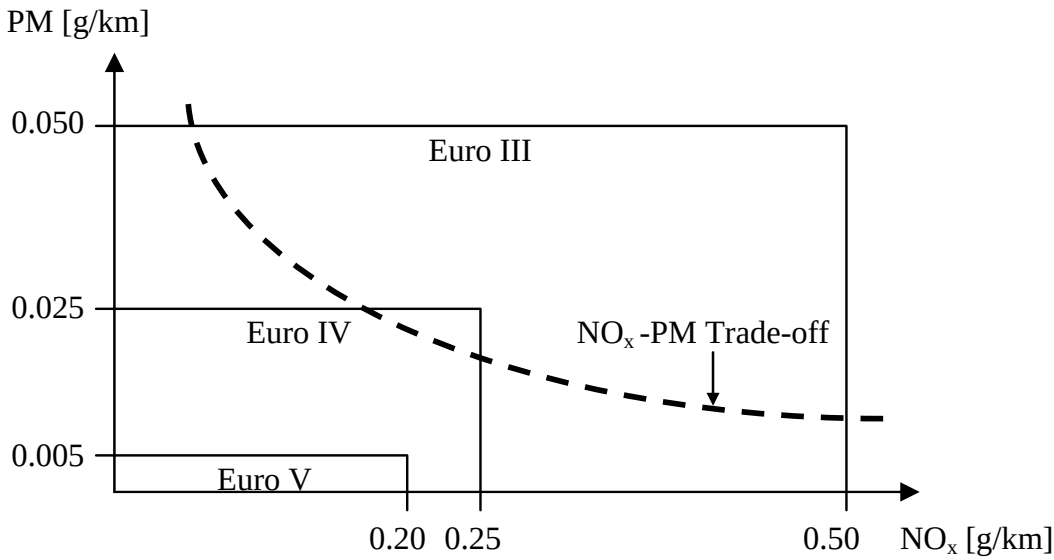

Figure 1.1: The NO_x-PM trade-off effect for diesel engines [10]

tance and low costs. SiC offers high thermal conductivity and high melting temperature. Sintered metal filters (SMF) have been more recently developed, showing high filtration efficiency and high fabrication flexibility [10].

The critical issue concerning DPFs is their regeneration. Soot deposition leads to an increase of the pressure drop across the DPF, decreasing the fuel efficiency of the engine. To regenerate the filter, the carbon contained in PM is oxidized into CO and CO_2. In the following, the term "diesel soot" will be defined as the solid fraction (SF) and the part of soluble organic fraction (SOF) which may be adsorbed on it (see in Figure 1.2). The major problem is that soot can only be oxidized at temperatures higher than 550°C to 600°C with the oxygen contained in the exhaust gas. Generally, the exhaust gas temperature does not exceed 250°C (urban) or 400°C (non-urban) at normal driving conditions [13]. A possible solution is to use an active system to increase the exhaust gas temperature or the soot temperature [14]. But it implies to use another energy source, meaning additional costs. Furthermore, high regeneration temperatures could easily damage the filter. Therefore, the use of passive systems, which decrease the oxidation temperature of soot through the use of catalysts is the preferred way to regenerate DPFs.

There are two catalytic regeneration strategies used on the market: the continuously regenerating trap (CRT) and the fuel borne catalyst (FBC) processes. The CRT process combines an oxidation catalyst to transform the NO contained in exhaust into NO_2 and a DPF, where NO_2 can oxidize soot at temperatures of 250-350°C. This process is however very sensitive to sulfur and should be used with sulfur-free

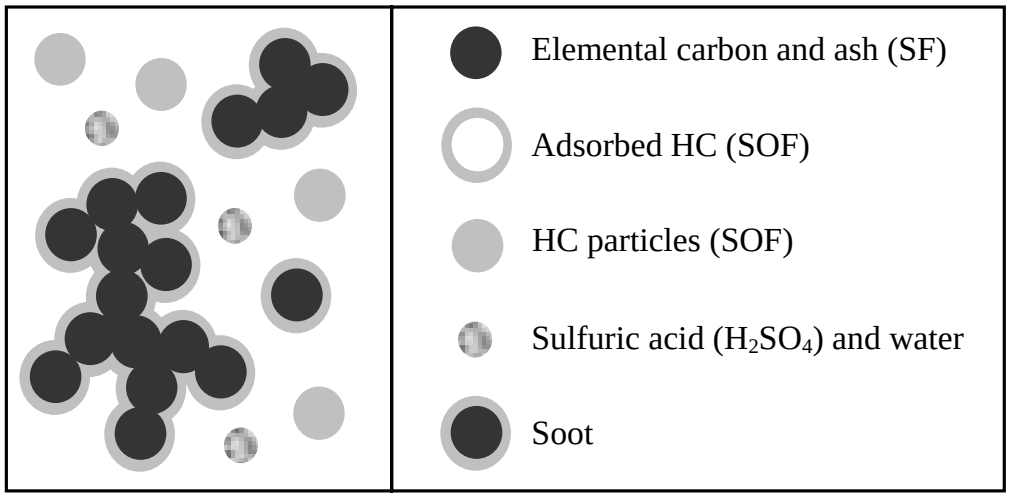

Figure 1.2: Schematic representation of the PM composition [10]

diesel only. CRT can only be applied in trucks where the ratio of NO_2 to soot is higher than 8. The FBC is used for passenger cars. Organometallic compounds of transition metals (e.g. cerium, iron) or noble metal (e.g. platinum) additives are mixed with the fuel, leading to the formation of metal or metal oxide catalyst-doped soot during the combustion in the engine. This catalyst can then lower the soot oxidation temperature from 600°C to 450°C inside the DPF [11], but it is not sufficient to regenerate it continuously. Regularly, if the pressure drop through the filter is too high, additional post-injections of diesel fuel are performed to increase the exhaust gas temperature and oxidize the soot. This FBC process has the added inconvenience of producing some ash which permanently accumulates in the DPF. Hence, it should be changed every 100 000 to 150 000 km [11].

Research is now oriented towards alternative processes to regenerate the DPF. To avoid the ash accumulation and achieve a continuous regeneration, the idea is to apply the catalyst directly to the filter. Such DPFs are however not effective in regards to the soot oxidation yet, because the contact between soot and catalyst is too poor. The use of intermediate washcoat to enhance the surface area of the catalyst is intensively studied.

1.3 Mechanisms of catalytic soot oxidation

Thermal and catalytic oxidation of soot (or more generally of carbon) have been widely studied [15]. While a unified mechanism was proposed for the thermal

carbon oxidation [16], the mechanisms of the catalytic carbon oxidation remain largely unknown. At the atomic scale, two mechanisms have been proposed. In the electron transfer mechanism, the catalyst can activate the carbon itself by making it more susceptible to oxidation [17]. This theory, based on a redistribution of the π-electrons in the carbon matrix, has never really been confirmed by experiments. Today, the oxygen transfer mechanism has been widely accepted as the general mechanism for the carbon oxidation [18, 19]. In this theory, the catalyst is considered as a renewable activated oxygen donor.

On a macroscopic scale, both mechanisms proposed depend on the contact between catalyst and carbon. Most catalysts require physical contact with carbon (direct catalysis), leading to two modes of attack represented in Figure 1.3: edge recession and channeling [20]. Edge recession is thought to occur when the interaction between catalyst and carbon forms strong interfacial bonds. If the interfacial bonds are not strong enough, the channeling attack occurs. It was proposed that metal atoms, which adsorb oxygen dissociatively and readily form oxides, establish strong interfacial bonds, leading to edge recession. On the contrary, metal atoms which adsorb oxygen non-dissociatively and tend to remain in the noble state do not exhibit strong interfacial bonds and result in channeling [21, 22].

Without physical contact (indirect catalysis) the catalyst could still act as a renewable activated oxygen donor. But activated oxygen radicals recombine themselves too rapidly in the gas phase before reaching carbon. For supported catalysts, it was proposed that activated oxygen could migrate on the support to the carbon. This is called the spillover effect theory [24], illustrated in Figure 1.4. Otherwise, the catalyst could also catalyze other oxidation reaction of the gas phase. It could accelerate the transformation of NO to NO_2, which can oxidize the carbon (CRT). Or it can oxidize the CO from the thermal carbon oxidation to CO_2, releasing some heat that can accelerate the carbon combustion (auto thermal reaction).

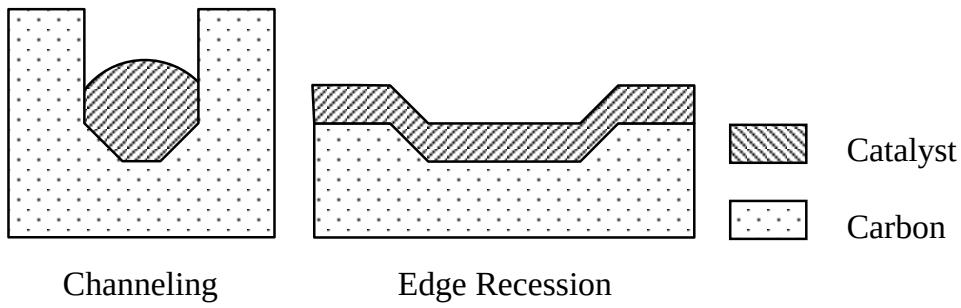

Figure 1.3: Comparison of channeling and edge recession attacks [23]

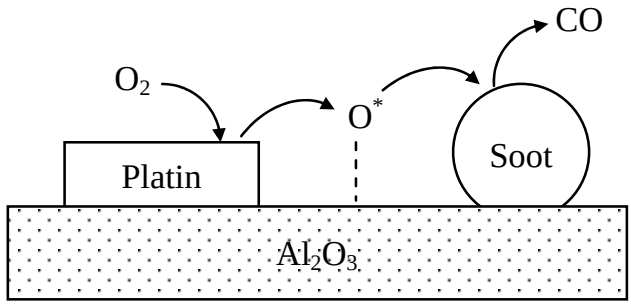

Figure 1.4: Schematic representation of the spillover effect [25]

There is a vast array of materials exhibiting a catalytic activity for oxidation reactions. The two major families are transition metals which form relatively unstable oxides and metal oxides with oxygen storage capacity (OSC) [26]. In the transition metals family, noble metals generally present a higher level of activity for oxidation reactions (HC and CO oxidation in exhaust aftertreatment for example) and a higher resistance to sulphur poisoning. However, they are more expensive than the transition metals (e.g. iron, cobalt, nickel, copper). Platinum is the most commonly noble metal used. OSC metal oxides can cycle between two valence states, adsorbing and releasing oxygen. Ceria (CeO_2, Ce_2O_3) has been widely used in TWC. Other OSC materials include oxides of iron, manganese or copper. Some transition metals such as iron could catalyze an oxidation reaction as metal as well as metal oxides.

According to the previous discussion, it appears that the two catalyst families suitable for an oxidation reaction adsorb oxygen differently depending on their OSC. It is thus highly probable that the mechanisms involved in the direct or the indirect catalytic oxidation of carbon differ from one family to another. The proposition of a unified theory for the catalytic carbon oxidation should consequently combine the mechanisms involved for each of these families. The present work is focused on the understanding of the catalytic soot oxidation with a catalyst of the noble metal family: platinum. It may help in the global comprehension of the catalytic soot oxidation. It should be completed with a study of a catalyst from the metal oxide family.

1.4 Platinum as a soot oxidation catalyst

In comparison with metal oxides, the literature on catalytic soot oxidation with platinum is limited to a few authors [25, 27–30]. Indeed, it was frequently thought

that the platinum was inactive in regard to the diesel soot oxidation. However, the physical contact required for a direct soot catalysis in air was mostly not fulfilled.

Neeft et al. [31] and van Setten et al. [32] defined operationally the contact between a catalyst and soot. They achieved "loose" contacts by filtering soot aerosol on a catalytic filter, by dipping a catalytic filter in a soot dispersion, or by mixing soot and catalyst powder with a spatula. "Tight" contacts were obtained by mixing mechanically soot with the catalyst powder in a ball mill for example. Samples prepared with "tight" contact showed soot oxidation at much lower temperatures than samples prepared with "loose" contacts. These studies reinforce the fact that some catalysts require a physical contact to be active.

Oi-Uchisawa et al. [27, 33–35] mixed with a spatula platinum supported on metal oxides catalysts with carbon black to achieve what they termed a "loose" contact. The evolution of CO_2 production was followed during temperature programmed oxidation (TPO) under various gas conditions. The catalytic activity was evaluated by the temperature of the CO_2 peak (see in Figure 1.5). Supported platinum catalysts does not exhibit any activity in air. Setiabuti et al. [36] and Matsuoka et al. [37] performed similar experiments with synthetic and pyrolytic soot and came to the same conclusions. Neri et al. [25], on the contrary, reported an activity of a platinum supported on an Al_2O_3 catalyst on the soot oxidation in air. They proposed the spillover effect theory to explain these results. However, they used soot from a diesel engine mixed mechanically with platinum-doped alumina catalyst, so that the conditions of a "tight" contact between platinum and soot were also certainly fulfilled, enabling the catalytic soot oxidation in air.

From these different studies, it appears that, when the physical contact conditions between platinum and soot are not fulfilled, the direct catalytic oxidation of soot in

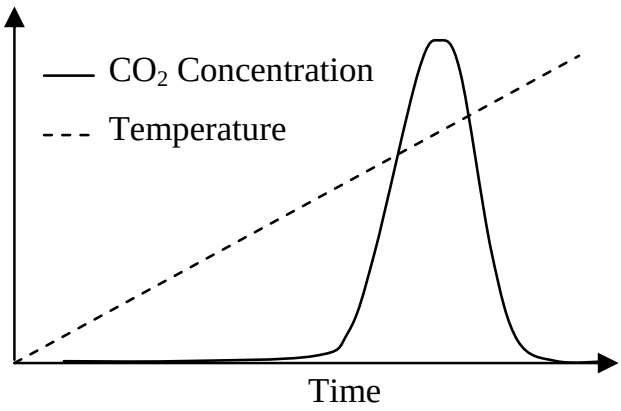

Figure 1.5: Example of temperature programmed oxidation (TPO)

air can not happen. But the role of a possible spillover effect on the intermediate support is not clear. Weber et al. [28] mixed a platinum and a carbon aerosol from a spark discharge generator (SDG) in parallel ("loose" contact) or in series ("tight" contact). They observed as the other authors, that platinum was only active for the "tight" contact conditions. But in this case, no intermediate support was used, so that the often cited spillover effect could not play any role. Platinum is thus an active catalyst for the soot oxidation in air when a "tight" contact between platinum and soot particles is achieved. This is also valid in absence of any intermediate.

Most of the published experiments have been performed on a laboratory scale to study the catalysis mechanisms. Experiments on engine beds in real conditions with platinum FBC or platinum on a coated DPF have only been performed recently.

Jelles et al. [30] performed engine experiments using a platinum FBC and filters coated with platinum. It was found that the platinum contained in soot (from the platinum FBC) does not influence the oxidation rate of soot. The platinum concentrations used were very low (2 wt% Pt in FBC, corresponding to ca. 0.0002 platinum-to-soot mass ratio) and the platinum particles were supposed to be too small (atomic dispersion) to even have any catalytic activity. Otherwise, the platinum present on the filter did not have any effect on the balance temperature (the lowest temperature where an equilibrium between the rate of soot collected and oxidized is found) when running the oxidation under air conditions. If the catalytic activity of platinum under "tight" contact conditions was proven, its application on real engine beds condition seems to depend on other parameters, such as the platinum quantity and the platinum particle size.

Seipenbusch et al. [29, 38] studied the influence of the platinum surface area and of the platinum particle size on the carbon oxidation. They deposited soot (from laser ablation) and platinum nanoparticles on a SiO_2 surface, and exposed it to air at different temperatures. The reaction rate was found to first decrease with the platinum surface area for low surface areas, and then increase with the platinum surface area for high surface areas. Seipenbusch et al. proposed the presence of both a direct oxidation mechanism and a spillover effect. However, the very low activation energy found for the thermal soot oxidation in air makes the validity of the method used questionable. The influence of the platinum particle size was unfortunately not investigated under air atmosphere.

To conclude, if the catalytic activity of platinum under "tight" contact conditions was proven, its application as FBC or coated filter remains unclear. Moreover, the question of the influence of the platinum quantity and particle size in the case of such "tight" contact was still not solved.

1.5 Presentation of the objectives

From a technological point of view, the great challenge in the next years is to develop coated DPFs that can achieve the same regenerating performance as a FBC - or better. As the contact between catalyst and soot established on a coating or with FBC is not the same, it is necessary to clear if it is possible to achieve the same catalytic effect on both systems. This work was chosen to be focused on platinum as a reference catalyst for the noble metal family. It should be kept in mind that the mechanisms involved with platinum will probably be different from those involved with metal oxide family. From the literature review, it appears that a direct catalysis mechanism can only happen by a "tight" contact between platinum and soot. Assuming that this "tight" contact is achieved, it is then necessary to know which parameters influence the catalysis. Following the literature review, it seems that the platinum quantity and particle size could play a role in the direct catalysis. It should also be interesting to know if the platinum location (inside the soot agglomerate or on the soot surface) is relevant. Indeed with a platinum coated DPF, the platinum particles could only be located at the surface of the filtered soot, and not in the soot agglomerate as for FBC.

The objectives of this work could be summed up in two questions. First, from the scientific point of view: do the platinum quantity, platinum particle size and platinum location influence the catalysis in FBC systems? And secondly, from the technological point of view: is it possible to achieve the same catalytic effect between platinum and soot on a coated DPF as the one obtained using a FBC? The answer to the first question could help to improve the catalytic effect of FBC systems. The answer to the second question should determine the development possibilities of coated DPF to achieve the same performance as FBC.

The first requirement to achieve these objectives is to define the catalytic effect of the platinum, independently of the experimental conditions and the soot used. This is performed in Chapter 2, dealing with the theory of heterogeneous reactions and the identification of the kinetic parameters for both thermal and catalytic oxidation. Chapter 3 presents the two experimental set-ups used to measure the catalytic effect of soot, as powder or as an aerosol collected on a filter. Chapter 4 deals with the characterization of different soot sources. The aim is to determine which soot parameter (structure, composition) influences the thermal soot oxidation, and to compare the thermal soot oxidation of synthetic soot sources with the one of diesel soot. Experiments on established DPF technologies for FBC and coated DPFs are discussed in Chapter 5. Chapter 6 presents the influence of the platinum quantity, platinum particle size and platinum location using model FBC systems. The

possibility to achieve the same catalytic effect on coated filter than using FBC is studied in Chapter 7. A conclusion on the results achieved, the answer to the two fundamental questions and the future research fields is exposed in Chapter 8.

Chapter 2

Methodology

The aim of this chapter is to define an appropriate parameter, describing the catalytic effect of platinum on the soot oxidation. To be able to compare the results obtained here with the ones in literature, it is necessary that the parameter used is independent of the experimental conditions. Most authors define a catalytic "activity" of a soot oxidation catalyst only in terms of the ignition or peak temperature during temperature programmed oxidation (TPO) experiments. The temperature of the peak depends however on the experimental conditions used. On the contrary, kinetic parameters of a reaction are independent of the experimental conditions. The first part of this chapter is thus focused on the method to obtain a global kinetic law from isothermal or single ramp experiments in the case of the thermal soot oxidation. The second part concentrates on the influence of the platinum catalyst on the parameters of the kinetic law of the soot oxidation. The pre-exponential factor ratio between catalytic and thermal soot oxidation is finally selected as the parameter describing the catalytic effect of platinum.

2.1 Identification of kinetic parameters for the thermal soot oxidation

The thermal oxidation of soot is an exothermic reaction between oxygen and carbon contained in the soot. In this section, soot is assumed to be pure carbon (without any ash or HC adsorbed on the surface). There are two reaction paths to oxidize carbon, producing carbon dioxide CO_2 and carbon monoxide CO, CO can additionally be oxidized in CO_2 (Equations 2.1, 2.2 and 2.3). In the following, these elementary processes are assimilated as one global oxidation reaction, and no distinction is made between the reaction products. This does not affect the way of calculating

the kinetic parameters of the global thermal carbon oxidation.

$$C + \frac{1}{2} O_2 \rightarrow CO \qquad (\Delta_r H^0 = -100{,}5 \ \ kJ/mol) \tag{2.1}$$

$$C + O_2 \rightarrow CO_2 \qquad (\Delta_r H^0 = -393{,}5 \ \ kJ/mol) \tag{2.2}$$

$$CO + \frac{1}{2} O_2 \rightarrow CO_2 \tag{2.3}$$

2.1.1 Reaction rates and kinetic law

The oxidation of carbon is a heterogeneous reaction between one solid phase, the carbon, and one gaseous phase containing oxygen. The oxidation takes place at the interface between the two phases, where oxygen gets into contact with carbon. At this interface, the reaction products (CO and CO_2) are emitted into the gas phase. Therefore, the interface is always moving. This reactive interface is called the reaction front of the oxidation [39].

The global reaction rate r of the carbon oxidation in a closed reactor can be described as the loss of remaining mass of carbon m_c per unit of time t (Equation 2.4). This definition is not entirely satisfying, because the reaction rate is an extensive variable depending on the reactor size. It is possible to define a specific reaction rate, related to an extensive parameter of the system. Rigorously, as the oxidation takes place on the reaction front, the specific reaction rate can only be defined as an interfacial reaction rate r_i, where S_i is the reaction front surface, varying with the reaction time (Equation 2.5) [40]. If the interfacial reaction rate is constant on the entire reaction front surface, then r and r_i are related by the Equation 2.6.

$$r = -\frac{dm_c}{dt} \qquad [kg/s] \tag{2.4}$$

$$r_i = -\frac{1}{S_i} \frac{dm_c}{dt} \qquad [kg/s.m^2] \tag{2.5}$$

$$r = r_i \, S_i \tag{2.6}$$

The interfacial reaction rate r_i can be described with a kinetic law, independently of the experimental conditions used. The kinetic law is generally reduced to a function of temperature T and of reactant concentrations $[C]$ and $[O_2]$ (Equation 2.7). k_i is the reaction rate constant related to the interfacial reaction rate r_i. k_i depends on the temperature following the Arrhenius law (Equation 2.8). E_a is the

energy of activation of the reaction (kJ/mol) and $k_{0,i}$ the pre-exponential factor. $k_{0,i}$ represents the value of k_i at an infinite temperature. The units of k_i and $k_{0,i}$ depend on the units of the reactant concentration functions $f([C])$ and $f([O_2])$. R is the gas constant.

$$r_i = k_i \, f([C]) \, f([O_2]) \qquad [kg/s.m^2] \tag{2.7}$$

$$k_i = k_{0,i} \, exp(-\frac{E_a}{RT}) \tag{2.8}$$

The kinetic law of a homogeneous reaction presents a reaction order for each reactant depending on the elementary processes of the reaction. Concerning the interfacial reaction rate, the reaction order of carbon in the Equation 2.7 is zero and the function $f([C])$ is equal to 1 [39]. The function $f([O_2])$ depends on the partial pressure of oxygen p_{O_2} with the reaction order n_{O_2} (Equation 2.9). The interfacial reaction rate can thus be described by Equation 2.10, with $k_{0,i}$ having the same unit of r_i, kg/s.m^2.

$$f([C]) = 1 \qquad f([O_2]) = {p_{O_2}}^{n_{O_2}} \tag{2.9}$$

$$r_i = k_{0,i} \, exp(-\frac{E_a}{RT}) \, {p_{O_2}}^{n_{O_2}} \tag{2.10}$$

Generally, the reaction front of an heterogeneous reaction is unknown and not measurable. It is thus more convenient to calculate a specific reaction rate related to a known extensive parameter. The conversion rate r_s is commonly used (Equation 2.11). It is the rate of the conversion X defined by the Equation 2.12, with $m_{c,0}$ representing the initial mass of carbon.

$$r_s = \frac{dX}{dt} \qquad [1/s] \tag{2.11}$$

$$X = (m_{c,0} - m_c)/m_{c,0} \tag{2.12}$$

Assuming that the interfacial reaction rate r_i is constant on the entire reaction front surface S_i, the conversion rate r_s can be related to r_i by the Equation 2.13. The evolution of the reaction front surface with the reaction time will be defined as the initial reaction front surface $S_{i,0}$ multiplied by a function of the conversion $f(X)$, depending itself on the reaction time through X (Equation 2.14). As $k_{0,i}$ and $S_{i,0}$ are unknown, a global Arrhenius pre-exponential factor k_0 was defined (Equation 2.15). Finally, the conversion rate of the carbon oxidation can be modeled with a kinetic law depending on four kinetic parameters: k_0 in 1/s, E_a in kJ/mol, and $f(X)$ and the dimensionless n_{O_2} (Equation 2.16).

$$r_i \, S_i = r_s \, m_{c,0} \tag{2.13}$$

$$S_i = S_{i,0} \, f(X) \tag{2.14}$$

$$k_0 = k_{0,i} \, \frac{S_{i,0}}{m_{c,0}} \tag{2.15}$$

$$r_s = k_0 \, exp(-\frac{E_a}{RT}) \, f(X) \, {p_{O_2}}^{n_{O_2}} \tag{2.16}$$

2.1.2 Kinetic analysis of isothermal experiments

Thermogravimetric analysis (TGA) is a popular method to measure reaction rates in heterogeneous kinetics [41]. Soot is placed in a crucible inside an oven and the mass and the temperature of the solid are measured as a function of time. The temperature can be controlled to perform isothermal or temperature ramp experiments. The TGA device used in this work is described in detail in Chapter 3.

The major disadvantage of this technique is that it is not possible to perform a mixing of the solid phase. Therefore mass transport (oxygen diffusion) or heat transfer limitations could arise during the oxidation. Some propositions (sample dilution with an inert solid or limited sample size) were made to minimize them, but it is impossible to avoid them completely [42]. The aim of this section is to determine the global kinetic parameters of the soot oxidation (Equations 2.1 and 2.2), not the intrinsic kinetic parameters for each elementary reaction process. Thus, it was decided not to take into account the mass transport or heat transfer limitation contributions in the global kinetic parameters. But to compare soot samples with each other, these contributions have to be kept constant. Therefore, soot samples with constant weight (not diluted) were studied.

Generally, kinetic parameters of the conversion rate (k_0, E_a, $f(X)$ and n_{O_2}) are determined by performing isothermal experiments. A quantity of 10 mg soot (Printex U soot from Degussa) was put in the crucible. The oven was run under a nitrogen flow (60 ml/min) until the isothermal temperature was reached. Then the flow was switched to oxygen, and the mass m_c was recorded. The conversion and the conversion rate could be calculated as explained before (Equations 2.11 and 2.12). Isothermal experiments were performed at various temperatures (450°C to 650°C) and various oxygen concentrations (5% to 40%). Linear regressions (minimization of the least squares) were performed to determine E_a and n_{O_2}. Then, $f(X)$ and k_0 were determined with the help of a chemical or a morphological model for $f(X)$.

2.1.2.1 Determination of E_a and n_{O_2}

To determine the activation energy E_a in the Equation 2.16, isothermal experiments at various temperatures were performed. The oxygen partial pressure was kept constant (20% O_2 in N_2). For each isotherm, the reaction rate was calculated at defined conversions: X = 0.1, 0.2, ..., 0.9. For each conversion, ln(r_s) was represented as a function of 1/T and a linear regression was performed to calculate the activation energy. On the Arrhenius plot (Figure 2.1), two reaction zones could be observed. At high temperatures (T > 550°C, 1000/T < 1.25 1/K) the plot is no more linear: the conversion rate is partially controlled by mass transport mechanisms (oxygen diffusion) or heat transfer. At lower temperatures (T < 550°C, 1000/T > 1.25 1/K) the plot is perfectly linear: the reaction is chemically controlled (no mass transport limitation). It is the zone were the true chemical activation energy can be calculated. The average activation energy in this zone was found to be E_a = 160 $\pm$ 3 kJ/mol. This is consistent with literature, where E_a in the range 150 - 170 kJ/mol appears frequently for different soot sources [43–46].

To determine the influence of the oxygen partial pressure on the conversion rate, isotherms at various partial pressure (5% to 40%) were performed. The isotherm temperature was chosen at 525°C (the highest temperature of the chemical regime). For each partial pressure, the conversion rate was calculated at defined conversions (X = 0.1 to 0.9). A linear regression between ln(r_s) and ln(p_{O_2}) was performed

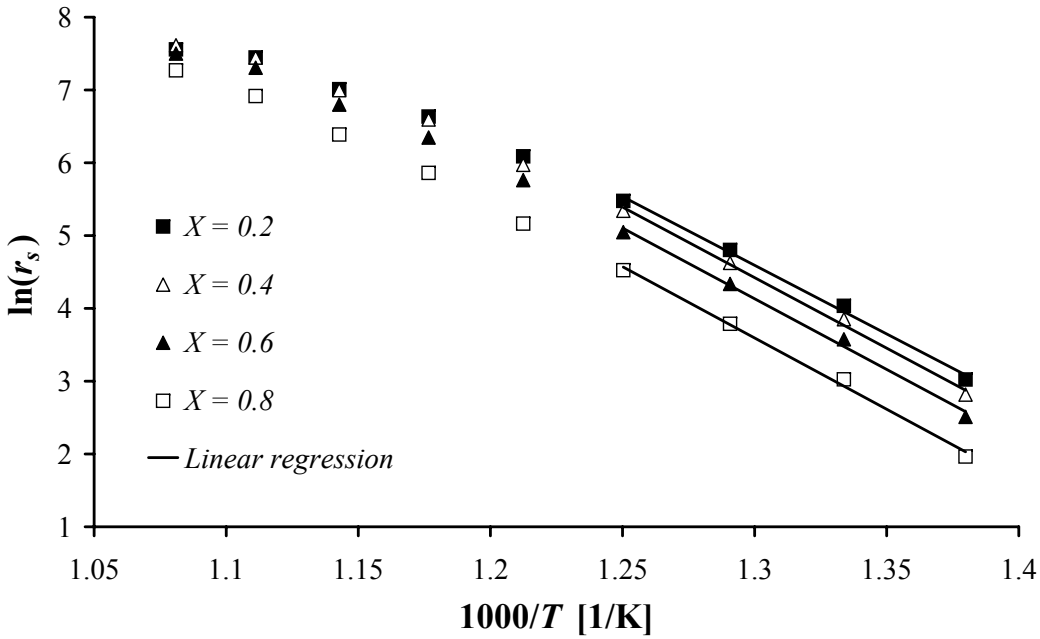

Figure 2.1: Arrhenius plot for PrintexU soot at various conversions

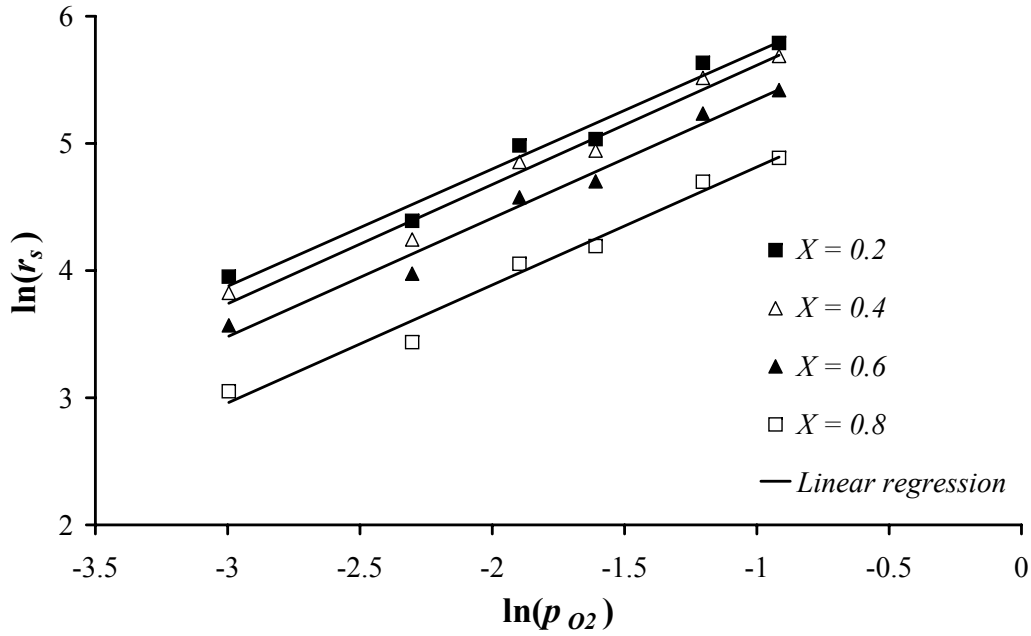

Figure 2.2: Linear regression between the conversion rate and the O_2 partial pressure for PrintexU soot at various conversions

(Figure 2.2). The order of reaction in oxygen was found to be 0.96 ± 0.02 at 525°C. This agrees with literature where the order of reaction in oxygen was reported to be unity [15, 45, 47, 48]. In the following, it was assumed that the reaction order in oxygen remains constant over the entire temperature range.

2.1.2.2 Determination of $f(X)$ and k_0

To determine the function $f(X)$ and k_0, the data of the isotherms at 450 - 525°C with 20% oxygen were used. As the partial pressure of oxygen and the temperature are constant during the experiment, it is possible to represent the conversion rate as a function of the conversion (Figure 2.3). There are chemical and morphological models in literature to describe the function $f(X)$. The simplest one is the chemical "pseudo reaction order model" (PRO, Equation 2.17, [41]). The experiment shows that the conversion rate first increases with conversion (corresponding to an increase of the reaction front surface - pore opening) before decreasing. Morphological models as the "pore growth model" (PG, Equation 2.18, [41]) can describe such phenomena (Figure 2.4).

$$f_1(X) = (1 - X)^m \tag{2.17}$$

$$f_2(X) = m\,(1 - X)\,(-ln(1 - X))^{(1-1/m)} \tag{2.18}$$

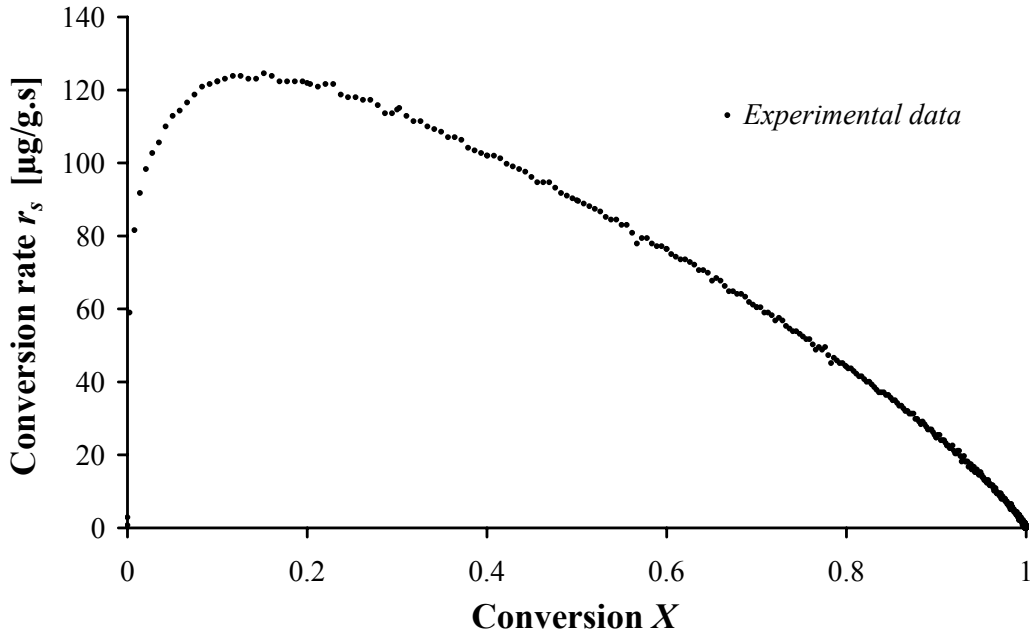

Figure 2.3: Conversion rate for PrintexU soot oxidation at 500°C and 20% O_2

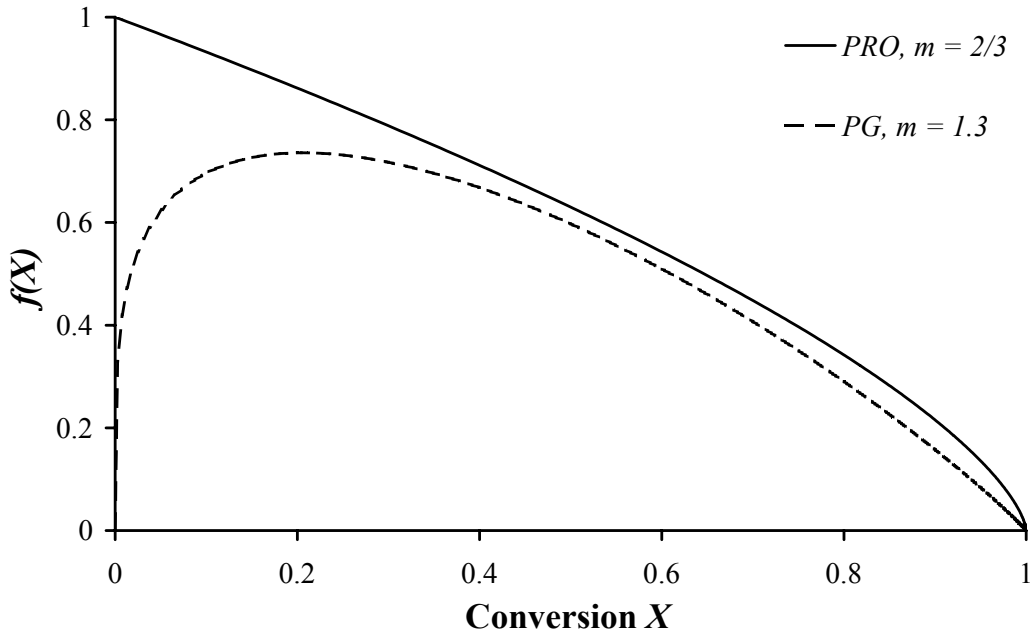

Figure 2.4: Examples of PRO and PG models for different m parameters

The parameter m of the PRO and PG models, and the resulting pre-exponential factor k_0 were calculated by linear regression for the four isothermal experiments. The average for the four temperatures was calculated. The curve showing r_s as a function of X was first interpolated for X varying from 0 to 1 with a step of 0.0025. Then, the linear regression was performed for both PRO and PG models with the following linearisation of the model (Equations 2.19 and 2.20). The coefficients A and B of the linearisation, the correlation coefficient CC and the parameters m and k_0 (assuming E_a and ${p_{O_2}}^{n_{O_2}}$ known from the last paragraph) of the two models are given in Table 2.1.

$$ln(r_s) = ln(k_0\,{p_{O_2}}^{n_{O_2}}) - \frac{E_a}{RT} + m\,ln(1-X) \tag{2.19}$$

$$ln(r_s) = A + B\,ln(1-X)$$

$$m = B \qquad k_0 = exp(A + \frac{E_a}{RT})/{p_{O_2}}^{n_{O_2}}$$

$$ln(\frac{r_s}{1-X}) = ln(m\,k_0\,{p_{O_2}}^{n_{O_2}}) - \frac{E_a}{RT} + (1-1/m)\,ln(-ln(1-X)) \tag{2.20}$$

$$ln(\frac{r_s}{1-X}) = A + B\,ln(-ln(1-X))$$

$$m = 1 - 1/B \qquad k_0 = exp(A + \frac{E_a}{RT})/(m\,{p_{O_2}}^{n_{O_2}})$$

Table 2.1: Parameters and correlation coefficients of the PRO and PG models

Model	A	B	CC	m	k_0 [1/s]
PRO	4.5 ± 1.3	0.74 ± 0.03	0.99 ± 0.01	0.74 ± 0.03	$4.0 \pm 0.4 \times 10^7$
PG	4.9 ± 1.4	0.20 ± 0.03	0.94 ± 0.04	1.25 ± 0.05	$4.7 \pm 0.5 \times 10^7$

The final kinetic law for each model is written in Equations 2.21 and 2.22. For the PG model, the parameter m was included in the constant k_0. The two models are compared with the isotherm experimental curve at T = 500°C. The conversion rate r_s is drawn as a function of X on the Figure 2.5. It appears clearly that an isotherm could not be modeled properly by the pseudo reaction order model for conversions < 0.1. Unlike the PRO model, the PG model can describe the experiment on the entire conversion range. For isothermal experiments, it seems also that the PG model is the most adapted one. Independently of the model used, the activation energy and the reaction order in oxygen are 160 kJ/mol and 0.96 respectively, which is consistent with the literature [15, 43–46].

$$PRO: \tag{2.21}$$

$$r_s = 4.0 \times 10^7 \, exp(-\frac{160 \times 10^3}{RT}) \, (1-X)^{0.74} \, {p_{O_2}}^{0.96}$$

$$PG: \tag{2.22}$$

$$r_s = 5.8 \times 10^7 \, exp(-\frac{160 \times 10^3}{RT}) \, (1-X) \, (-ln(1-X))^{(1-1/1.25)} \, {p_{O_2}}^{0.96}$$

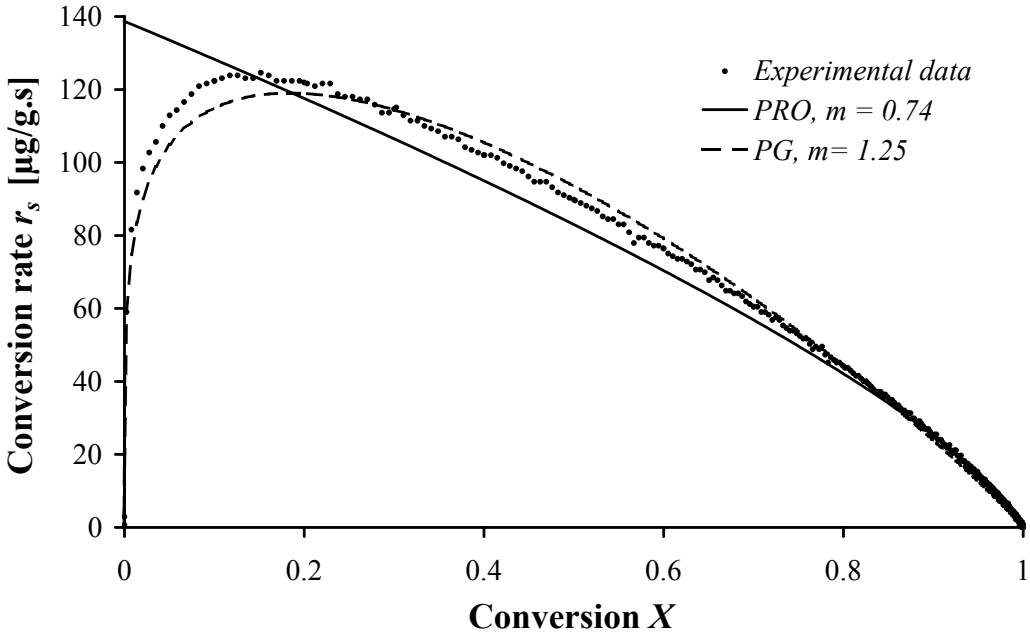

Figure 2.5: Comparison of the PRO and PG models with the experimental Printex-U soot oxidation at 500°C and 20% O_2

2.1.3 Kinetic analysis of a single ramp experiment

To determine the four kinetic parameters of the conversion rate kinetic law (k_0, E_a, n_{O_2} and $f(X)$) with isothermal experiments, at least five isotherms are needed (three points for the Arrhenius plot and three points to determine the dependence on the oxygen partial pressure). Assuming that the reaction order in oxygen is constant and equals 1 [15], three experiments are still needed. To gain time, it was decided to reduce the number of experiments, and perform just a single ramp experiment for each soot sample. Therefore, it was necessary to find a method to calculate all the kinetic parameters from a single ramp experiment.

2.1.3.1 Theoretical comments

Theoretically, it is not possible to derive all the kinetic parameters from a single ramp experiment. Indeed, it was shown that the same conversion curve could be generated using different kinetic models with different Arrhenius parameters [49]. Thus one specific kinetic model $f(X)$ has to be assumed to determine the kinetic parameters.

The preceding part has shown that the PG model is more adapted to describe isothermal experiments on the whole conversion range than the PRO model. However the applicability of the PG model under nonisothermal conditions has been widely discussed. The PG model includes contributions from distinct reaction processes, which may have very different temperature dependence [41]. Therefore, it should not be used to describe ramp experiments. It was thus decided to use the PRO model to describe the kinetic law of a single ramp experiment.

Assuming the PRO model, the kinetic parameters k_0, E_a, n_{O_2} and m have to be calculated by an appropriate method. Slovak [50, 51] proposed to use a direct non-linear regression method, which is described below. The kinetic law model obtained with this method for a single ramp experiment (PRO-Slovak) was compared with the kinetic law models obtained from the isothermal experiments (PRO and PG models) to validate the method.

2.1.3.2 Description of the direct non-linear regression

As seen before, the conversion rate can be written with the Equation 2.16. Two important assumptions are made in the method of Slovak. Firstly, the evolution of the reaction front surface follows the pseudo reaction order model (Equation 2.17). Secondly, the oxygen partial pressure remains constant and independent of the temperature during a ramp (as it was also assumed with isothermal experiments). Then the conversion rate can be written as following (Equation 2.23) with k'_0 including k_0 and the oxygen partial pressure dependence (Equation 2.24).

$$r_s = k_0\, exp(-\frac{E_a}{RT})\, f(X)\, {p_{O_2}}^{n_{O_2}} \tag{2.16}$$

$$f_1(X) = (1-X)^m \tag{2.17}$$

$$\frac{dX}{dt} = k'_0\, exp(-\frac{E_a}{RT})\, (1-X)^m \qquad [1/s] \tag{2.23}$$

$$k'_0 = k_0\, {p_{O_2}}^{n_{O_2}} \qquad [1/s] \tag{2.24}$$

Assuming that the time step between two measurements of X is small enough, the derivative in Equation 2.23 can be replaced by differences (Equation 2.25). Knowing the initial point of the TG-curve, X_0 and T_0 at t_0 = 0, further points of the curve can be calculated from the relation 2.26. The kinetic parameters will be calculated step by step with a non linear regression based on the least squares method [50, 51].

$$\Delta X = k_0' \, exp(-\frac{E_a}{RT}) \, (1 - X)^m \, \Delta t \tag{2.25}$$

$$X_i = X_{i-1} + k_0' \, exp(-\frac{E_a}{RT_{i-1}}) \, (1 - X_{i-1})^m \, (t_i - t_{i-1}) \tag{2.26}$$

2.1.3.3 Validation of the method

A temperature ramp from 50°C to 700°C (10 K/min) was performed with 10 mg PrintexU soot. The flow rate was adjusted at 60 ml/min flow rate with 20% oxygen in nitrogen. The conversion rate was plotted as a function of the temperature. The kinetic parameters calculated with the model of Slovak are summed up in Table 2.2. For comparison, the kinetic parameters found under isothermal conditions (with the PRO and the PG model) are also listed in Table 2.2. The experimental curve and the three modeled curves showing the conversion as a function of the temperature are drawn in Figure 2.6.

The activation energy found with the ramp experiments is the same as the one found with isothermal experiments. The major difference between the PRO-Slovak obtained from a single ramp experiment (with the Slovak method) and PRO model obtained from several isothermal experiments is the pseudo reaction order m. Applying the PRO model to a ramp experiment, m is underestimated, leading to an overestimation of the conversion at high temperatures. The PG model underestimates the conversion for $X < 0.5$ and overestimates it for $X > 0.5$. A possible explanation is that this model could not be applied for ramp experiments [49].

Table 2.2: Parameters and correlation coefficients of the PRO and PG models

Model	E_a [kJ/mol]	m	k_0 [1/s]	n_{O_2}	k_0' [1/s] (p_{O_2} = 0.2)
PRO-Slovak	160	0.9	?	?	8.27×10^6
PRO	160	0.74	4.03×10^7	0.96	8.60×10^6
PG	160	1.25	4.67×10^7	0.96	9.96×10^6

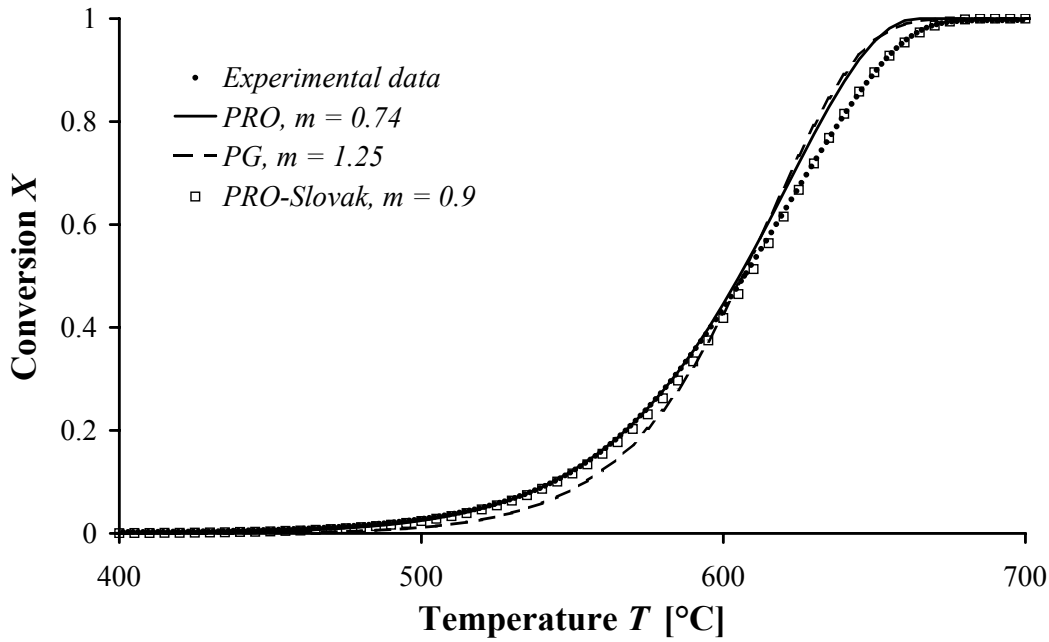

Figure 2.6: Comparison of the Slovak, PRO and PG model to the experimental oxidation of PrintexU soot for a temperature ramp (10 K/min, 20% O_2)

The Slovak model does not permit to calculate separately the pre-exponential factor k_0 and the reaction order in oxygen n_{O_2}, but it allows calculating the energy of activation, and the pseudo reaction order in carbon from one ramp experiment. E_a and k_0' were found to be comparable with the ones obtained with the two isothermal models. Therefore, the Slovak method can be used to calculate the activation energy E_a, the pseudo reaction order m (assuming a PRO model) and the pseudo pre-exponential factor k_0'. In the following, TGA experiments were performed with temperature ramps to gain time. It was further assumed that all the soot sources could be modeled with a PRO model. The kinetic parameters were calculated with the method of Slovak. To be able to compare the kinetic parameters with each other, a constant partial pressure in oxygen (20% oxygen in nitrogen) was used.

2.2 Definition of the catalytic effect of platinum

The aim of this section is to be able to evaluate the effect of a catalyst on the soot oxidation. It is thus necessary to compare the effect of two different catalysts on the same soot, but also the effect of one common catalyst on two different soot sources. Therefore, the definition of the catalytic effect should be relative to the soot oxi-

dized. The definition of a catalyst and its catalytic "activity", "degree", "efficiency" or "effect" is first discussed. The outline of the Arrhenius and Eyring equations is used to support the definition of the catalytic effect used here. Assumptions made regarding the kinetic law of the catalytic oxidation are discussed. The catalytic effect is finally defined as the pre-exponential factor ratio between the catalytic and the thermal soot oxidation, with the other kinetic parameters being kept constant.

2.2.1 Notion of catalyst, definition of the catalytic effect

A catalyst is a substance that can accelerate the rate of a reaction, or lower the temperature at which the reaction occurs, without being consumed by it. The presence of the catalyst can not change the free enthalpy of the reaction $\Delta_r G$. The equilibrium state at the end of the reaction remains constant: a catalyst can not allow a reaction that is thermodynamically impossible. A catalyst has the possibility to form an intermediary reactant with one or several reactants. The formation of this intermediate should correspond to an easier reaction path than the one without catalyst (see in Figure 2.7). The intermediate reacts alone or with another reactant in one or more steps to produce the products of the reaction and regenerate the catalyst. One step of the non-catalytic reaction is also replaced by one or more reactive steps. The free activation enthalpy of the catalytic reaction $\Delta^{\neq} G_1$ is lower than the one of the non-catalytic reaction $\Delta^{\neq} G$.

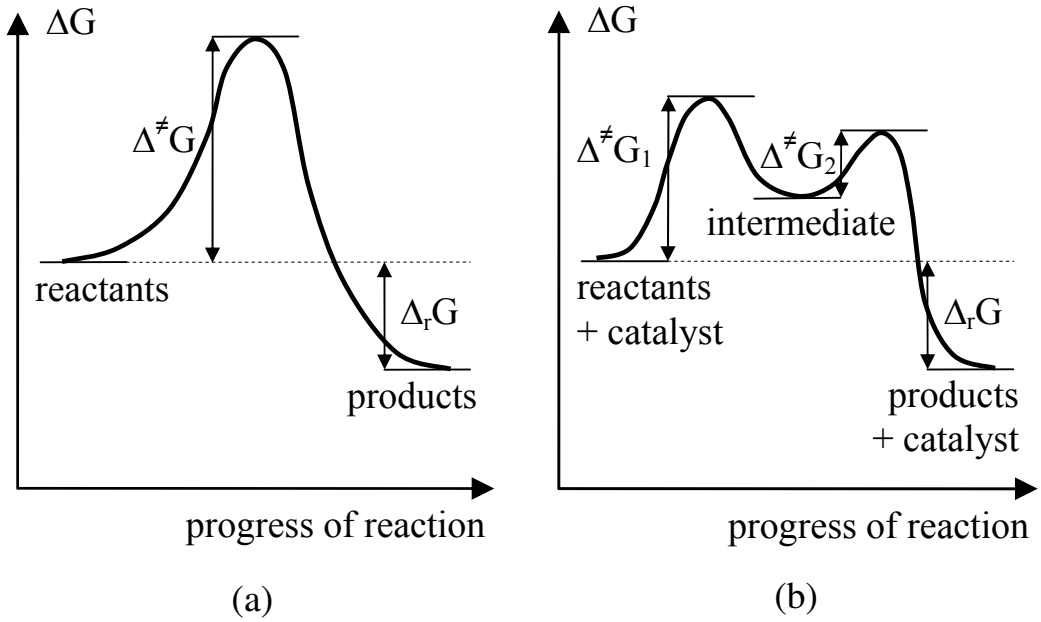

Figure 2.7: Reaction path without catalyst (a) and with catalyst (b)

Most authors working on the catalytic soot oxidation define the catalyst activity in terms of the ignition or the peak temperature during temperature programmed (TPO) experiments. This definition has the advantage of being easily applicable but the disadvantage of depending on the experimental conditions used. In heterogeneous catalysis between a gas and a solid, the degree of activity of a catalyst is described by the turn over of number (TON) and the catalytic efficiency by the turn over of frequency (TOF). The TON is defined as the number of catalytic transformation in respect to the number of active sites (without unit), and the TOF is the TON per unit of time (in [1/s]). Transferring this definition to a gas-solid-solid system (as the O_2-soot-platinum system) is quite complicated. Indeed, as the mechanisms of the catalysis remain unknown, the active sites that should be taken into account remain undefined too. Are they the active sites of carbon, where the oxidation happens, or the active sites of platinum, which adsorbed O_2? Seipenbusch et al. [38] defined the TOF for the catalytic soot oxidation as the number of reacted carbon atoms per number of platinum surface atoms and reaction time. We want to study if the catalytic effect depends on the platinum quantity and platinum particle size (Chapter 4). It is therefore more convenient to find a definition independent of the platinum active sites. Returning to the original definition of a catalyst explained before, the catalytic effect will be characterized in the following from the free enthalpy of the reaction, which is a parameter independent of the experimental conditions used and of platinum active sites.

To access the free enthalpy of a reaction, it is necessary to relate it to the parameters of the kinetic law describing the conversion rate. The kinetic and thermodynamic parameters of an elementary process could be related by comparing the Arrhenius equation (Equation 2.27) with the Eyring equation (Equation 2.28). Both equations describe the temperature dependence of the elementary process rate constant k.

Arrhenius equation:
$$k = k_0\, exp(-\frac{E_a}{RT}) \qquad [1/s] \tag{2.27}$$
$$ln(k) = ln(k_0) - \frac{E_a}{RT}$$

Eyring equation:
$$k = \frac{k_B\, T}{h}\, exp(-\frac{\Delta^{\neq} G}{RT}) \qquad [1/s] \tag{2.28}$$
$$ln(k) = ln(\frac{k_B\, T}{h}) - \frac{\Delta^{\neq} H}{RT} + \frac{\Delta^{\neq} S}{R}$$

The Arrhenius equation (Equation 2.27) is based on the collision theory (developed theoretically for gas phase reactions) and is founded on empirical observations. It supposes that particles must colloide with the correct orientation and with

sufficient kinetic energy if the reactants are to be converted into products. The pre-exponential factor k_0 represents the collision rate multiplied by a steric factor. The Eyring equation (Equation 2.28) is a theoretical construct based on the transition state model that can be applied for gas, condensed or mixed phase reactions (all situations where the simple collision model is not very helpful). The pre-exponential term is known as the universal constant for a transition state. k_B is the Boltzmann constant equals to 1.381×10^{-23} J/K, and h the Planck constant equals to 6.626×10^{-34} J.s, so that the universal constant for a transition state is ca. $6 \times 10^{+12}$ 1/s at room temperature.

The free activation enthalpy $\Delta^{\neq}G$ can be decomposed in an activation enthalpy term $\Delta^{\neq}H$ and an activation entropy term $\Delta^{\neq}S$ (Equation 2.29). A comparison between both Arrhenius and Eyring equations (Equation 2.30) allows to relate the activation energy E_a to the activation enthalpy $\Delta^{\neq}H$ (Equation 2.31), and the Arrhenius pre-exponential factor k_0 to the activation entropy $\Delta^{\neq}S$ (Equation 2.32). Hence, a decrease of the free activation enthalpy $\Delta^{\neq}G$ means a decrease of the activation energy E_a and/or an increase of the pre-exponential factor k_0 (Equation 2.33).

$$\Delta^{\neq}G = \Delta^{\neq}H - T\,\Delta^{\neq}S \tag{2.29}$$

$$\frac{dln(k)}{dT} = \frac{E_a}{RT^2} = \frac{1}{T} + \frac{\Delta^{\neq}H}{RT^2} \tag{2.30}$$

$$E_a = \Delta^{\neq}H + RT \tag{2.31}$$

$$k_0 = \frac{k_B\,T}{h}\,exp(\frac{\Delta^{\neq}S}{R} + 1) \tag{2.32}$$

$$\Delta^{\neq}G = E_a - RT\,ln(\frac{k_0\,h}{k_B\,T}) \tag{2.33}$$

For an elementary process, the free activation enthalpy $\Delta^{\neq}G$ can be directly related to the activation energy E_a and the Arrhenius pre-exponential factor k_0 (Equation 2.33). It was here assumed that the same relation exists for the global carbon oxidation into CO and CO_2 in presence or absence of platinum. So that both the activation energy E_a and the Arrhenius pre-exponential factor k_0 of the kinetic law could be affected by a catalytic effect. As it is essential to have just one parameter describing the catalytic effect, some assumptions have to be made on the kinetic law to be able to separate the contributions of E_a and k_0 on $\Delta^{\neq}G$.

2.2.2 Hypothesis on the kinetic law

An illustration of calculation problems of the kinetic parameters for the catalytic soot oxidation is plotted in the Figure 2.8. The thermal and catalytic (with various platinum-to-soot mass ratio) oxidation of Vulcan soot was performed in a TGA device. The obtained conversion curves were modeled with the Slovak method. The resulting kinetic parameters are summed up in Table 2.3. The temperature T_{50} and the conversion rate $r_{s,50}$ defined at a conversion X = 0.5 are also added. It appears that the catalyst decreases the temperature T_{50}. Concerning the reaction rate $r_{s,50}$, it increases for low platinum-to-soot mass ratio, but for mass ratio superior to 0.05, it remains constant. The T_{50} temperature would have been a good parameter describing the catalytic effect. However, it depends first on the experimental conditions used, and second, on the type of soot used.

The method of Slovak to calculate the kinetic parameters m, k'_0 and E_a seems to not be applicable for catalytic oxidation. Indeed, it appears that the three parameters are linked together (they all increase or decrease) but have no relation with the variation of the temperature T_{50}. The values of k'_0 are higher for catalyst oxidations than for the thermal oxidation. It could be explained by an augmentation of the free entropy during the catalysis, but the values are abnormally high in comparison with literature. Besides, the energy of activation E_a increases too, where it is supposed

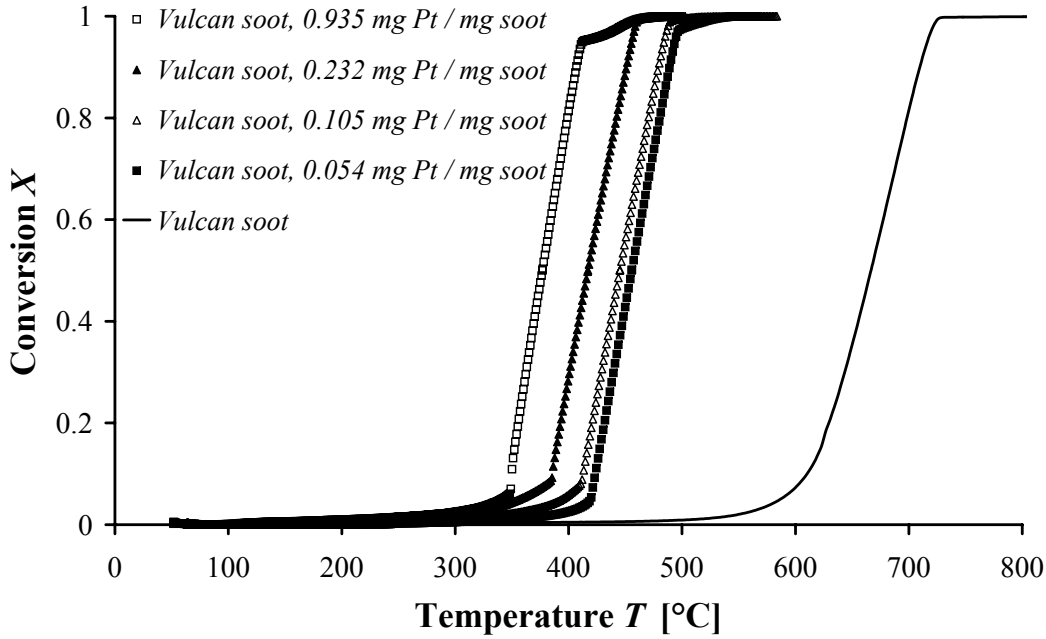

Figure 2.8: Conversion curve for thermal and catalytic oxidation of Vulcan soot with various platinum-to-soot mass ratio (10 K/min, 20% O_2)

Table 2.3: Kinetic parameters from the Slovak method for the conversion curves of Vulcan soot with various Pt-to-soot mass ratio

Platinum-to-soot mass ratio [mg Pt / mg soot]	m -	k'_0 [1/s]	E_a [kJ/mol]	T_{50} [°C]	$r_{s,50}$ [μg/g.s]
0	0.9	1.3×10^{8}	191	667	1517
0.054	1.5	1.1×10^{13}	212	456	2050
0.105	1.3	1.6×10^{11}	185	445	2016
0.232	1.2	1.6×10^{10}	165	417	2025
0.935	1.9	3.4×10^{15}	218	377	2037

to remain constant or decrease during catalytic oxidation. There are good reasons for suspecting that the fact that the three parameters vary in the same direction is a computational artefact [41]. The method of Slovak can not be used to calculate the kinetic parameters and achieve the free activation enthalpy of catalytic soot oxidation. As it is impossible to perform isothermal experiments for each catalysis, two assumptions were made on the kinetic law to evaluate quickly the free activation enthalpy of catalytic soot oxidation.

The first hypothesis is that the function $f(X)$ describing the evolution of the reaction front surface with the conversion is the same for thermal or catalytic soot oxidation. Physically, it means that the number of active sites where the carbon can receive oxygen atoms remains the same with or without catalyst, during the whole reaction process. This assumption is consistent with the oxygen transfer theory described in Chapter 1 [18, 19]. Platinum particles just act as activated oxygen donors, but will not create or inhibit active sites on the carbon. Following the oxygen transfer theory, it will thus be assumed that the function $f(X)$ obtained with the method of Slovak for the thermal soot oxidation remains unchanged in the case of catalytic soot oxidation.

The second hypothesis should allow to define the catalytic effect by omitting one kinetic parameter. It has been demonstrated that the catalytic effect (a decrease of the free activation enthalpy) could result in both a decrease of the activation energy E_a and an increase of the pseudo Arrhenius pre-exponential factor k'_0. Isothermal experiments on Vulcan soot were performed to achieve the exact contribution of these two parameters. The corresponding Arrhenius diagram for a fixed conversion is plotted in Figure 2.9 for both thermal and catalytic (with 0.054 platinum-to-soot mass ratio) soot oxidation. The two linear regressions lead to two parallel straight lines with the same slope but different intersections. The catalytic effect results in an increase of the Arrhenius pre-exponential factor for a constant activation energy.

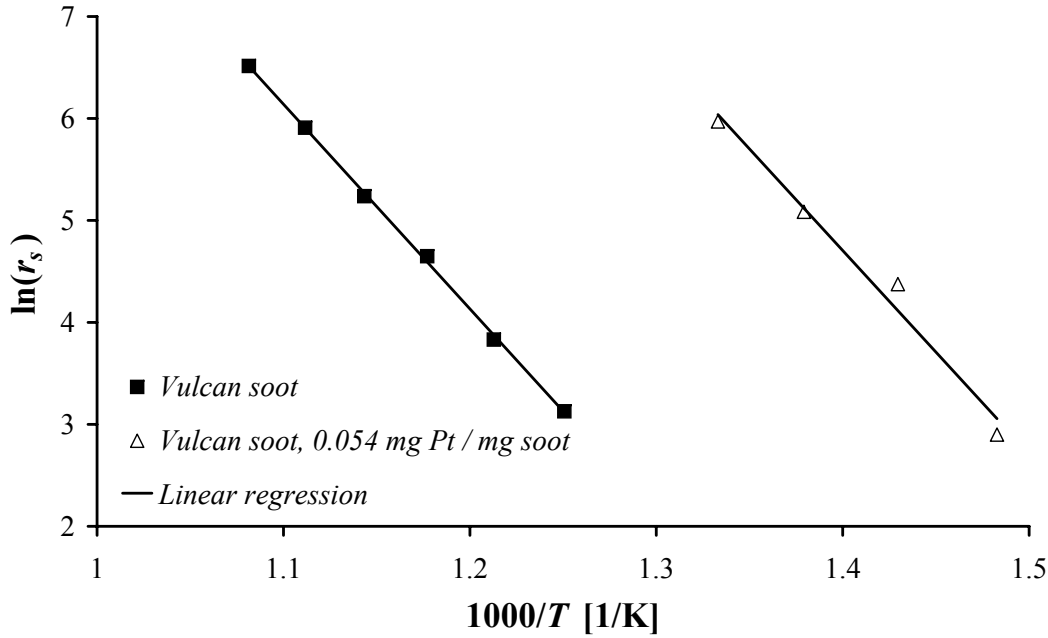

Figure 2.9: Arrhenius plot for Vulcan soot and Vulcan soot with 0.054 mg Pt / mg soot

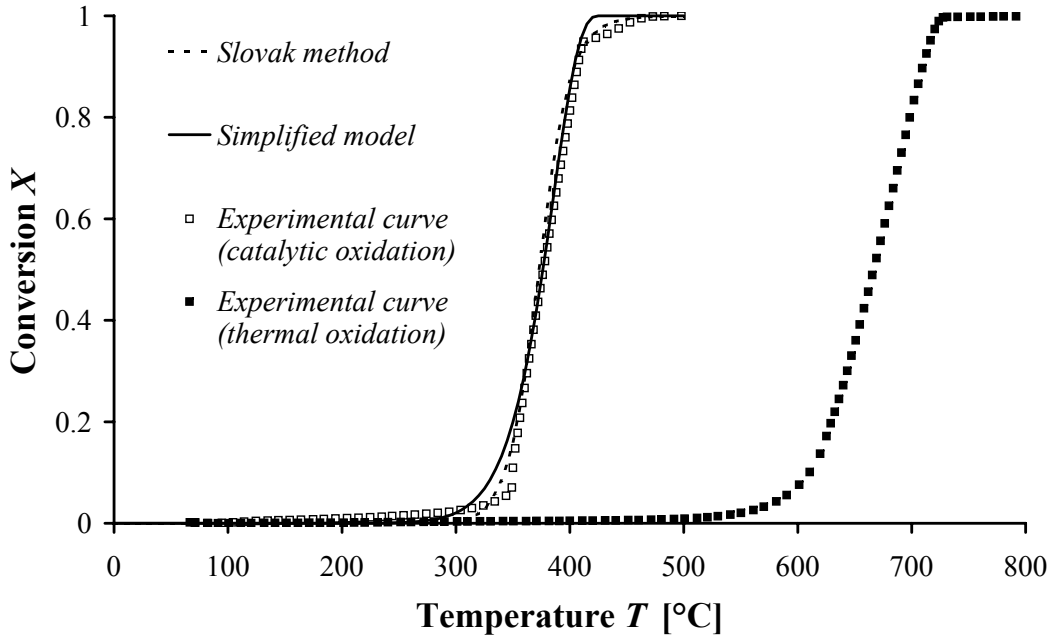

Figure 2.10: Experimental conversion curve for the catalytic oxidation of Vulcan soot with 0.935 mg Pt / mg soot and the corresponding Slovak and simplified model (10 K/min, 20% O_2)

Physically, it means that the catalytic effect is only due to an increase of the frequency of the carbon conversion into CO and CO_2, and that the energy required for this conversion remains constant. This is fully in accordance with the oxygen transfer theory described in Chapter 1.

The kinetic parameters of a catalytic soot oxidation were calculated from the one of the thermal oxidation. The kinetic parameters m_{th}, $k'_{0,th}$ and $E_{a,th}$ of the thermal soot oxidation are first calculated with the Slovak method. Then the catalytic conversion curve (conversion versus temperature) is modeled with the same m and E_a parameters ($m_{cat} = m_{th}$ and $E_{a,cat} = E_{a,th}$) but by adjusting the pseudo pre-exponential factor $k'_{0,cat}$. An example of the experimental and modeled conversion curves by the method of Slovak and by the actual simplified method is plotted in Figure 2.10. The kinetic parameters of the simplified model are presented in the Table 2.4. The simplified method can also model the conversion curve of catalytic oxidation properly, making it a robust method to determine the pseudo pre-exponential factor $k'_{0,cat}$.

Table 2.4: Kinetic parameters from the simplified model for the conversion curves of Vulcan soot

Platinum-to-soot mass ratio [mg Pt / mg soot]	m -	k'_0 [1/s]	E_a [kJ/mol]	T_{50} [°C]
0	0.9	1.3×10^{8}	191	667
0.054	0.9	3.8×10^{10}	191	456
0.105	0.9	4.9×10^{10}	191	445
0.232	0.9	1.1×10^{11}	191	417
0.935	0.9	3.0×10^{11}	191	377

2.2.3 Pre-exponential factor ratio between catalytic and thermal oxidation

Figure 2.11 displays the temperature T_{50} as function of the logarithm of the pseudo pre-exponential factor k'_0 issued from the Table 2.4. The temperature T_{50} is proportional to the logarithm of the pre-exponential factor k'_0. This relation can be explained easily. Indeed, the temperature T_{50} is defined by the temperature achieved for a conversion of X = 0.5. It depends thus on the three kinetic parameters m, k'_0 and E_a. As m and E_a are kept constant for thermal or catalytic oxidation, the exponential of temperature T_{50} varies linearly with k'_0, and the temperature T_{50} varies

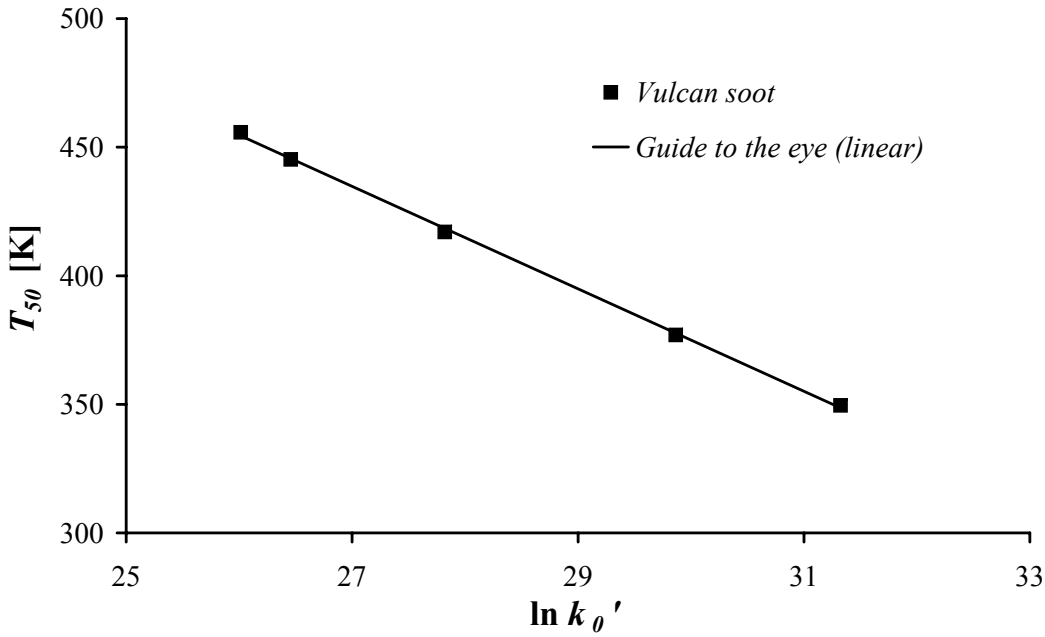

Figure 2.11: Temperature T_{50} versus the logarithm of the pre-exponential factor k'_0 for the catalytic Vulcan soot oxidation

linearly with the logarithm of k'_0. The exponential of the temperature T_{50} could have been used to define a catalytic effect. But the relation between $exp(T_{50})$ and k'_0 depends on m and E_a. And the kinetic parameters m and E_a are not the same for all the soot sources. To be able to compare two catalytic effects of the same catalyst on two different soot sources, it is not possible to compare the temperatures T_{50}.

Otherwise, to be able to compare the effect of two different catalysts on the same or different soot sources, it is necessary to define the catalytic effect as a relative value to the corresponding thermal soot oxidation. Thus, the catalytic effect will be defined as A, the ratio of the pseudo pre-exponential factor for the catalytic oxidation on the pseudo pre-exponential factor for the thermal soot oxidation, with the kinetic parameters m and E_a being kept constant (Equation 2.34).

$$A = \frac{k'_{0,cat}}{k'_{0,th}} \tag{2.34}$$

$$\text{with} \quad m_{cat} = m_{th} \quad \text{and} \quad E_{a,cat} = E_{a,th}$$

Chapter 3

Experimental equipment

The method to calculate the catalytic effect $A = k'_{0,cat} / k'_{0,th}$ of the catalytic soot oxidation on the basis of the conversion curve was developed in the previous chapter. Two test benches were used to perform soot oxidation experiments and obtain the conversion curves. The first and commonly used equipment is a thermogravimetric analysis device (TGA). It allows to oxidize a soot powder bed and is presented in the first part of this chapter. But it does not permit to investigate the soot oxidation directly on a filter. It was thus decided to develop a test bench with a reactor allowing to oxidize soot collected on sintered metal filters (SMF), described in the second part of this chapter. For both methods (TGA and reactor), conversion curves were obtained by plotting the reaction conversion as function of the soot temperature. Concerning the reactor, a radiation model was developed to calibrate the soot temperatures measured with an infrared camera on the SMF surface.

3.1 Thermogravimetric analysis

The thermogravimetric analysis consists of measuring the variation of mass of a sample subjected to a temperature program in a controlled atmosphere. The TGA device used in this work is a SESTYS Evolution 12, commercially available by Setaram. The operation principle is exposed in Figure 3.1.

The TGA balance is fitted with a beam articulated on a torsion ribbon and can measure in the range $\pm$ 200 mg. The soot powder sample is first put in a 1 cm^3 silica crucible. Then the crucible is hung from one end of the beam (with the other end taking the rebalancing tare) and introduced in the furnace chamber consisting of a 18 mm water cooled alumina tube. The carrier gas mixture is adjusted from 0 to 100 ml/min and from 0 to 100% O_2 in N_2. Carrier gas flows from the bottom to

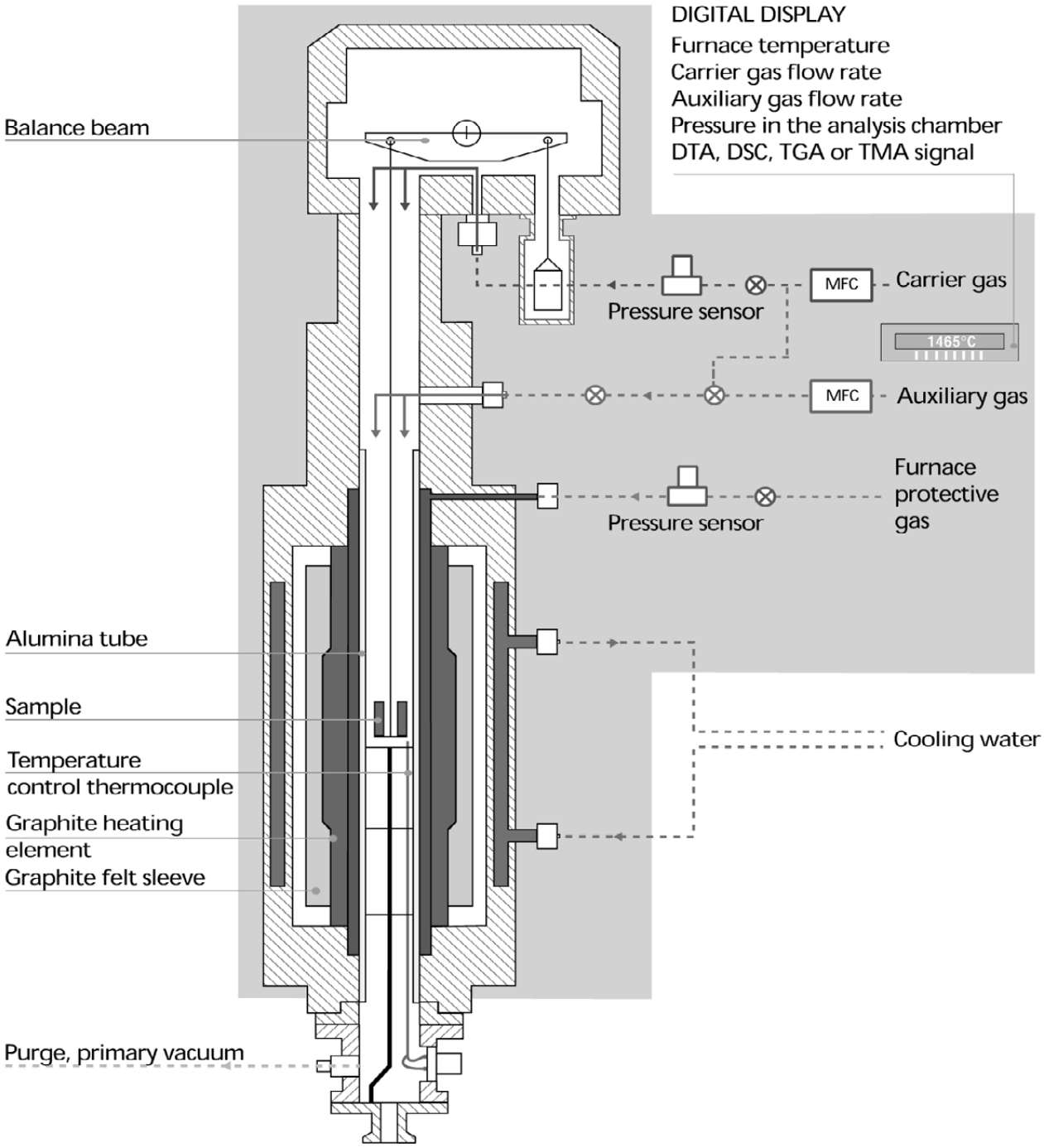

Figure 3.1: TGA Operation principle (from Setaram prospectus)

the top of the furnace. The oven temperature can be controlled with a thermocouple to perform isothermal or temperature ramp experiments from ambient temperature to 1000°C.

The temperature of the sample is recorded with an additional thermocouple placed just under the crucible. The momentary mass of the soot remaining in the crucible m_c is recorded by the balance with a resolution of 0.03 μg. The conversion X can be easily calculated from the remaining mass of soot by Equation 3.1, with $m_{c,0}$ the initial soot mass. Plotting the conversion as a function of the temperature give the conversion curve.

$$X = (m_{c,0} - m_c)/m_{c,0} \tag{3.1}$$

Temperature ramp experiments of 10 K/min were performed under a synthetic air atmosphere (20% O_2 in N_2) and a 60 ml/min flow rate. Three PrintexU soot samples of about 10 mg (effective: 9.9 mg, 9.7 mg and 9.7 mg) were oxidized using the temperature ramp conditions, to determine the reproducibility. The conversion curves are presented in Figure 3.2, and their differences in term of temperature for a conversion of 0.5 were found to be lower than $\pm$ 5 K. Applying the method of Slovak to calculate the kinetic parameters, the energy of activation was found to be 160 $\pm$ 1 kJ/mol with the other kinetic parameters k'_0 and m remaining constant. The reproducibility of the TGA experiment is thus excellent.

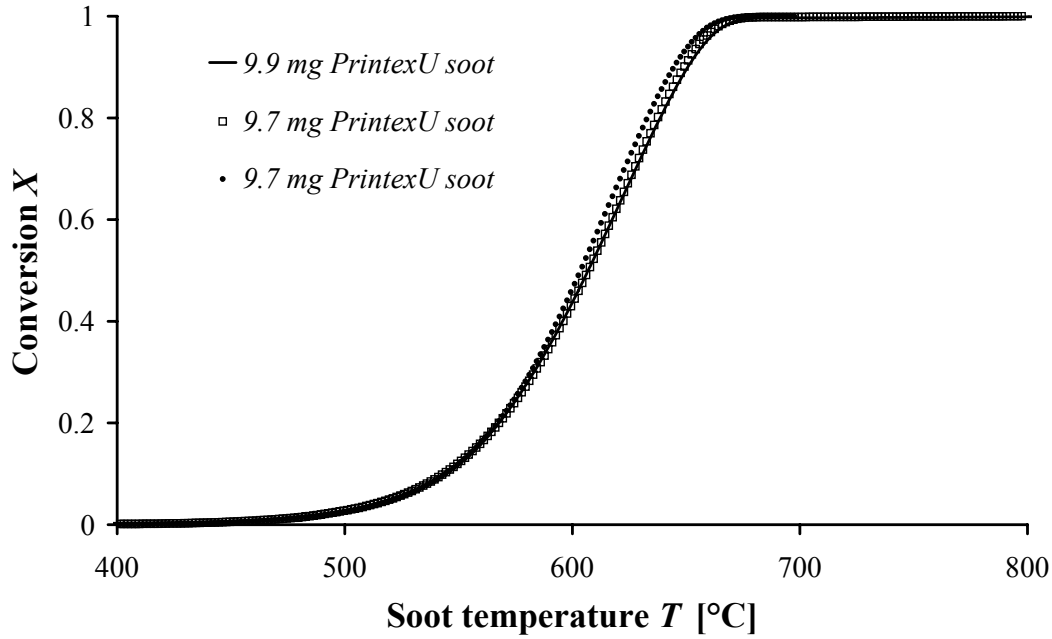

Figure 3.2: Reproducibility of the 10 mg PrintexU soot oxidation in TGA device (20% O_2 in N_2, 60 ml/min and 10 K/min ramp)

3.2 Soot oxidation on sintered metal filters

The test bench to investigate the soot oxidation on sintered metal filters (SMF) was constructed and developed at Robert Bosch GmbH, as part of this thesis. It consists of a reactor at laboratory scale in which a SMF can be exposed to a thermal treatment under varying gas atmospheres. The soot temperature and the reaction product concentrations were measured simultaneously. System control and data acquisition were performed with Labview and Irbis softwares. Conversion curves can be obtained from the recorded data after having calibrated the gas analyzer and the measured soot temperature. The model for the temperature calibration was validated with thermocouple measurements (code available in Appendix A).

3.2.1 Test bench presentation

Description of the test bench is divided into three parts. First, the characteristics of the sintered metal filter used in this work are given. The reactor developed to oxidize soot collected on this SMF is presented in a second part. Finally, measurement techniques and data acquisition methods are regrouped in a third part.

3.2.1.1 Sintered metal filter sheets

The filter used in this study is a sintered metal filter commercially available by HJS (Figure 3.3). For this thesis, it has the advantages of being easy to handle (flexible, easy to cut) and electrical conductive. The filter consisted of an expanded metal

Figure 3.3: Sintered metal filter

(canvas filled with powder) of iron, chrome and nickel. Before any utilization, the filter sheets are pre-oxidized for one hour at 800°C in air to stabilize the material before further temperature treatment takes place.

As experiments on an entire filter would require high gas quantities, it was decided to reduce the filter size to a more convenient laboratory dimension. Depending on the engine operating point, the exhaust gas flow rate varies between 0 and 400 m^3/h for a 2 liters direct injected diesel motor (Euro 3). It corresponds to a maximal face velocity of 6.73 cm/s for sintered metal filter with typical geometry (1.65 m^2 filter surface for 4.4 l filter volume). With a 10 l/min gas flow rate, ca. 25 cm^2 filter surface is required to obtain the same 6.73 cm/s face velocity. It was thus decided to use square filter sheets of 5 $\times$ 5 cm. However, as the sheets have to be clamped on two sides in the reactor, final sheet sizes of 6 $\times$ 5 cm were cut.

3.2.1.2 Reactor

After being loaded with soot, the filter has to be oxidized in an appropriate reactor. A reactor was developed to measure simultaneously the soot temperature with thermography and the reaction product concentrations (CO and CO_2) with a gas analyzer. The reactor was designed as a stainless steel chamber housing the SMF sheet, equipped with gas inlet and outlet, and a window for thermography measurements (Figure 3.4, left side). As the temperature loss would have been to high through the window if only heating the gas phase, it was decided to heat the filter

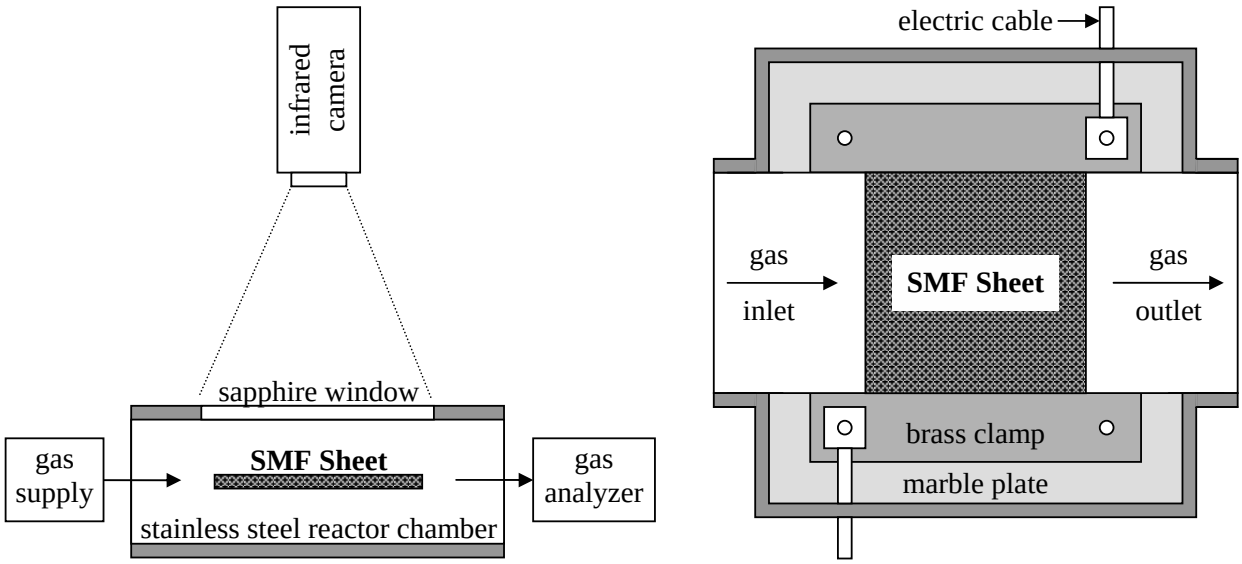

Figure 3.4: Plan of the reactor

directly by electric current (from 0 to ca. 170 A) through the sheets. Two electric cables are connected to the SMF sheet through two brass clamps. These pincers were embedded in marble plate to be electrically insulated from the stainless steel wall of the reactor.

Figure 3.4 (right side) shows the reactor chamber with a filter mounted between the two brass clamps. The gas flows from left to the right, parallel to the filter surface. The internal face of the chamber was coated with a black paint (Pyromark serie 2500 commercially by Helling GmbH). A thermocouple was glued to the internal face of the chamber to get the temperature of the reactor. The reactor can be closed with a cover containing a sapphire window. Sapphire is transparent in the midwave infrared (3-5 μm). A copper foam was installed in the channel gas inlet to homogenize the profile of the gas flow. The reactor was placed in an aluminium box with insulated materials for security.

3.2.1.3 Measurements techniques

The test bench is composed of the reactor, a gas supply and a gas analyzer, a power supply, a data logger for thermocouples, an infrared camera and a computer to control the system and acquire the data (see in Figure 3.5).

Nitrogen and oxygen are supplied through two mass flow controllers - MFC (MKS GmbH), and conducted to the reactor. At the reactor outlet, a part of the gas (measured with a mass flow meter - MFM) is pumped through a filter (2 μm diameter pores) and diverted into the 3 channels of the gas analyzer (Rosemount GmbH). Oxygen, carbon monoxide and carbon dioxide concentrations are measured simultaneously in three parallel cuvettes. The oxygen concentration is measured with a paramagnetic oxygen sensor between 0 and 100%. Carbon monoxide and dioxide concentrations are measured with non-dispersive infrared analyzer (NDIR) between 0 and 5000 ppm and 0 and 16% respectively (see in Table 3.1). The gas flow path is described in Figure 3.6.

An infrared camera (VarioTHERM commercially available by InfraTec GmbH) suspended above the reactor is used to measure the soot temperature through the sapphire window. The camera measures the infrared radiation emitted by the soot in the midwave spectral range (3.4 - 5 μm). Camera technical specifications are regrouped in Table 3.2. The camera consists of a focal plane array with 256 $\times$ 256 platinum silicide detectors. A stirling cooler is integrated inside the camera to cool down the detectors. The camera can measure temperatures from -25 to 1200°C with an accuracy better than 0.1 K at 30°C and a maximal frequency of 50 Hz.

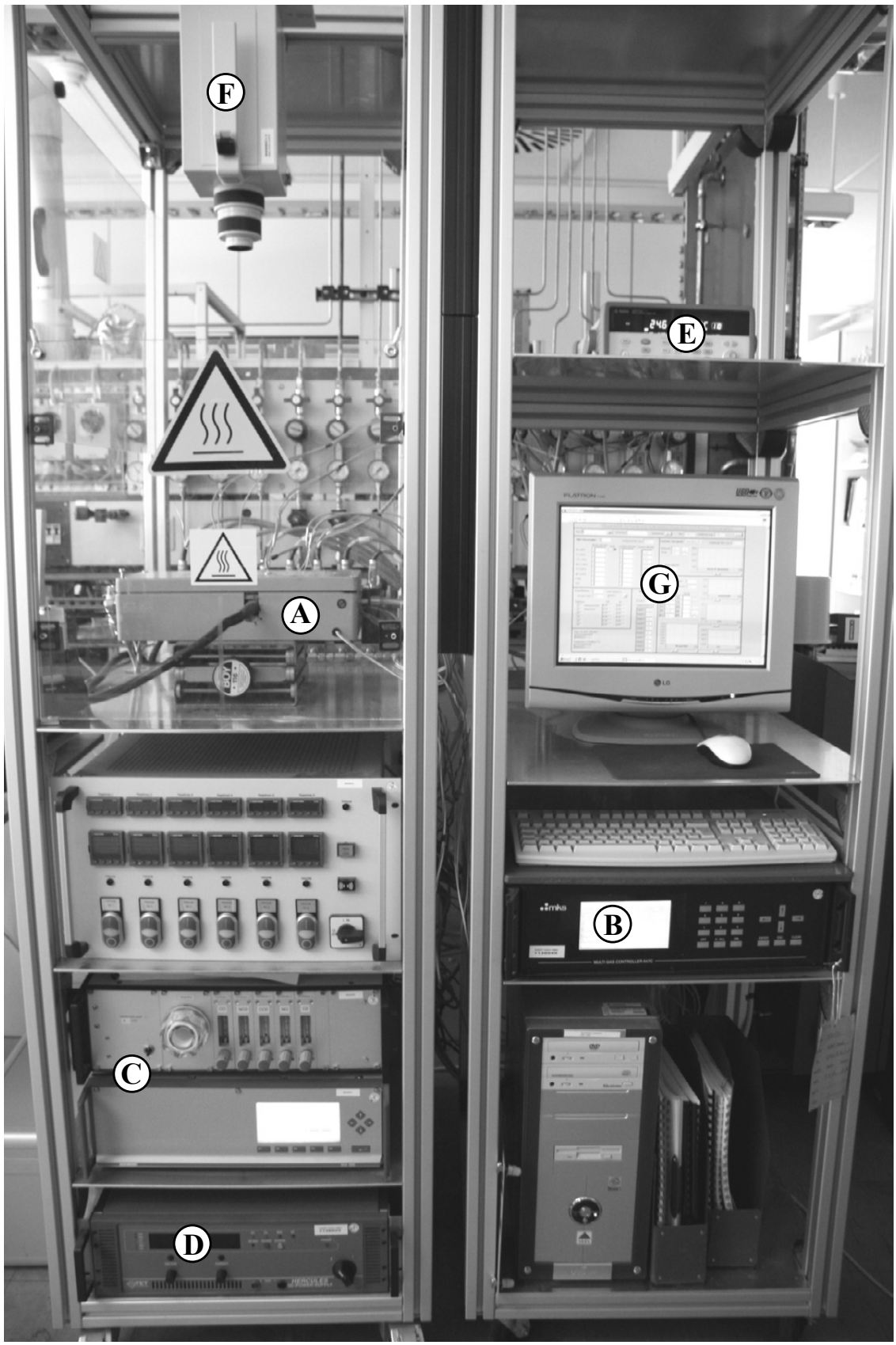

Figure 3.5: Test bench with reactor (A), gas supply (B), gas analyzer (C), power supply (D), data logger (E), infrared camera (F) and computer (G)

Table 3.1: Characteristics of the gas supply and gas analyzer

Gas supply	Composition	Range
N_2	100%	0 - 10 l/min
O_2	100%	0 - 2 l/min
Gas analyzer	Method	Range
O_2	paramagnetic	0 - 100%
CO	NDIR	0 - 5000 ppm
CO_2	NDIR	0 - 16%

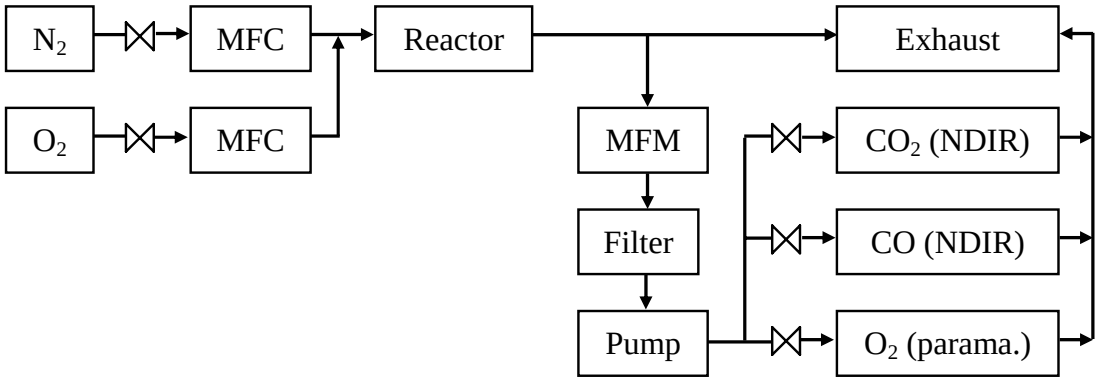

Figure 3.6: Gas flow path in the testbench

Table 3.2: Technical specification of the infrared camera (from InfraTec GmbH prospectus)

Spectral range	3.4 - 5 μm
Image principle	Focal plane array (256 $\times$ 256)
Detector, cooling	Platinum silicide, Stirling Cooler
Temperature range, accuracy	-25 to 1200°C, 2 K
Temperature resolution (30°C)	0.1 K
Time resolution	1 - 50 Hz

The power to heat the filter is supplied by a Hercules (TET Electronic) device. Currents from 0 to 200 A can be supplied. SMF sheet resistance of the samples used is about 10 mΩ at room temperature and increases with temperature. Thus a maximal power of 400 W can be applied. A current of 170 A is enough to raise the filter temperature to more than 800°C. A current ramp of 2 A/min corresponds to a temperature ramp of 10 K/min. Thermocouples were placed inside the reactor and at the gas analyzer inlet to control the evolution of the corresponding temperatures. A data logger allows to record all the temperatures measured by the thermocouples.

The test bench control was assured through two independent softwares. The software Irbis Process (available by InfraTec GmbH) records thermal images and Irbis Plus (also available by InfraTec GmbH) is then used for their evaluation. The temperature average on an image part corresponding to the visible filter surface can be calculated. Then a temperature profile of image series can be performed. The resulting temperature to time data (1 s step) are available in ASCII-format. The software Labview is the interface between all the other components of the test bench, and the computer. Figure 3.7 presents the data flow between Labview and the test bench components. Data coming from the data logger (temperatures) and the gas analyzer (concentrations) are read and recorded by Labview. The gas supply and power supply are controlled by Labview (read and written data). All the data managed by Labview are recorded as a function of time with a 1 s step and are available in Excel-format.

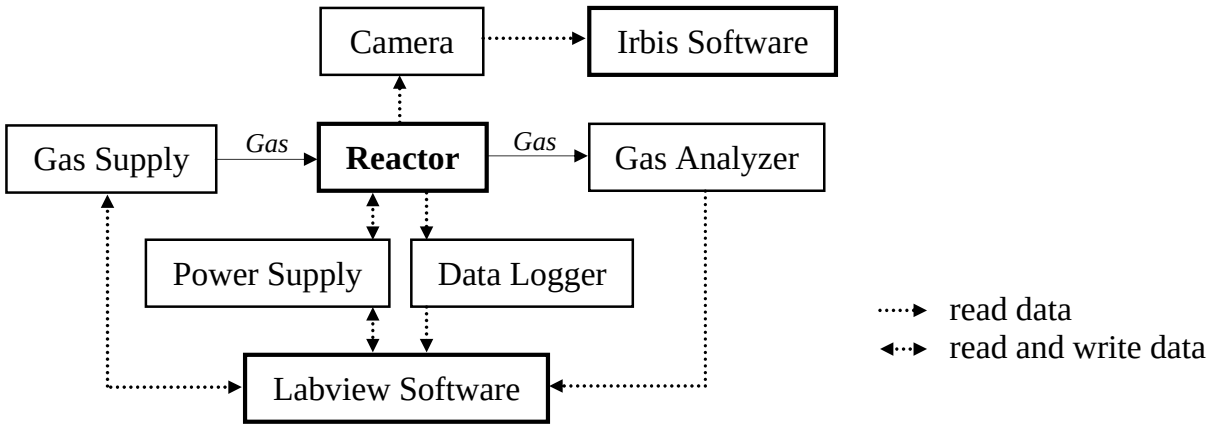

Figure 3.7: Information flow for test bench control and data acquisition

3.2.2 Test bench calibration

The soot temperature recorded by the infrared camera and the reaction product concentrations measured by the gas analyzer have to be calibrated. The infrared camera measures a radiation. From this radiation, with the assumption that the emissivity of the object emitting this radiation equals that of a black body, a temperature is calculated. This assumption could not be applied directly in the case of the SMF as its emissivity has first to be determined. Therefore, a model was developed to calculate the real temperature on the filter surface, and it was experimentally validated with temperature readings from a thermocouple. The emissivity of the filter and of soot were also measured with the aid of a reference black body. Concerning the reaction product concentrations, it was verified that the reactor itself does not emit any CO or CO_2. It was also verified that the filter and the reactor do not catalyze the CO to CO_2 by oxidation in the gas phase. When these temperature and reaction product concentrations calibration are completed, it is possible to calculate the conversion of C into CO and CO_2 from the CO and CO_2 concentrations, and to plot it as a function of the temperature to obtain the conversion curve.

3.2.2.1 Temperature calibration

A radiation model for the reactor was developed based on heat radiation theory. The model was experimentally validated comparing the temperature measured by the infrared camera and corrected by the model with the temperature measured by a thermocouple. The model was then used to determine the filter and the soot emissivity. These parameters are essential for applying the model to soot oxidation experiments.

Radiation model for the reactor

The temperature measured by the infrared camera is based on the theory that every body at the absolute temperature T radiates energy. This energy is composed of electromagnetic waves of different wavelengths λ. Planck's law describes the relation between the radiation Φ and the temperature T of a black body, depending on the wavelength λ (Equation 3.2) [52]. The infrared camera measures the radiation on a defined wavelength range. The integration of Planck's law on this range gives the relation between the radiation and the temperature of a black body. For the VarioTHERM infrared camera, this relation is given by the Equation 3.4 [53].

$$\Phi(T,\lambda) = \frac{c_1}{\lambda^5\,(exp(\frac{c_2}{\lambda T}) - 1)} \quad [W/m^3] \tag{3.2}$$

$$c_1 = 3.7418 \times 10^{-16} \quad [W.m^2] \qquad c_2 = 1.4388 \times 10^{-2} \quad [m.K] \tag{3.3}$$

$$\Phi(T) = \frac{c_1\,\delta\lambda}{{\lambda_{av}}^5\,(exp(\frac{c_2}{\lambda_{av}\,T}) - 1)} \quad [W/m^2] \tag{3.4}$$

$$\lambda_{av} = 4.5 \times 10^{-6} \quad [m] \qquad \delta\lambda = 3 \times 10^{-6} \quad [m] \tag{3.5}$$

In theory, a completely black body is an ideal body which for each temperature and each wavelength, absorbs all the incident radiation. This can be illustrated by the following balance (see in Figure 3.8). An incident radiation Φ_i arrives on a body surface. A fraction ρ of the radiation is reflected (reflexivity), a fraction α is absorbed (absorptivity), and a fraction τ is transmitted (transmissivity). The conservation of energy imposes that the sum of the reflexivity, the absorbance and the transmissivity is equal to 1 (Equation 3.6). Bodies are often characterized by their emissivity ϵ, that is equal to the absorptivity α (Kirchhoff law, Equation 3.7). So that the Equations 3.6 and 3.7 leads to the balance Equation 3.8. For a black body, the absorptivity α - and consequently the emissivity ϵ - are equal to 1 for all wavelengths. In reality, black bodies do not exist and the objects are called gray bodies, having emissivity ϵ comprised between 0 and 1. It will be assumed that all gray bodies of this work are diffusive. This means that the emissivity ϵ is independent of the wavelength.

$$\rho + \alpha + \tau = 1 \tag{3.6}$$

$$\alpha = \epsilon \tag{3.7}$$

$$\rho + \epsilon + \tau = 1 \tag{3.8}$$

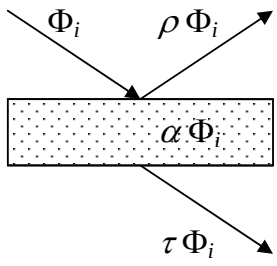

Figure 3.8: Energy balance relative to an incident radiation on a surface body

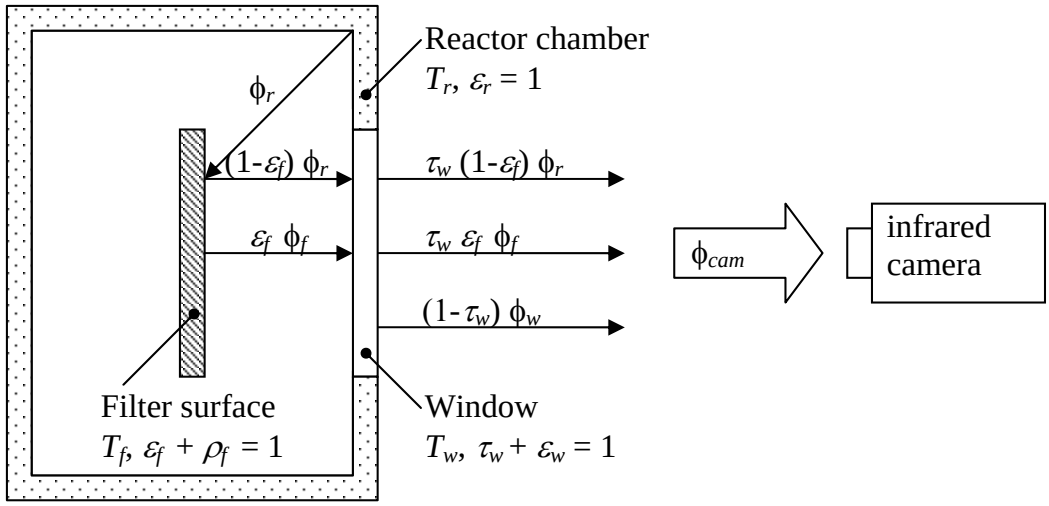

Figure 3.9: Contribution of radiations emitted by the filter surface, reactor chamber and window on the radiation measured by the infrared camera

The infrared camera measures the incident radiation, Φ_{cam} on its detectors. This radiation results from contributions of the filter surface, the reactor chamber, and the sapphire window (see in Figure 3.9). In fact, the filter surface emits a radiation $\epsilon_f\ \Phi_f$, with ϵ_f being the emissivity of the filter. As the filter is a gray body, it can thus reflect incident radiation with the reflexivity ρ_f = 1 - ϵ_f. The reactor chamber emits also a radiation Φ_r. The reaction chamber was painted with a black lacquer which can be assumed to act as a black body (emissivity ϵ_r = 1). The sapphire window is a transparent object with a known transmissivity τ_w. The window was assumed to not reflect any radiation, it emits thus itself a radiation $\epsilon_w\ \Phi_w$, with ϵ_w = 1 - τ_w. The emissivity of the exterior reactor surface and the surroundings were considered to be negligible: the temperature of these objects remains at room temperature during an experiment. Finally, the incident radiation measured by the infrared camera Φ_{cam} can be described with the Equation 3.9. Thus, the filter surface temperature T_f can be calculated from Φ_{cam} and Planck's law (Equation 3.4) , leading to the Equation 3.10.

$$\Phi_{cam} = \tau_w(\epsilon_f\ \Phi_f(T_f) + (1-\epsilon_f)\ \Phi_r(T_r)) + (1-\tau_w)\ \Phi_w(T_w) \tag{3.9}$$

$$\Phi_f(T_f) = \frac{1}{\epsilon_f}\,[\frac{\Phi_{cam} - (1-\tau_w)\ \Phi_w(T_w)}{\tau_w} - (1-\epsilon_f)\ \Phi_r(T_r)] \tag{3.10}$$

To calculate the temperature at the surface of the filter from the incident radiation on the infrared camera, it is necessary to know the temperature and emissivity of the reactor chamber, the temperature and transmissivity of the sapphire window and the emissivity of the filter surface. The model is validated in the next section.

Experimental validation

A thermocouple was soldered onto the filter surface which was then covered with a reference black lacquer of emissivity equal to 0.98 (commercially available by Helling GmbH). Thus the emissivity of the filter surface was assumed to be ϵ_f = 0.98. The same lacquer was used to paint the reactor chamber. As it does not have any influence on the results of the model, it was decided to assume that the emissivity of the reactor chamber ϵ_r is equal to 1. The temperature of the reactor chamber was measured through the thermocouple glued on the internal face of the reactor chamber. The transmissivity spectrum of the sapphire window was given by the producer and τ_w was found to be equal to 0.81 in the wavelength range of the infrared camera. The temperature of the sapphire window was assumed to be the same as the temperature of the rector chamber.

Knowing all the parameters of the model presented in Figure 3.9, experiments were performed to validate it. The painted filter with the soldered thermocouple was put inside the reactor, and a 2 A/min current ramp was performed up to 500°C (maximal temperature before the soldering breaks). The temperature of the filter surface and the reactor chamber were recorded through the soldered thermocouple. The camera records simultaneously the temperature T_{cam} of a black body corresponding to the incident radiation (related by the Equation 3.4). A program was developed with

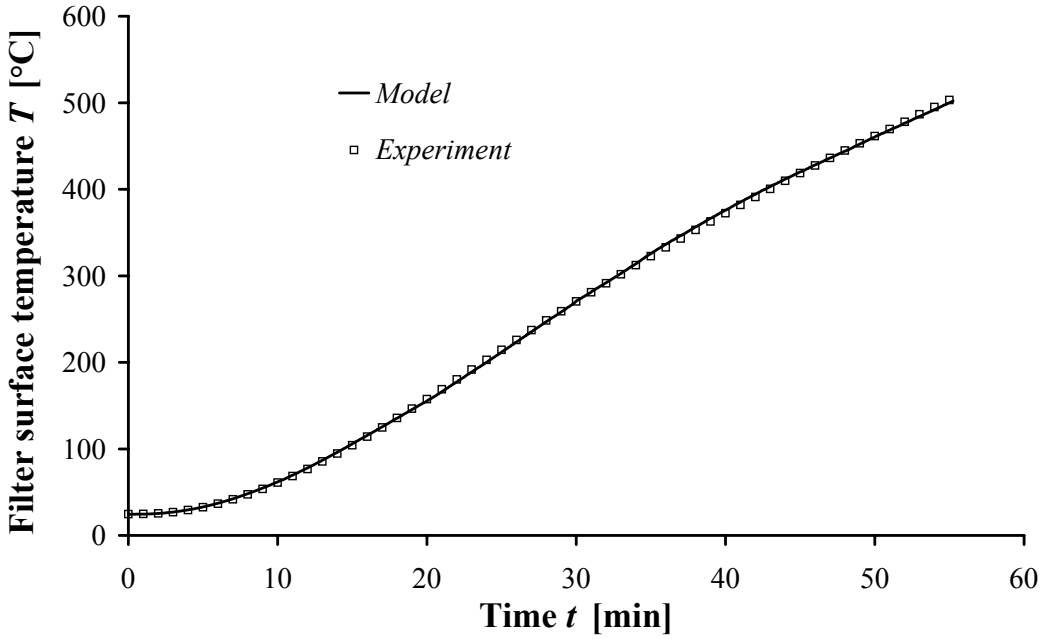

Figure 3.10: Comparison between the filter surface temperature T_f calculated by model and measured by thermocouple

the Engineering Equation Solver software, to calculate the temperature of the filter surface T_f from the temperature measured by the camera T_{cam} and the temperature of the reactor chamber T_r. The code is presented in Appendix A.

The comparison between the modeled and measured filter surface temperature is presented in Figure 3.10. It appears that over the examined temperature range (room temperature to 500°C), the differences between model and experiment are in a temperature range of $\pm$ 5 K. The temperature measured by the infrared camera can thus be corrected with the radiation model to obtain the real temperature of the filter surface. The model was not validated for temperatures higher than 500°C (soldering breakage). It will be however extrapolated for temperatures up to 800°C.

In order to use the model properly during the soot oxidation experiments, the filter surface emissivity, depending if soot is collected on the filter, has to be determined. This is the subject of the next section. Otherwise, all other radiation model parameters were obtained as previously: reactor chamber (ϵ_r = 1) and window (τ_w = 0.81) temperatures were assumed to be the same and measured through the thermocouple glued on the reactor internal face during the entire soot oxidation experiment.

Determination of the filter emissivity and of the soot emissivity

The filter and the soot emissivities were determined by comparison with the reference lacquer of known emissivity $\epsilon_{lacquer}$ equal to 0.98. A filter was painted on one half with the lacquer, the other half was kept plain. The filter was then submitted to a temperature ramp, and the emitted radiation was measured by the infrared camera. The two surfaces (plain or with lacquer) are at the same temperature T_f. But due to their different emissivity, the infrared camera measures two different radiations $\Phi_{cam,lacquer}$ and $\Phi_{cam,filter}$ for the two surfaces (Figure 3.11).

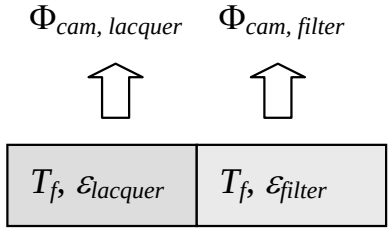

Figure 3.11: Experimental method to determine the filter emissivity based on the lacquer reference emissivity

Using the model as described in the preceding paragraph (T_w = T_r measured by a thermocouple, ϵ_r = 1, τ_w = 0.81), and knowing the emissivity of the lacquer, it is possible to calculate the temperature T_f of the filter, for the part covered with lacquer (Equation 3.11). Knowing the temperature T_f and the incident radiation measured for the plain filter, it is possible to calculate reversely the emissivity of the plain filter ϵ_{filter} (Equation 3.12). The same method is used with a filter covered an half with the lacquer, and an half with PrintexU soot, to calculate the emissivity of the soot, ϵ_{soot}.

$$\Phi_f(T_f) = \frac{1}{\epsilon_{lacquer}} \left(\frac{\Phi_{cam,lacquer} - (1-\tau_w)\,\Phi_w(T_w)}{\tau_w} - (1-\epsilon_{lacquer})\,\Phi_r(T_r) \right)$$

$$T_f = \frac{c_2}{\lambda_{av}\, ln(1 + \frac{c_1\,\delta\lambda}{\lambda^5\,\Phi_f})} \tag{3.11}$$

$$\epsilon_{filter} = \frac{\Phi_{cam} - \tau_w\,\Phi_r(T_r) - (1-\tau_w)\,\Phi_w(T_w)}{\tau_w(\Phi_f(T_f) - \Phi_r(T_r))} \tag{3.12}$$

The filter and the soot emissivity were determined for 12 temperatures varying from 250 to 750°C. As the emissivity varies with temperature (see in Figure 3.12), an average was performed to get the final values. The emissivity of the plain filter is ϵ_{filter} = 0.81 and the emissivity of the soot is ϵ_{soot} = 0.93. Averaging affects the calculated temperature of $\pm$ 2 K for the plain filter and $\pm$ 4 K for the soot on

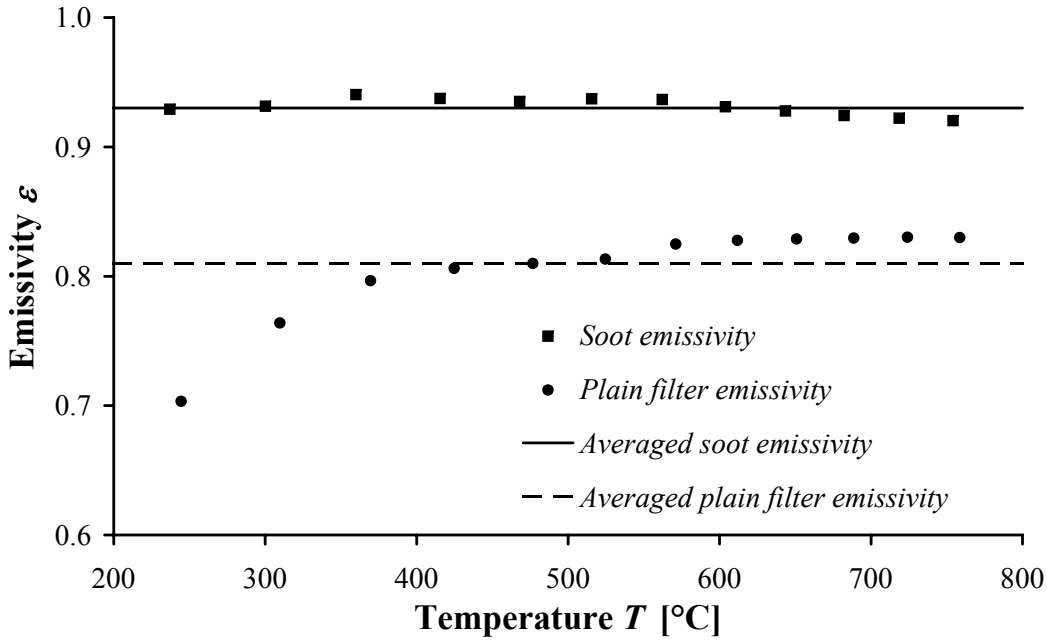

Figure 3.12: Filter and soot emissivity

the studied temperature range (250°C to 750°C). This difference is acceptable to justify to work with the average emissivity values. Knowing the emissivity of the soot and of the filter, it is possible to use the model to calculate the temperature emitted by a plain filter, or a filter covered with soot.

3.2.2.2 CO and CO_2 concentrations measurement

The conversion curves are calculated from the reaction product concentrations measured by the gas analyzer. It is thus necessary to assess that the measured concentrations really correspond to the primary products of the concentration. It was first verified that the reactor itself does not emit any CO and CO_2 in experimental conditions (notably from the carbon sealing on the reactor cover). The catalytic effect of the stainless steel surface in the reactor chamber and of the filter itself on the CO to CO_2 oxidation was also studied.

A filter was clamped inside the reactor, and the reactor closed with the cover. A 2 A/min current ramp was performed under a 10% O_2 atmosphere (4 l/min flow). The filter temperature was recorded with the infrared camera and corrected applying the radiation model. The CO and CO_2 concentrations were simultaneously recorded with the gas analyzer and plotted as a function of the temperature (Figure 3.13).

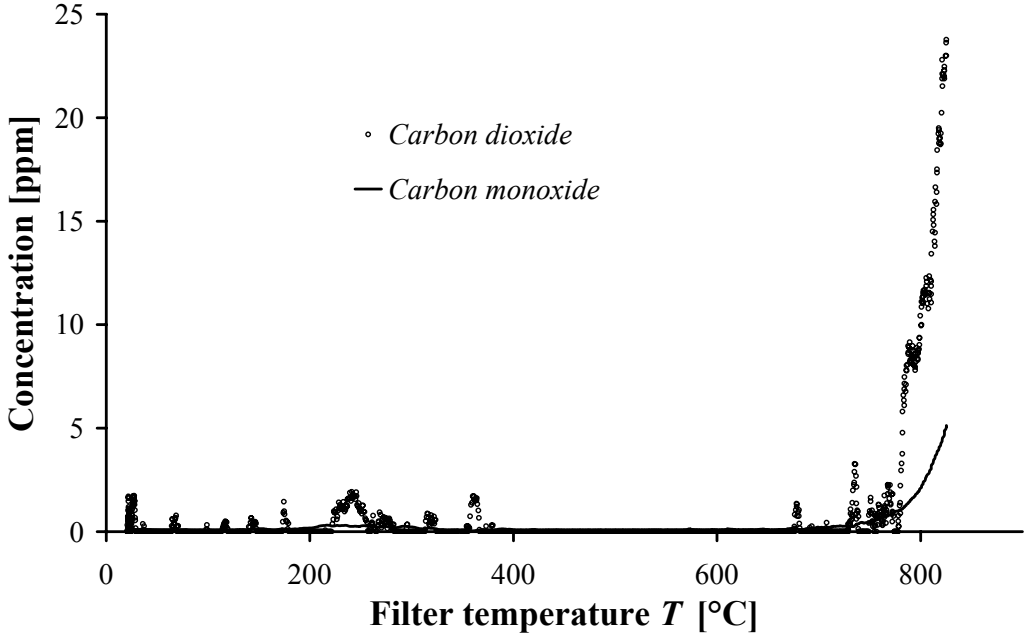

Figure 3.13: CO and CO_2 emitted from the reactor under a 10% O_2 atmosphere (4 l/min flow, 2 A/min ramp)

The reactor begins to emit some CO and CO_2 at about 750°C. This emission could be due to the carbon sealing. Indeed, the rector chamber temperature reaches about 200°C at a 750°C filter temperature. Thus the sealing temperature, which increases also with the filter temperature, can provoke CO and CO_2 emissions. However, the concentrations emitted are very low and do not exceed 5 ppm CO and 15 ppm CO_2 at 800°C. This will be considered negligible in regards to the 100 - 500 ppm concentrations CO and CO_2 emitted during the soot oxidation. Furthermore, the majority of experiments do not exceed the temperature of 750°C.

The same experiment was performed with two different CO concentrations at the reactor inlet. The aim is to verify that the reactor and the filter themselves do not catalyze the CO to CO_2 oxidation. The thermodynamic equilibrium of this reaction was first calculated as reference. The CO oxidation reaction was considered (Equation 3.13). The equilibrium constant K can be written as a function of the gas partial pressures p_{CO_2}, p_{CO}, and p_{O_2}, and the relative pressure P inside the reactor (Equation 3.14). At the thermodynamic equilibrium, the equilibrium constant can be related to the standard free enthalpy of the reaction $\Delta_r G^0$ (Equation 3.15). This last one can be calculated knowing the standard free enthalpy of formation $\Delta_f G^0$ of each species involved in the reaction (Equation 3.16). The $\Delta_f G^0$ are given in thermodynamic tables as a function of the temperature (see in Appendix B). Thus for fixed O_2 and CO concentrations, the partial pressure in CO_2 as a function of the temperature can be calculated with the Equation 3.17.

$$2CO + O_2 \rightarrow 2CO_2 \tag{3.13}$$

$$K = \frac{P\, {p_{CO_2}}^2}{{p_{CO}}^2\, p_{O_2}} \tag{3.14}$$

$$ln(K) = -\frac{\Delta_r G^0}{RT} \tag{3.15}$$

$$\Delta_r G^0 = -2\Delta_f G^0(CO_2) + 2\Delta_f G^0(CO) + \Delta_f G^0(O_2) \tag{3.16}$$

$$p_{CO_2} = \left(\frac{{p_{CO}}^2\, p_{O_2}}{P}\, exp\left(-\frac{\Delta_r G^0}{RT}\right)\right)^{\frac{1}{2}} \tag{3.17}$$

Two temperature ramps (2 A/min) were performed with 10% O_2 and 2000 and 500 ppm CO in N_2 respectively (4 l/min). The relative pressure P inside the reactor was supposed to be equal to 1. The CO_2 concentration at the reactor outlet was measured with the gas analyzer and compared with the one obtained from thermodynamic equilibrium (see in Figure 3.14). For the whole temperature range, the

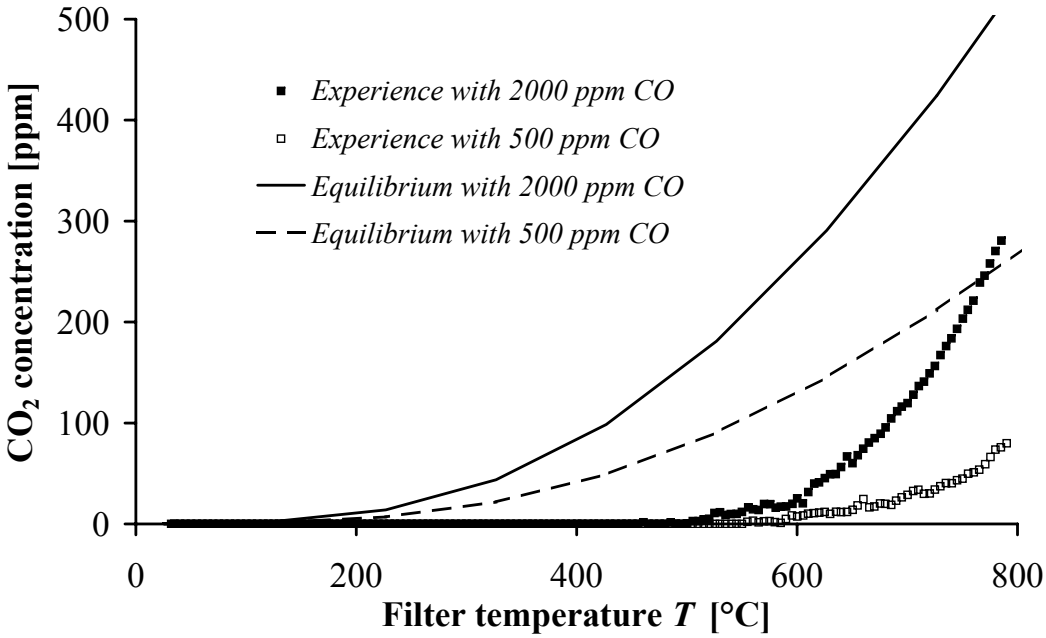

Figure 3.14: CO_2 concentration from the CO oxidation in a 10% O_2 and 500 or 2000 ppm CO in N_2 atmosphere (4 l/min flow, 2 A/min ramp)

CO_2 concentration measured by the reactor is inferior to the one reached by an equilibrium. The reaction 3.13 does not reach the equilibrium and is also not catalyzed by the reactor and/or the filter surface. The measured CO to CO_2 ratio will also be considered as the true ratio of primary reaction products.

3.2.2.3 Determination of the conversion curves from CO and CO_2 concentrations

Oxidation experiments in the reactor were conducted with the following conditions: a temperature ramp of about 10 K/min achieved by a current ramp of 2 A/min and a volumetric flow rate Q = 4 l/min with 10% O_2 in N_2. From the temperature measured with the infrared camera, it is possible to calculate the real temperature of the filter surface by the radiation model. From the CO and CO_2 concentrations, it is possible to calculate the momentary mass of dissipated carbon $m_{c,d}$ (Equations 3.18 and 3.19). Integrating the momentary mass $m_{c,d}$ for $i = 0$ to $i = n - 1$ gives the conversion at the time t_n (Equation 3.20). Thus, it is possible to plot the conversion as a function of temperature and obtain the conversion curve.

The reproducibility of the conversion curves was found to be $\pm$ 5 K at the temperature T_{50} (temperature achieved at the conversion 0.5). Figure 3.15 presents the

reproducibility of the oxidation of PrintexU soot. Three oxidations were performed at the same experimental conditions and an initial mass of soot of 10.2 ± 0.9 mg. The temperature T_{50} was found to be 635°C ± 2 K. The temperature difference at the end of the curve is due to the fact that the experiments with 9.4 mg was stopped 50°C sooner as the two other ones. This has no influence on the calculated T_{50} temperature.

$$m_{c,d} = ([CO] + [CO_2])\, Q\, \rho \tag{3.18}$$

$$m_{c,d} = ([CO] + [CO_2])\, Q\, \frac{PM}{RT} \tag{3.19}$$

$$X(t_n) = \sum_{i=0}^{n-1} \frac{m_{c,d,i} + m_{c,d,i+1}(t_{i+1} - t_i)}{m_{c,d,n}} \tag{3.20}$$

The conversion curves obtained here from experiments in the reactor can not be used to determine kinetic parameters. Indeed, the calculated soot temperature is only correct as long as soot is present on the filter. But at a certain time of the oxidation, there is no more soot on the filter, so that the filter surface under the soot layer appears. Then the emissivity to use in the radiation is no longer the soot emissivity ϵ_{soot} = 0.93 but the filter emissivity ϵ_{filter} = 0.81. Therefore, the calculated temperature is no more accurate. This emissivity difference can lead to a

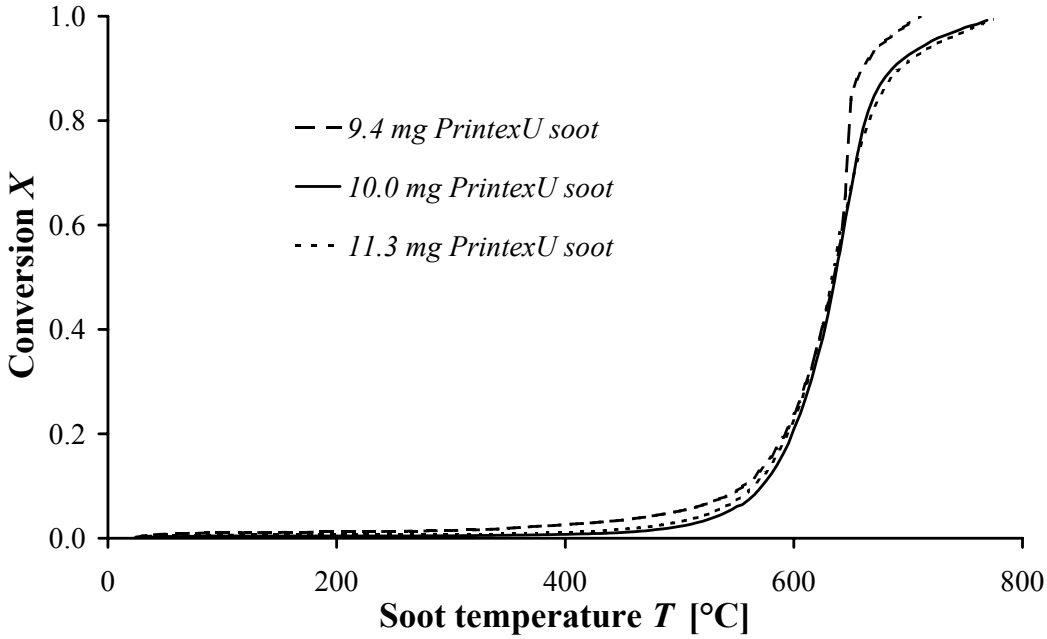

Figure 3.15: Reproducibility of the 10 mg PrintexU soot oxidation in reactor with 10% O_2 in N_2, 4 l/min and 2 A/min ramp)

large temperature difference: when a temperature of 750°C is calculated with ϵ_{soot}, then 795°C are calculated with ϵ_{filter}. Therefore, the end of the conversion curves should be theoretically shifted to higher temperatures.

As the evolution of the surface emissivity from ϵ_{soot} to ϵ_{filter} remains unknown, the soot temperature was calculated with ϵ_{soot} for the entire temperature range. But this temperature can not be used then to calculate kinetic parameters. The consequence is that the temperature difference ΔT_{50} = $T_{50,cat}$ - $T_{50,th}$ is used as the parameter to define the catalytic effect for oxidation performed in the reactor. The temperature difference ΔT_{50} is logarithmic proportional to the catalytic effect A = $k'_{0,cat}$ / $k'_{0,th}$. But it should be kept in mind that ΔT_{50} is related to the soot sources used and consequently, ΔT_{50} from different soot sources could not be compared with each other.

3.2.3 Comparison with TGA experiments

To compare experiments performed in the TGA device with the one performed inside the reactor, it is necessary to use similar experimental conditions. The PrintexU soot oxidation was studied in the two experimental equipments.

The mass of the soot sample used in the TGA and on the SMF inside the reactor was chosen to be the same and kept constant along this study to minimize the influence of mass transport and heat transfer limitations. In the case of periodic regeneration in diesel cars equipped with a diesel particle filter (DPF), soot loadings between 4 and 8 g soot per liter filter volume are generally required to start the oxidation. It corresponds to 25 to 50 mg soot on SMF sheets used in this thesis. However, a soot bed with high soot quantity promotes large heat transfer and mass transport in TGA. To reduce them, it is better to work with low soot quantities [15, 42]. A compromise with 10 mg soot sample (for both TGA and reactor experiments) was decided.

A temperature ramp of 10 K/min was chosen to perform the experiments in the TGA. For the reactor, it corresponds to a current ramp of 2A/min. For TGA, all experiments were performed under 20% O_2 in N_2 atmosphere and with 60 ml/min flow rate. This was dictated to be in accordance with previous studies. For the reactor, all experiments were performed under 10% O_2 in N_2 atmosphere and with 4 l/min flow rate. This corresponds to the real exhaust gas conditions. TGA and reactor experiments were thus performed with different oxygen concentration and flow rate. As long as mass transport and heat transfer limitations are negligible in

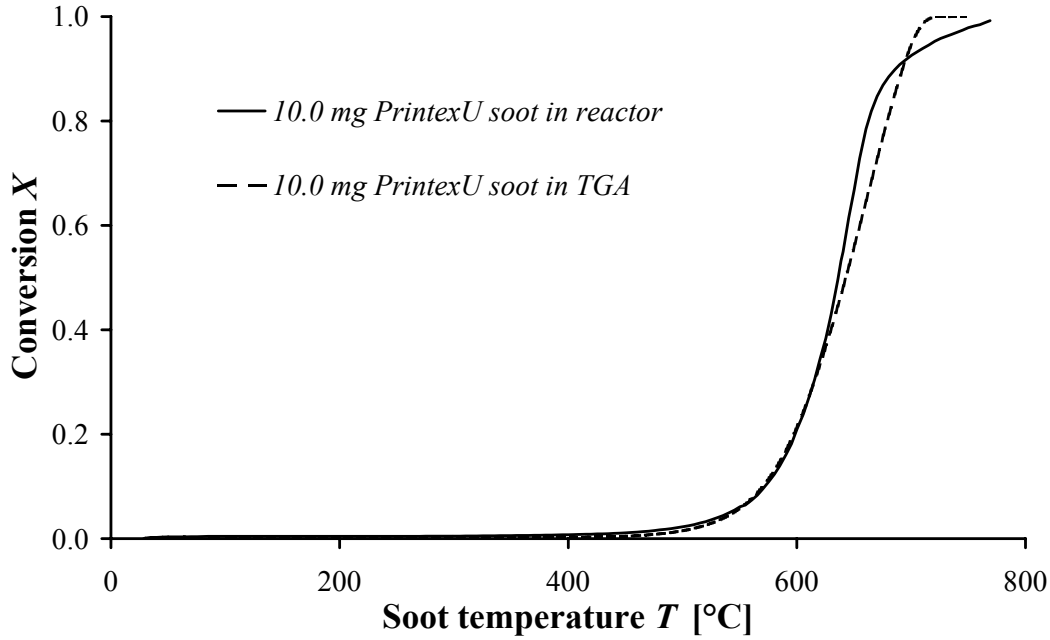

Figure 3.16: Comparison between the PrintexU soot oxidation in TGA with and in reactor (10 K/min, 10% O_2 in N_2)

the soot cake, the flow rate should not have any influence of the conversion curves. On the contrary, as shown in Chapter 1, the oxygen concentration plays a role in the oxidation rate. Thus, one experiment was performed in TGA with a 10% O_2 in N_2 atmosphere to compare it with a reactor experiment.

The conversion curves of the TGA and reactor experiment with 10 mg PrintexU soot, 10 K/min ramp, 10% O_2 in N_2 are plotted in Figure 3.16 (60 ml/min and 4 l/min flow rate, respectively). Until a conversion of about $X = 0.5$, both conversion curves have a similar shape. From $X = 0.5$, the conversion in the reactor is higher than the conversion in the TGA. This can be easily explained by the change of emissivity on the filter surface. Indeed, the soot temperature is calculated with the emissivity of the soot. At the end of the reaction, there is no more soot on the filter, and the real emissivity is the one of the filter. Thus, with the radiation model, the soot temperature is underestimated at high temperature.

Finally, experiments in the TGA or in the reactor give about the same temperature T_{50} (635°C for the reactor against 640°C for the TGA), but the radiation model does not allow to model the end of the conversion curve perfectly for the reactor. Thus, no kinetic parameters are calculated for the conversion curves obtained with reactor experiments. The temperature difference ΔT_{50} is used in this case as the parameter to define the catalytic effect within a soot source.

Chapter 4

Thermal soot oxidation

In order to investigate the catalytic soot oxidation by platinum, different soot sources were used along this work, as powder or as aerosols. So as to determine if the future results obtained for these different soot sources can be further applied in real diesel particle filters, it is essentially to compare their oxidation behavior with the one of a reference diesel soot. It was decided to examine in this chapter the influence of the soot structure and composition on the kinetic parameters of the thermal soot oxidation. Although no systematic trend was found, the soot presenting the closest conversion curve shape to the one of the reference diesel soot is also the one with the closest structure and composition parameters. Diesel soot characteristics were nevertheless observed to vary with diesel engine, so that all soot sources investigated can be used as a model for diesel soot.

4.1 Soot production, sampling and storage

Six different soot sources including two diesel soot sources were studied in this work. The production and sampling methods of these soot sources (as powder or as aerosol) are first exposed. Two soot sources were commercially available as powder and were transformed into the aerosol phase by atomizer (PrintexU and Vulcan soot). Two other ones were produced directly as aerosol with a spark discharge generator (SDG) or by pyrolyzing toluene. A diesel driven micro-cogenerator and a diesel engine were used to produce two diesel soot aerosols. The particle agglomerate size distribution was measured by a scanning mobility particle sizer (SMPS) for all soot produced directly as aerosol: spark discharge generator soot, pyrolysis soot and both diesel soot types. All soot can be collected by aerosol filtration on sintered metal filter (SMF) sheets. The storage conditions of the soot loaded sheets and of the soot powders are discussed in the second part of this section.

4.1.1 Synthetic soot in powder form: PrintexU and Vulcan

Two synthetic soot types supplied as powder were commercially available: PrintexU soot, a flame soot supplied by Degussa AG and Vulcan soot, an amorphous furnace carbon black supplied by DeNora.

To collect synthetic soot in powder form on a SMF sheet and oxidize them in the reactor, they first have to be transformed into the aerosol phase. An atomizer aerosol generator ATM 220 from Topas (see in Figure 4.1) was used to nebulize the soot suspended in a solution. The essential part of the aerosol generator is a stainless steel atomizer. It works as a two-stream nozzle based on the injection principle. The glass wall facing the nozzle outlet acts as a collision separator: large droplets return into the solution resulting in a defined particle size distributed aerosol. Compressed air is supplied through an HEPA-Filter to the atomizer. A pressure reducer controls the compressed air pressure (readable on a gauge), and thus the volumetric flow rate of the aerosol.

A solution of 1 g soot mixed with 30 ml water and 10 ml isopropanol was used. The solution was placed in an ultrasonic bath to achieve a good dispersion of the soot in the solution. The atomizer was operated with 4 bar, corresponding to a volumetric flow rate of about 4 l/min. The aerosol droplets were filtered through a SMF sheet. The SMF sheet was heated (ca. 120°C) during the filtration to remove the water and isopropanol. The filtered soot mass flow rate on a sheet was about 30 mg/h.

The soot structure, and consequently the soot oxidation behavior, can change during the suspension step. The aerosol generator was only used with PrintexU soot to compare experiments performed in the TGA device and in the reactor (Chapter 3).

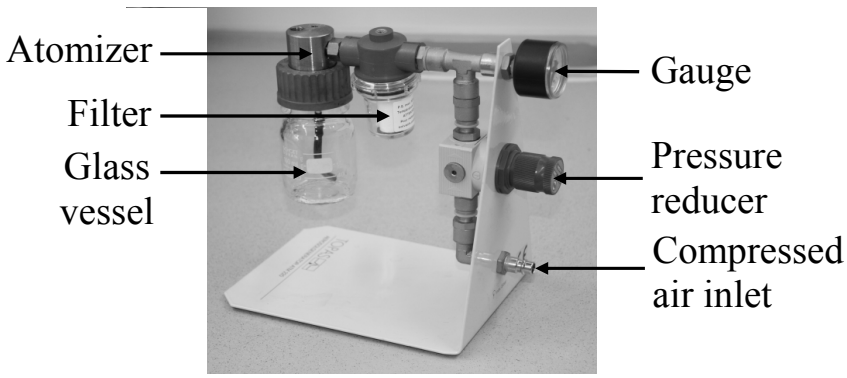

Figure 4.1: Photo of the aerosol generator ATM 220 from Topas

4.1.2 Spark discharge generator soot aerosol

Soot collecting experiments from a spark discharge generator (SDG) were performed at the Institut für Mechanische Verfahrenstechnik und Mechanik (IMVM) of the Universität Karlsruhe. A SDG was used to produce nano-particulate carbon aerosol by erosion and vaporization of two carbon electrodes in a spark discharge loop. The loop consists of two carbon electrodes, connected in parallel to one or more capacitors and a high voltage power supply (see in Figure 4.3). A carrier gas flows between the carbon electrodes, generating the aerosol.

The discharge was performed regularly with a 50 nF capacity, a distance of about 3 mm between electrodes and a capacitor charge current of 2 mA. Nitrogen was used as carrier gas through the electrodes with a volumetric flow rate of 10 l/min, leading to the production of a continuous carbon nano-particulate aerosol with a mass flow rate of about 4 mg/h. The particle agglomerate size distribution of the SDG soot aerosol was measured by a scanning mobility particle sizer (SMPS) and is represented in Figure 4.2. The mean mobility diameter was found to be about 70 nm. The volumetric flow rate through the SMF sheet during the soot collecting is controlled by a critical nozzle placed after the filter.

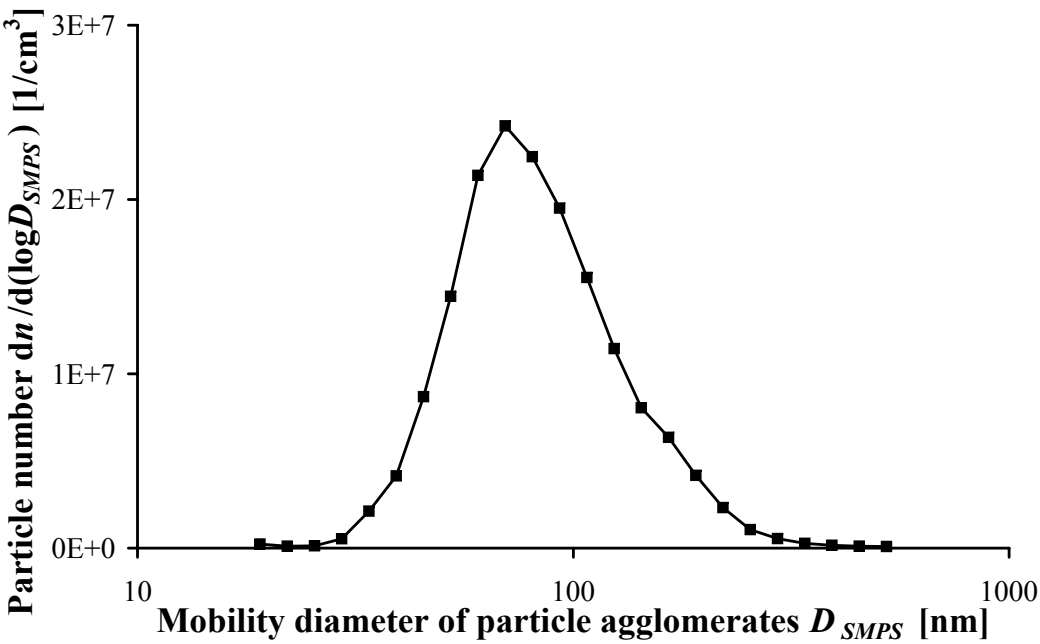

Figure 4.2: Size distribution of the particles agglomerate produced by a SDG (50 nF capacity, 10 l/min N_2)

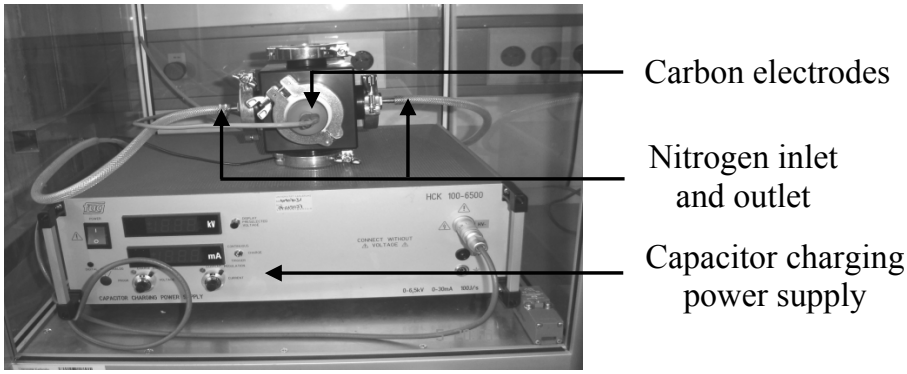

Figure 4.3: Photo of the SDG of the IMVM - Universität Karlsruhe

4.1.3 Pyrolysis soot aerosol

Pyrolysis soot was produced on a test bench at the institute for aerosol and sensor technology (IAST) of the university of applied sciences, Aargau in northwestern Switzerland. A high temperature furnace (1300°C) was used to synthesize soot by pyrolyzing a toluene aerosol. Argon was used as carrier gas and flowed through a toluene bubbler with a volumetric flow rate of 0.07 l/min. The resulting toluene droplet aerosol was first diluted with a 2.54 l/min flow rate of argon, and then led through the furnace. The furnace consists of a ceramic tube, where the toluene aerosol was pyrolyzed. With the test bench, a soot aerosol was produced with a mass flow of about 10 mg/h (see in Figure 4.4).

The soot aerosol was conducted through a diluter working with filtered air. The aerosol can be pumped directly (without any dilution) through an SMF sheet. The flow rate through the filter is controlled by a critical nozzle of 1.83 l/min. Alternatively, the aerosol can be diluted by the filtered air with a dilution ratio of 740, before conducting it through a scanning mobility particle sizer (SMPS). The particle agglomerate size distribution after dilution is plotted in Figure 4.5. The mean mobility diameter was found to be about 110 nm.

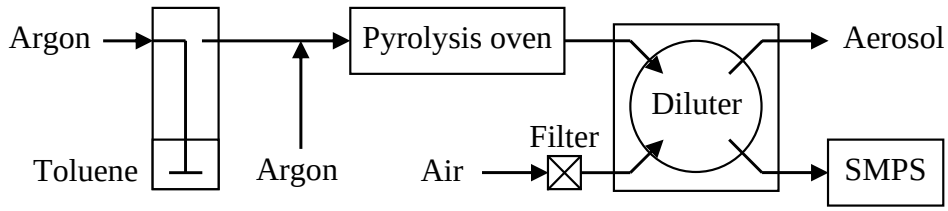

Figure 4.4: schematic representation of a pyrolysis oven

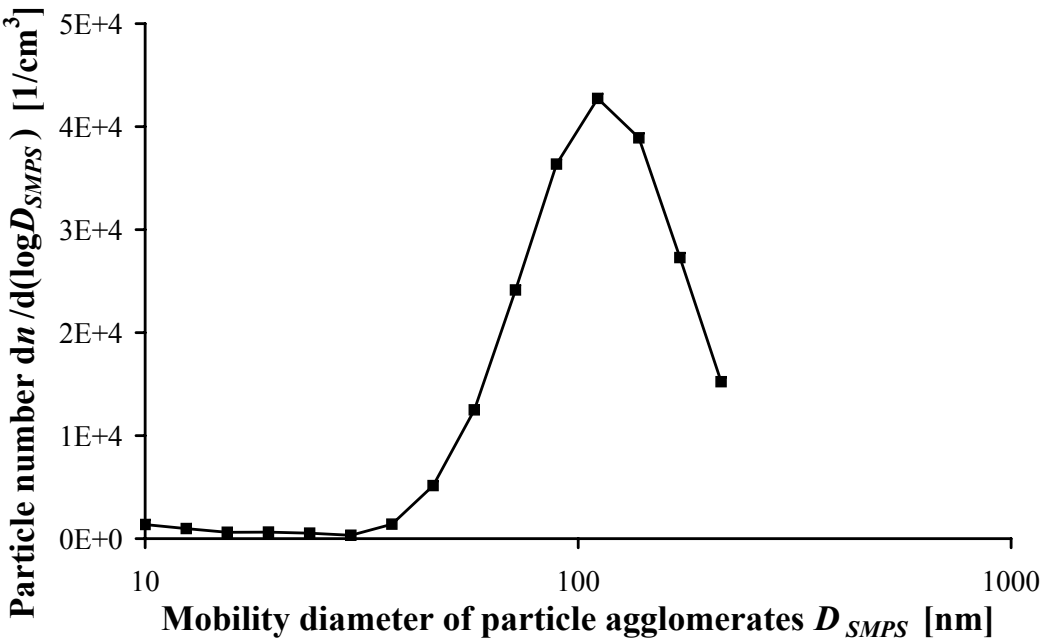

Figure 4.5: Size distribution of the particles agglomerate produced by pyrolyzing toluene

4.1.4 Diesel soot aerosols

A first diesel soot source was provided by a micro-cogenerator driven with a naturally aspirated direct injected diesel engine, commercially available by Senertec. In this study the engine was always operated at the maximal power of 6 kW to achieve dry soot (with few HC adsorbed on it) and high soot concentration in the exhaust. Sulfur-free diesel fuel was used (< 10 ppm). A part of the soot aerosol (10 l/min) was pumped from the main exhaust gas pipe with a mass flow of ca. 20 mg/h. The sampling was performed on heated SMF (about 120°C) to avoid the condensation of water vapor present in the exhaust (about 10%). The particle agglomerate size distribution was measured with a SMPS and an mobility mean diameter of 110 nm was found (Figure 4.6).

A second diesel soot source was provided from the section of industrial catalysis of the Delft university of technology in the Netherlands. A three cylinder Lister-Petter (LPW3) direct injected and water cooled diesel engine was used. The engine was operated at 75% load corresponding to 7.5 kW power, with low sulfur Shell V-power fuel (ca. 10 ppm S). Soot was collected by passing a part of the exhaust gas through a glass fiber filter until the back pressure reached 0.2 - 0.3 bar.

Both of these diesel soot sources do not necessary represent diesel soot emitted

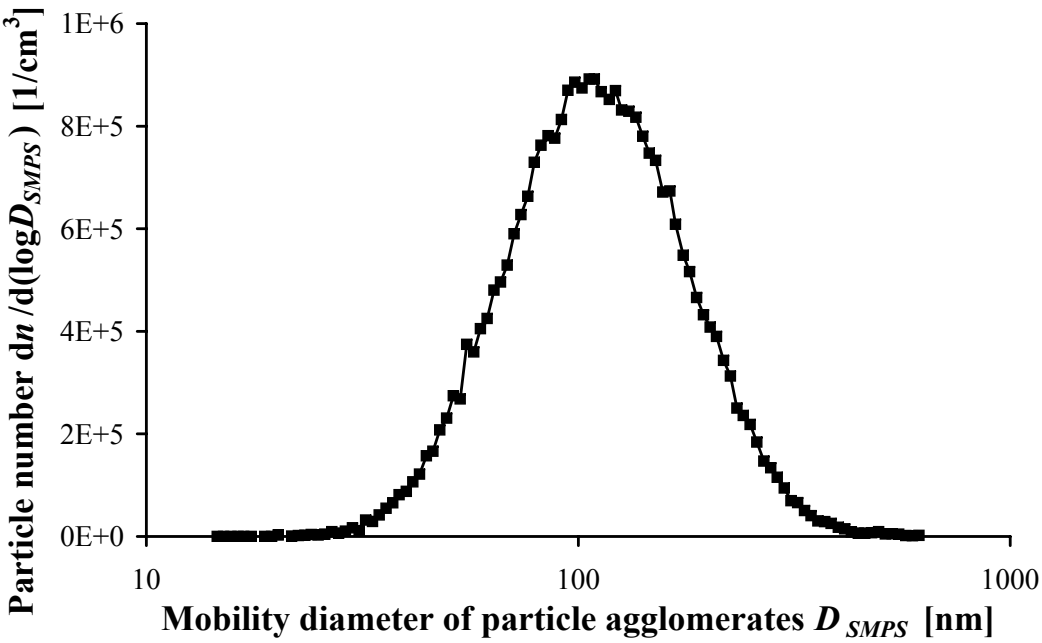

Figure 4.6: Size distribution of the particles agglomerate produced by a micro-generator by maximal power (6 kW)

from a modern engine. Furthermore, the soot composition and structure change with the operating conditions of the engine. But a reference diesel soot has to be defined for this study. In the following, the first diesel soot source provided by the micro-cogenerator is chosen as the representative one and is considered to be the reference diesel soot. The second diesel soot source is only considered as an alternative diesel soot source, and called LPW3 diesel soot.

4.1.5 Soot storage

After the soot was collected on SMF sheets, the filters were transferred and stored in closed vessel before oxidizing them in the reactor. If soot powder was needed (TGA experiments), soot would carefully be scraped off the filter, and then stored in a closed vessel, too. The commercially available PrintexU soot and Vulcan soot were already supplied as powders in closed vessels. Adsorption of oxygen or desorption of hydrocarbon can happen during storing and during transfer, due to the high porosity of soot. It was assumed that the equilibrium between adsorbed and desorbed species is reached after a short time and does not change anymore. Thus, it was decided to study the soot under the current room conditions, avoiding complicated storage and transfer problems to the different soot analysis.

4.2 Soot characterization

Soot was characterized in terms of composition and structure. Soot powder was sampled and submitted to various analysis methods. The soot composition was characterized by elemental analysis (EA) for carbon, hydrogen, nitrogen, oxygen and sulfur. The soot structure was determined by the BET surface area (following the method of Brunauner, Emmet and Teller), and the soot primary particle size was measured by transmission electron microscopy (TEM). For soot produced as aerosol the mean mobility diameter was measured by scanning mobility particle sizer (SMPS). This knowledge should help to understand the oxidation properties of the different soot sources and find the soot that models diesel soot the best.

4.2.1 Soot composition

The six soot sources were characterized by their elemental composition, their surface area and their structure. The elemental analysis was performed following the ASTM D 5291 standard method for carbon, hydrogen, nitrogen and oxygen, and the DIN EN ISO 20884 standard method for sulfur. Analysis results are grouped in Table 4.1. The unaccounted-for mass (less than 0.1 wt%) is probably silicon, aluminium and metals [15]. The bulk density of soot was calculated from the measured elemental composition, without taking into account the rest of mass.

Table 4.1: Characterization of the composition of different soot sources

Soot	PrintexU	Vulcan	SDG	pyrolysis	ref. diesel	LPW3 diesel
C [wt%]	96.0	99.0	86.7	96.5	90.9	94
H [wt%]	0.7	0.1	0.6	1.4	1.4	1.3
N [wt%]	0.5	0.1	8.0	<0.1	0.9	1.8
O [wt%]	2.4	0.2	4.5	1.9	6.6	2.6
S [wt%]	0.293	0.530	0.129	0.010	0.121	0.200
rest [wt%]	0.11	0.07	0.07	0.09	0.08	0.10
ρ [g/cm^3]	2.182	2.255	1.968	2.188	2.063	2.135

The reference diesel soot was found to be composed of about 91 wt% carbon, and a non negligible oxygen fraction (6.6 wt%). Such high oxygen fraction was already found elsewhere [54], where fourier transform infrared spectroscopy (FTIR) analysis revealed strongly bonded oxygen in form of C=O, C-O-C, C-O-H and some aromatic structures. Hydrogen (1.4 wt%) is certainly present in form of adsorbed

hydrocarbons. But as the motor was run with its maximal power, soot is expected to contain only a small content of hydrocarbons. More than 1000 ppm sulfur were found, probably originating from lubricating oil. Traces of nitrogen were also measured. LPW3 diesel soot differs form the reference diesel soot by a lower oxygen fraction (2.6 wt%), and consequently an higher carbon fraction (94 wt%).

Both synthetic soot sources, PrintexU and Vulcan, were found to have higher amount of carbon (96 and 99 wt%, respectively) and higher amount of sulfur (ca. 3000 and 5000 ppm, respectively) than diesel soot. Vulcan soot is a high pure carbon, but PrintexU soot contains some traces of hydrogen and nitrogen, and also some oxygen (2.4 wt%). SDG soot has a specific composition with a lower amount of carbon compared to diesel soot (only 87 wt%). This is compensated by a high amount of nitrogen (8 wt%) and also some oxygen (4.5 wt%). Nitrogen found in SDG soot is probably present as adsorbed species during the production or the storage. Pyrolysis soot was found to have an higher amount of carbon than diesel soot (97 wt%), but the lowest sulfur amount of all soot sources (100 ppm, close to the resolution limit of the apparatus). The hydrogen amount (1.4 wt%) revealed the presence of some adsorbed hydrocarbons on pyrolysis soot.

From the composition point of view, PrintexU soot and pyrolysis soot are the closest to the reference diesel soot. Vulcan soot shows a very high carbon and sulfur fraction, and SDG soot high oxygen and nitrogen fractions.

4.2.2 Soot structure

Three different methods were used to characterize the soot structure. The surface area was determined by the BET method (Brunauer, Emmet and Teller). The soot was first preheated three hours at 300°C. Then the adsorption isotherm was performed with nitrogen at 77 K. TEM micrographs were performed on a Phillips CM12 working at 120 kV. The soot powder was deposited with a pincer on a SiO_2 frit. Using a Gatan multiscan camera 600HP allows a maximal magnification of 750,000 with a maximal resolution of 0.1 nm. The soot mean primary particle diameter d_{TEM} and the standard deviation δ_{TEM} were calculated from 50 to 100 measurements on micrographs. The specific surface area S_{TEM} was calculated from the real size distribution measured on micrographs and the soot bulk density ρ. The mean mobility diameter of the particle agglomerate D_{SMPS} determined by SMPS was also indicated for soot produced as aerosol. All the results are presented in Table 4.2, and a micrograph for each soot source is shown in Figure 4.7.

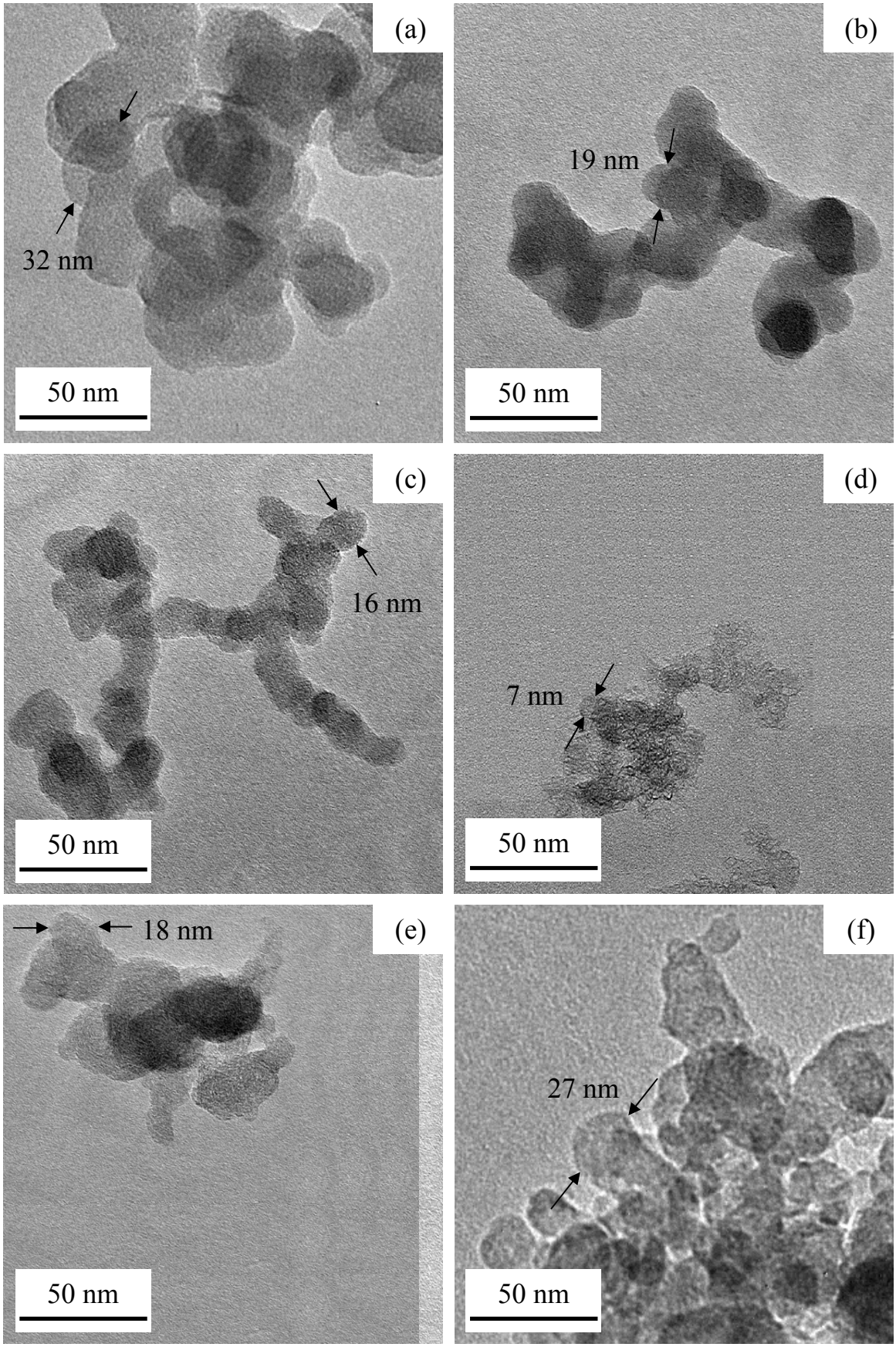

Figure 4.7: TEM images of PrintexU soot (a), Vulcan soot (b), pyrolysis soot (c), SDG soot (d), reference diesel soot (e) and LPW3 diesel soot (f)

Table 4.2: Characterization of the structure of different soot sources

Soot	PrintexU	Vulcan	SDG	pyrolysis	ref. diesel	LPW3 diesel
d_{TEM} [nm]	32	19	7	16	18	27
δ_{TEM} [nm]	8	4	2	3	5	10
S_{TEM} [m^2/g]	87	149	472	175	171	121
S_{BET} [m^2/g]	99	235	699	142	158	114
D_{SMPS} [nm]	-	-	70	110	110	-

The reference diesel soot aerosol was found to form agglomerates with a mean mobility diameter of 110 nm (measured by SMPS). Agglomerates contain primary particles of about 18 nm mean diameter (measured on micrographs). LPW3 diesel soot differs from the reference diesel soot by a higher primary particle size (27 nm mean diameter). PrintexU and Vulcan soot were found to be composed of primary particles of 32 nm and 19 nm mean diameter, respectively. Soot produced by the SDG form agglomerates of 70 nm mean mobility diameter. The primary particles measured by TEM were found to be very small (7 nm mean diameter). Such a small structure was already observed for SDG soot [55, 56]. Pyrolysis soot was found to have a similar particle agglomerate size distribution and similar primary particles (16 nm mean diameter) as the reference diesel soot.

The specific surface area calculated from the real size distribution obtained from TEM micrographs is 472 m^2/g for SDG soot. When compared with the measured BET surface area of 699 m^2/g, it suggests that some internal pore area is present. The same effect was observed for Vulcan soot. The BET surface area was found to be lower than the specific surface area obtained from TEM for the reference diesel soot and pyrolysis soot. It suggests that the agglomerate compactness masks the eventual presence of an internal pore area. For PrintexU and LPW3 diesel soot, the two methods exhibit comparable specific surface area.

Vulcan soot and pyrolysis soot present the closest structure to the one of the reference diesel soot. SDG soot exhibits very small agglomerates and primary particles.

4.3 Thermal soot oxidation in a TGA device

The thermal oxidation of the six soot sources was investigated in a TGA device. In a first part, the presence of adsorbed components on the soot surface is studied,

and the kinetic parameters of the thermal oxidation are calculated for each type of soot. Then, differences in soot oxidation behavior are discussed, according to the soot structure and composition, and the presence of adsorbed species. Pyrolysis soot was identified as the the best model for the reference diesel soot.

4.3.1 Presence of adsorbed species on soot

4.3.1.1 PrintexU and Vulcan soot

To detect the presence of any adsorbed species on the soot surface, the oxidation was performed in 20% O_2 ("normal"), and in 20% O_2 after a preheating ramp to 700°C (10 K/min) under N_2 ("preheated"). All other experimental conditions were identical: 60 ml/min flow and 10 mg soot sample. The PrintexU soot and Vulcan soot were first studied. As the normal and the preheated conversion curves do not present any difference, it was concluded, as expected, that no hydrocarbons or any other species were adsorbed on PrintexU and Vulcan soot (see in Figure 4.8).

The kinetic parameters obtained with the method of Slovak as explained in the previous chapter are summarized in Table 4.3. The modeled curves are also plotted

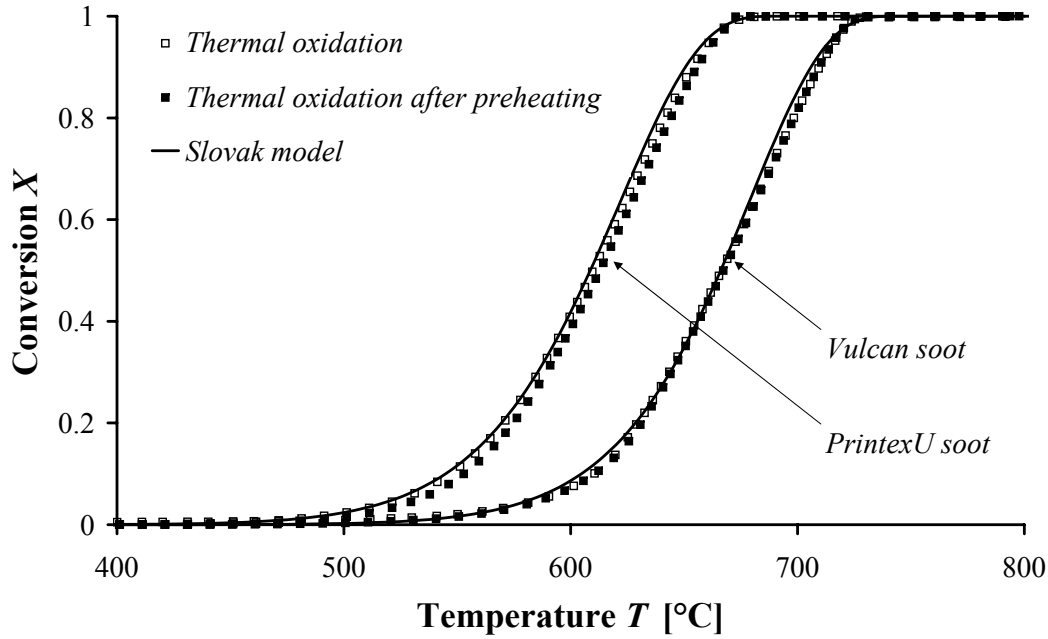

Figure 4.8: Conversion curve for PrintexU soot and Vulcan soot with or without a preheating ramp in N_2 (700°C), and corresponding Slovak model fits

Table 4.3: Kinetic parameters for the PrintexU and Vulcan soot thermal oxidation

Soot	m	k'_0 [1/s]	E_a [kJ/mol]	T_{50} [°C]
PrintexU	0.9	8.3×10^{6}	160	607
Vulcan	0.9	1.3×10^{8}	191	667

in Figure 4.8. The Vulcan soot oxidizes at higher temperatures than PrintexU. Both soot types show the same pseudo reaction order in carbon. The activation energies of PrintexU soot was already discussed in Chapter 2 and found to be in accordance with literature. For Vulcan soot, the activation energy was found to be 191 kJ/mol. This is comparable with literature where activation energies between 206 and 215 kJ/mol were reported for this type of soot [50]. The difference in activation energy between PrintexU soot and Vulcan soot is discussed in Section 4.3.2.

4.3.1.2 SDG soot

The presence of adsorbed species on SDG soot was also studied. A very distinct difference was found between the two conversion curves (Figure 4.9). From the sample mass difference before and after the preheating ramp, it was found that about 25 wt% of the soot desorbs in nitrogen. The kinetic analysis of Slovak is presented in Table 4.4 for these two curves. The direct oxidation of SDG soot could not be modeled properly with the Slovak model.

Species that desorb during the preheating ramp can not just be adsorbed hydrocarbons. Indeed, SDG soot is very porous and can adsorb more species than other soot sources, but such an amount of hydrocarbons is not present during the production method (just 0.6 wt% H was found in SDG soot). A better explanation would be that the oxygen present in the soot (4.5 wt%) oxidizes a part of the oxygen-bonded carbon atoms during the preheating ramp (C=O, C-O-C, C-O-H). The kinetic pa-

Table 4.4: Kinetic parameters for the SDG soot oxidation before and after preheating (700°C)

SDG soot	m	k'_0 [1/s]	E_a [kJ/mol]	T_{50} [°C]
normal	0	9.6×10^{-2}	36	600
preheated	0.3	5.2×10^{1}	78	614

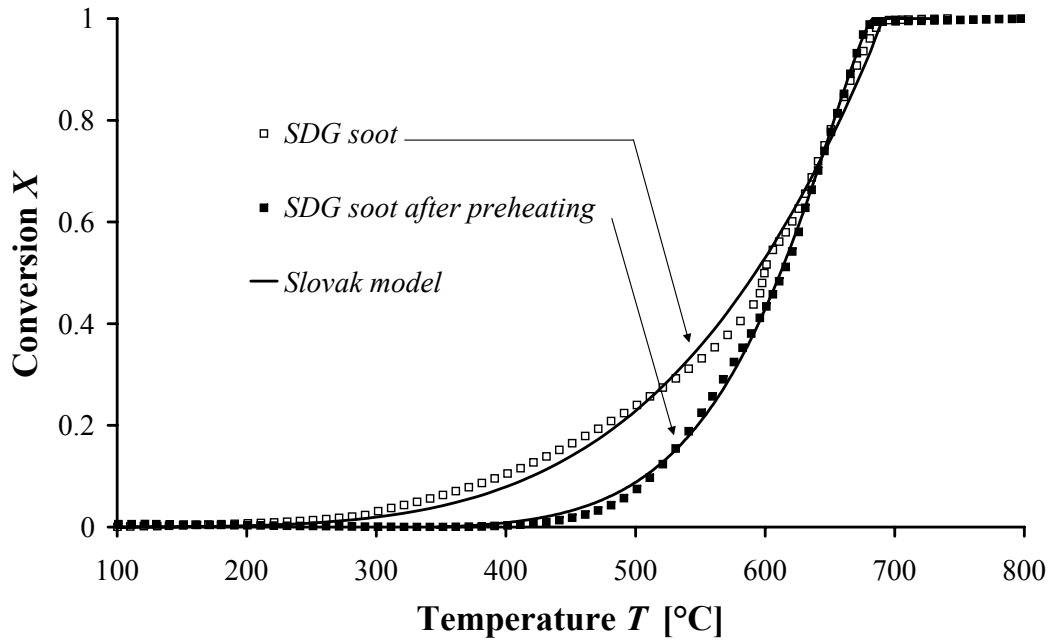

Figure 4.9: Conversion curve for SDG soot with or without a preheating ramp in N_2 (700°C), and corresponding Slovak model fits

rameters of the normal oxidation without preheating could not model the experiment very well. It can be supposed that oxygen-bonded carbon atoms oxidize with a different kinetic than the rest of soot, and affects the global oxidation kinetic that can not be consequently modeled with a global kinetic process.

The kinetic parameters after the preheating ramp are lower than the ones found for PrintexU and Vulcan soot. The activation energy is 78 kJ/mol. Using the model-free analysis of the Friedman method [57], Müller found an activation energy of 130 kJ/mol for the thermal oxidation of soot emitted from a spark discharge generator [56]. Otherwise, activation energy inferior to 100 kJ/nol were not reported in literature before for the thermal soot oxidation [15]. The application of the Slovak method to determine the kinetic parameters of the SDG soot oxidation is thus questionable. In the following, the catalytic effect of platinum on SDG soot is thus only determined by comparing the temperatures T_{50} of the thermal and the catalytic soot oxidation.

4.3.1.3 Pyrolysis soot

The presence of adsorbed species on pyrolysis soot was also studied. From the sample mass difference before and after the preheating ramp, it was found that

Table 4.5: Kinetic parameters of the pyrolysis soot oxidation before and after preheating (700°C)

Pyrolysis soot	m	k'_0 [1/s]	E_a [kJ/mol]	T_{50} [°C]
normal	0.8	1.1×10^6	140	575
preheated	0.8	1.4×10^7	159	584

about 5 wt% of the soot desorbed in nitrogen (Figure 4.10). The kinetic parameters obtained with the method of Slovak for the normal oxidation without preheating and for the oxidation after preheating are displayed in Table 4.5.

The presence of hydrocarbons (and consequently its desorption during the preheating) can possibly be justified by the relative high hydrogen composition (1.4 wt%) of pyrolysis soot. Their presence could be explained by an incomplete pyrolysis of toluene in the oven. The oxygen fraction present in pyrolysis soot is comparable with the one in PrintexU soot, and consequently probably too low to play a role during the preheating ramp. The contribution of any adsorbed species on pyrolysis soot is however very low regarding the oxidation reaction: the normal soot oxidation without preheating can be quite well modeled with the Slovak method.

The kinetic parameters k'_0 and E_a after the preheating ramp are higher than the ones for normal oxidation. This means that the oxidation of preheated pyrolysis soot happens at a higher activation energy than without it. This effect can be possibly due to a change in the soot surface state during the preheating ramp like a micropores closing. Or the hydrocarbons adsorbed on soot can liberate some heat during the normal oxidation, thus accelerating the carbon oxidation. The activation energy for the preheating oxidation was calculated to be 159 kJ/mol, which is included in the range 140 to 170 kJ/mol, that corresponds to most frequent values for various soot sources [15]. To avoid the contribution of the few adsorbed species, the catalytic effect of platinum on the pyrolysis soot is studied in the following after a preheating ramp.

4.3.1.4 Reference diesel soot

The reference diesel soot oxidation with and without a preheating ramp is presented in Figure 4.11. It was found experimentally that 18 wt% of soot had desorbed during the preheating ramp. Kinetic parameters of both conversion curves are displayed in Table 4.6.

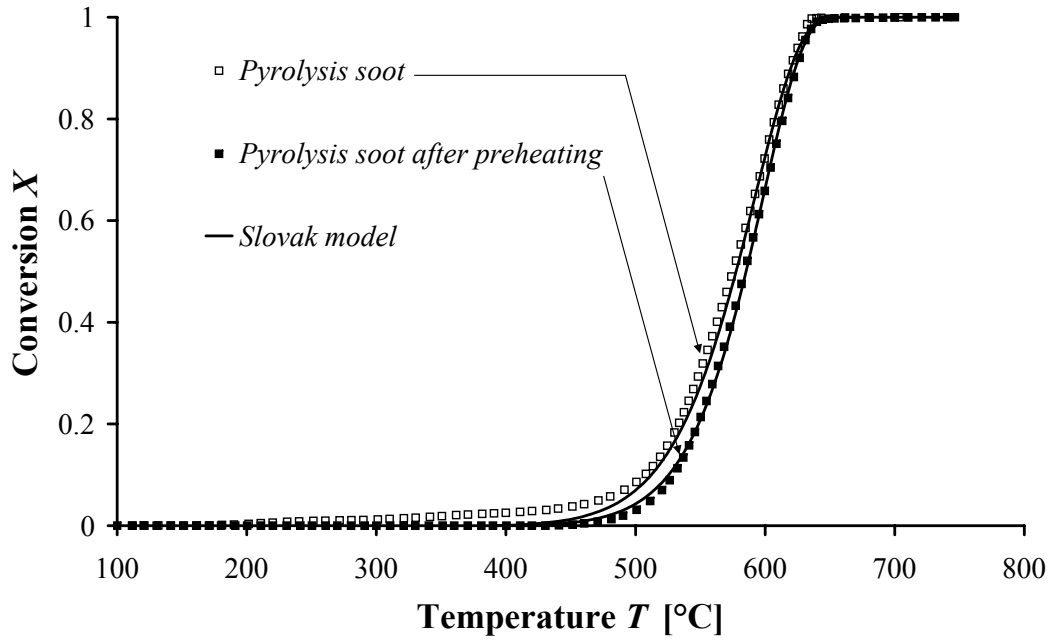

Figure 4.10: Conversion curve for pyrolysis soot with or without a preheating ramp in N_2 (700°C), and corresponding Slovak model fits

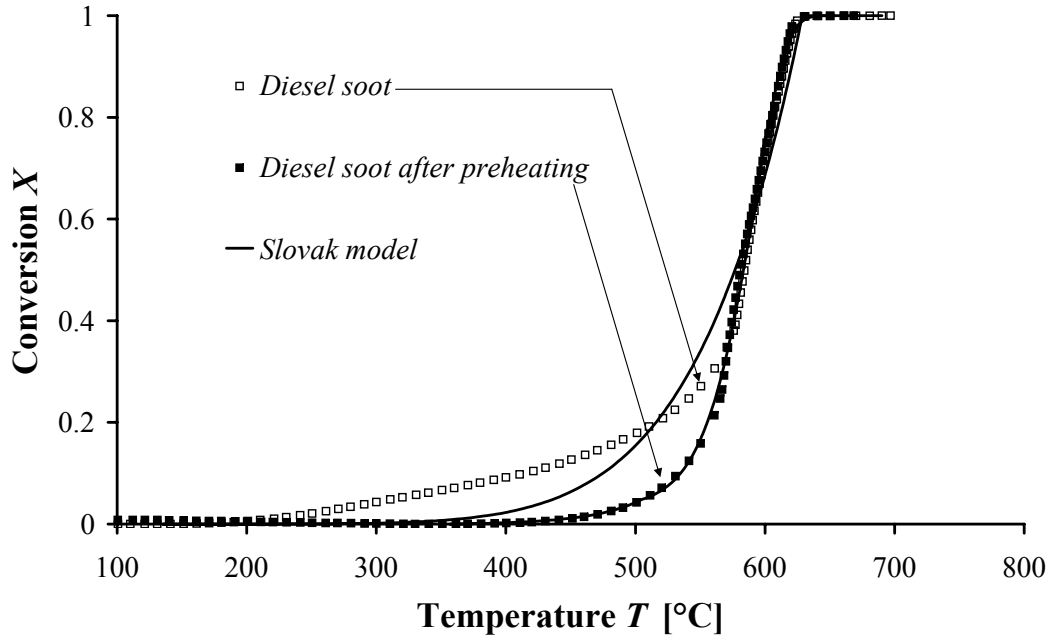

Figure 4.11: Conversion curves for the reference diesel soot with or without a preheating ramp in N_2 (700°C), and corresponding Slovak model fits

Table 4.6: Kinetic parameters for the reference diesel soot oxidation before and after preheating (700°C)

Diesel soot	m	k_0' [1/s]	E_a [kJ/mol]	T_{50} [°C]
normal	0	2.7×10^{1}	71	584
preheated	0.8	1.5×10^{10}	206	581

As it was the case for SDG soot, the normal oxidation of the reference diesel soot could not be modeled properly with a one step model. The desorption in N_2 can be likewise due to the desorption of adsorbed hydrocarbons and/or results of the oxidation of carbon atoms bonded to the oxygen present in the soot (6.6 wt%). It can thus be supposed that the oxidation of bonded carbon atoms affects the global oxidation behavior that can not be modeled as a one global kinetic process.

After a preheating ramp the activation energy is very high with 206 kJ/mol. It is at the upper boundary of the activation energies reported in literature for all soot sources (100 - 210 kJ/mol) [15]. As for SDG soot, the application of the Slovak method to determine the kinetic parameters of the reference diesel soot oxidation is questionable. However, this diesel soot type is in this work only used as reference soot and is not used to determine any catalytic effects.

4.3.1.5 LPW3 diesel soot

Figure 4.12 presents the conversion curves of the LPW3 diesel soot oxidation with and without a preheating ramp. The difference between the two curves can be explained by the presence of adsorbed species on LPW3 diesel soot. About 5 wt% of the soot was experimentally measured to desorb during the preheating ramp. The oxidation without preheating could not be modeled properly with the Slovak method (Table 4.7).

Table 4.7: Kinetic parameters for the LPW3 diesel soot oxidation before and after preheating (700°C)

LPW3 soot	m	k_0' [1/s]	E_a [kJ/mol]	T_{50} [°C]
normal	0	1.9×10^{2}	91	646
preheated	0.7	1.6×10^{7}	173	649

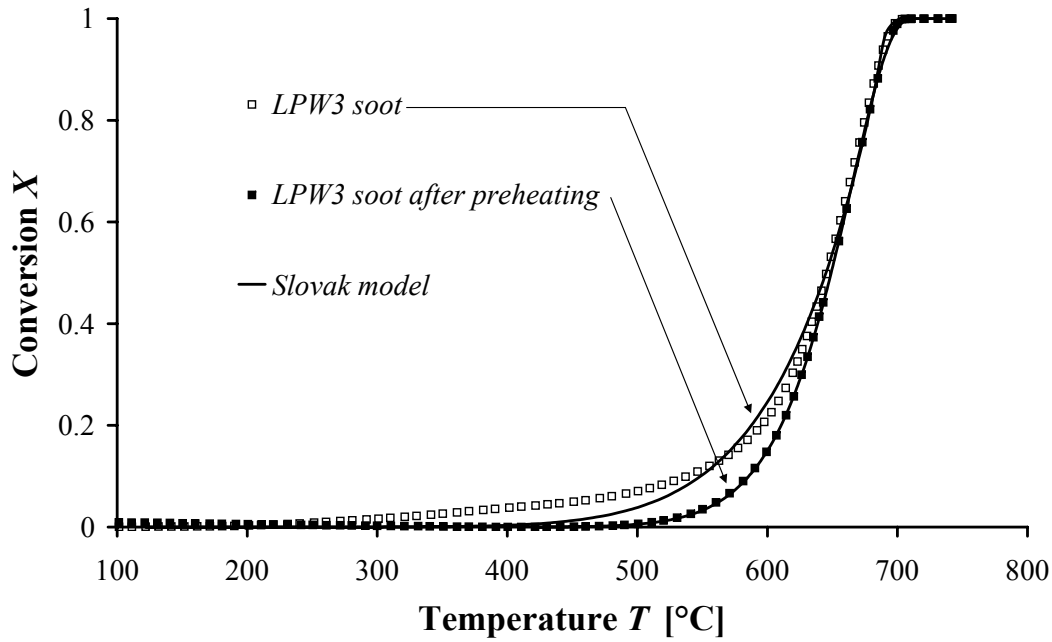

Figure 4.12: Conversion curves for LPW3 diesel soot with or without a preheating ramp in N_2 (700°C), and corresponding Slovak model fits

The desorption in N_2 is certainly due to the desorption of adsorbed hydrocarbons. As in the case of pyrolysis soot, the oxygen fraction is probably too low to affect the preheating. The activation energy for the oxidation after the preheating is 173 kJ/mol, which is comparable with literature [15]. Concerning the further investigation of the catalytic effect on the LPW3 soot oxidation, preheating ramp have to be performed to avoid the interaction of the desorption step.

4.3.1.6 Discussion

The presence of adsorbed species determines the shape of the conversion curve at low temperatures, and also whether a one-step kinetic model can be used. PrintexU soot and Vulcan soot do not contain any adsorbed species and could be modeled very well with the Slovak method in both cases.

Pyrolysis soot and LPW3 diesel soot contain a certain fraction of hydrocarbons. For pyrolysis soot, the fraction was so low that the normal oxidation could be quite well modeled with the Slovak method. The activation energy of the oxidation without preheating is lower than the one after preheating. A possible explanation is that the hydrocarbons adsorbed on soot can be oxidized during the normal oxidation liberating some heat and supporting the carbon oxidation. Another argumentation

is that the preheating affects the soot structure by closing micropores. The fraction of adsorbed species in LPW3 diesel soot was too high to applied the Slovak method on the normal oxidation (without preheating). In the following preheating ramps are performed for these two soot sources to avoid the influence of adsorbed species on the catalytic soot oxidation.

SDG soot and reference diesel soot also probably contain some adsorbed hydrocarbons, but not enough to explain the great part of soot that disappears during the preheating ramp. Both of them also contain a high fraction of oxygen. It was assumed that the carbon bonded to oxygen can be oxidized during the preheating (C=O, C-O-C, C-O-H and some aromatic structures). The normal oxidation could not be modeled with the Slovak method. Furthermore, the application of this method to determine the kinetic parameters of the oxidation after a preheating is also questionable. A very low activation energy was calculated for SDG soot, and a high activation energy was calculated for the reference diesel soot [15]. Performing isotherm experiments could help to determine the validity of the calculated kinetic parameters. In the following, to study the catalytic effect of platinum on SDG soot, only the temperature T_{50} is considered. Regarding the presence of adsorbed species, SDG is the soot that models the reference diesel soot the best.

4.3.2 Differences between synthetic and diesel soot

The oxidation behavior of the six soot sources are compared with each other after removing any adsorbed species, according to the soot structure and composition. Conversion curves of the thermal oxidation after a preheating to 700°C are summarized in Figure 4.13. The corresponding kinetic parameters from the Slovak model are summed up in Table 4.8. The temperature T_{50} indicates the position of the conversion curve relatively to the temperature axis. The activation energy E_a gives an

Table 4.8: Kinetic parameters for the six soot sources after preheating to 700°C

Soot	m	k'_0 [1/s]	E_a [kJ/mol]	T_{50} [°C]
PrintexU	0.9	8.3×10^{6}	160	607
Vulcan	0.9	1.3×10^{8}	191	667
SDG	0.3	5.2×10^{1}	78	614
pyrolysis	0.8	1.4×10^{7}	159	584
ref. diesel	0.8	1.5×10^{10}	206	581
LPW3 diesel	0.7	1.6×10^{7}	173	649

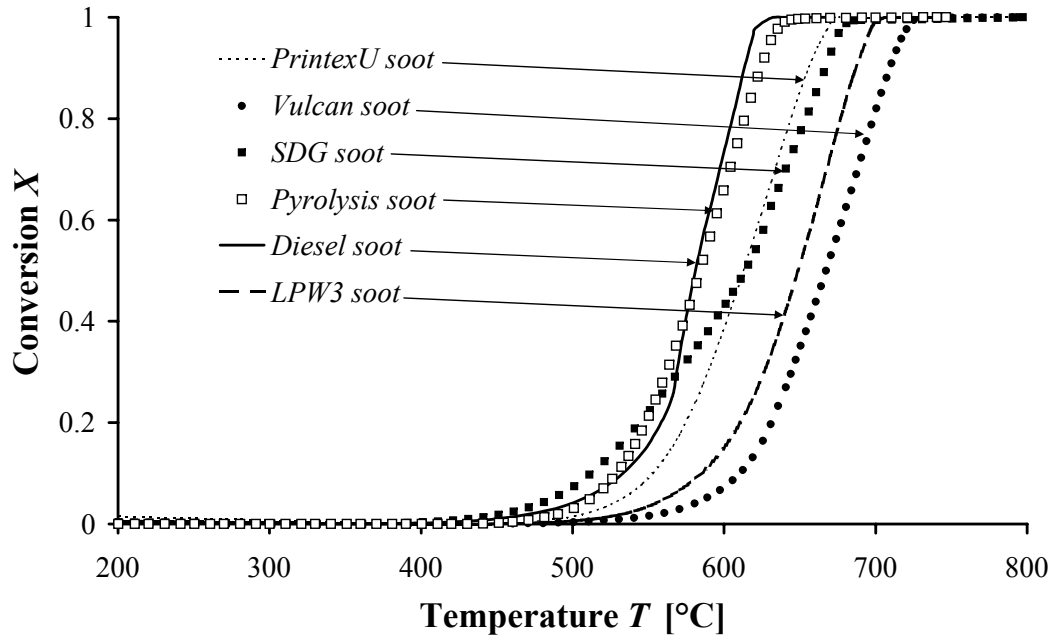

Figure 4.13: Conversion curves for the six soot sources after preheating to 700°C

information on the curve slope. A straight-forward dependence between the soot composition, the soot structure and the conversion curve shape parameters T_{50} and E_a could not be found.

It had been expected that soot with small primary particle diameter (determined on TEM micrographs) oxidizes at lower temperatures or with a lower activation energy. However, if SDG soot presents the lowest diameter and the lowest activation energy, it is not a systematic trend. Comparing two synthetic soot sources with each other, PrintexU soot and Vulcan soot, Vulcan soot presents the lower diameter, and also the higher temperature T_{50} and activation energy E_a. The structure is thus not the only parameter controlling the oxidation. Regarding the soot composition, Vulcan soot presents the highest carbon fraction, and the highest temperature T_{50}. It could be expected that soot without impurities oxidizes at higher temperatures or with a higher activation energy than soot containing impurities. However, this is also not a systematic trend. Comparing pyrolysis soot with LPW3 diesel soot gives a contra-example. Pyrolysis soot presents the higher carbon fraction but lower energy of activation and temperature T_{50}. No systematic trend regarding the influence of the soot structure and composition on the conversion curves shape was found. However, both of them play a certain role on it. Indeed, the soot presenting the closest conversion curve shape to the one of the reference diesel soot is the pyrolysis soot. Pyrolysis soot is also the only soot that presents both structure and composition parameters close to the reference diesel soot.

It was discussed that not only the soot structure, but also the soot nanostructure (length and curvature of the graphene segments in the soot primary particles) determines the soot oxidation [58]. It was found that soot presenting fullerene like structures such as SDG soot oxidizes at lower temperatures than well-graphitized soot [55, 56]. As Vulcan soot is an amorphous furnace carbon black, it is presumably more graphitized than the flame soot PrintexU for example, and it could explain why Vulcan soot oxidizes at high temperatures. The difference between the reference diesel soot and LPW3 diesel soot - two soot sources produced by diesel engines - can not be explained yet. The reference diesel soot was produced on a recent engine (2004) and LPW3 diesel soot on an old one (1996). It was argued that soot emitted from recent engines that fulfill the Euro 4 standard presents a more fullerene like nanostructure than soot emitted from old engines [55, 56]. This could explain why the LPW3 diesel soot oxidizes at higher temperatures than the reference diesel soot.

From the actual soot comparison, it can be concluded that pyrolysis soot models the reference diesel soot the best from a structure and an elemental composition point of view. Considering the presence of adsorbed species, SDG soot models the reference diesel soot the best. However, excepting Vulcan soot, all synthetic soot types (PrintexU, SDG and pyrolysis) present conversion curves comprised between the ones of the two diesel soot types (the reference diesel soot and LPW3 diesel soot). The shape of the conversion curve for Vulcan soot is additionally very closed to the one of LPW3 diesel soot, displaying a temperature shift lower as 20 K. It is consequently assumed that all the future results obtained on the synthetic soot types could be applied on real diesel soot.

Chapter 5

Catalytic soot oxidation by platinum using established DPF technologies

The aim of this chapter is to investigate the catalytic effect of platinum on the oxidation of diesel soot (LPW3 and reference diesel soot), using two established diesel particle filter (DPF) technologies: a fuel borne platinum catalyst (FBC) and a platinum coated sintered metal filter (SMF). The catalytic effect of the platinum FBC was investigated by thermogravimetric analysis (TGA), and observed to increase with the platinum quantity in the soot. This dependence will be discussed in more details in Chapter 6. The catalytic effect of the platinum coated SMF was investigated in the reactor presented in Chapter 3. An intermediate fibre supporting the platinum catalyst was applied onto the SMF. The fibre itself played a positive role on the soot oxidation but the platinum did not exhibit any catalytic effect, even with very high platinum quantities. The contact between platinum and soot particles was presumably too small, so that the possibility to achieve the same catalytic effect on a coated filter as using a FBC will be investigated in Chapter 7.

5.1 Fuel Borne Catalyst

In this part, the catalytic effect of a platinum FBC is investigated. Platinum-doped soot produced with different FBC concentrations was sampled from the LPW3 diesel engine and characterized by elemental analysis and TEM micrographs. This allows the determination of platinum quantity, location (in the soot agglomerate or on the soot surface), and particle size. The catalytic effect of the sample was determined from conversion curves obtained by TGA experiments. The catalytic effect was determined as $A = k'_{0,cat} \ / \ k'_{0,th}$, as defined in Chapter 2. Over the studied range, the catalytic effect increases with the total platinum quantity. However, due

to the sample characteristics, no conclusion concerning the form of this increase, the influence of the platinum particle size and influence of the platinum location could be made. This will be investigated in Chapter 6.

5.1.1 Production and characterization of platinum-doped soot

The preparation of the platinum-doped samples is first presented. The characterization methods used to determine the platinum quantity, the platinum location and the platinum particle size are briefly exposed and their results are discussed.

5.1.1.1 Production on an LPW3 diesel engine

The platinum-doped LPW3 soot samples were all produced and collected at the section of industrial catalysis of the Delft university of technology in the Netherlands. They originated from a platinum additive in the fuel of the LPW3 diesel engine. The LPW3 engine was already described in the Chapter 4. The engine was operated at 75% load. The platinum additive "Platinum Plus 3100SC" containing 2 wt% platinum was supplied by Clean Diesel Technologies, Inc. Shell V-power fuel with low sulfur content was used.

The standard procedure consists in homogeneously mixing the platinum additive with the fuel to achieve concentrations of 10, 20 and 50 ppm Pt in fuel. For each additive concentration, the engine was first operated on the new concentration for at least 24 h to prevent substantial memory effects. The engine exhaust pipe and the filter holder were cleaned before operating the engine again and beginning the soot sampling. When the back pressure reaches 200 - 300 hPa across the glass fibre filter, the soot was scraped off and stored in a bottle. From previous experiments performed at Delft, the emission factor (soot emission to fuel consumption ratio) is known to be rather high with 3.5×10^{-3}. Assuming that 50 wt% of the platinum recovered in the collected soot [59, 60], platinum-to-soot mass ratio (mg platinum / mg soot) of 0.0014, 0.0027 and 0.0068 are attended in the collected soot sample.

5.1.1.2 Characterization of the platinum quantity, location and particle size

The platinum quantity and the platinum location in the soot agglomerate or on the soot surface were both determined by elemental analysis (EA). Two different

Table 5.1: Platinum quantity and location in the platinum-doped soot

Pt in fuel	[ppm Pt in fuel]	10	20	50
expected Pt quantity	[mg Pt / mg soot]	0.0014	0.0027	0.0068
total Pt quantity	[mg Pt / mg soot]	0.0020	0.0030	0.0070
accessible Pt quantity	[mg Pt / mg soot]	0.0008	0.0018	0.0048
ratio: accessible Pt / total Pt	[%]	40	60	70

preparation methods were used. The following experimental procedure was performed to measure the soot quantity on the soot surface. The platinum-doped soot samples were dispersed in aqua regia (a mixture of nitric and hydrochloric acids: HNO_3 + 3 HCl). The fraction of platinum which is present on the soot surface - and consequently accessible to the aqua regia - dissolves in the solution. Soot possibly containing some platinum particles trapped inside the agglomerate was removed from the solution by filtration. The platinum concentration in the solution was then analyzed through inductive coupled plasma optical emission spectroscopy (ICP-OES).

To measure the total platinum quantity present in soot, an alternative experimental procedure was performed. Soot was first oxidatively removed from the sample with a mixture of nitric and sulfuric acid. Then the residue was dispersed in aqua regia. Thus, all the platinum present on and in the soot was dissolved in the solution. The platinum concentration in the solution was again determined by ICP-OES.

The platinum quantities are displayed as the ratio between the platinum mass and the soot mass (mg Pt / mg soot). The total and accessible quantities of platinum present in the three soot samples are grouped in Table 5.1. The experimentally determined total platinum quantities are in good agreement with the expected ones. The fraction of accessible platinum (or platinum present on the soot surface) increases with the total platinum quantity.

The platinum size was measured on TEM micrographs. A micrograph for each sample is presented in Figure 5.1. The mean diameter and the standard deviation are summarized in Table 5.2. With this technique, no platinum was observed for the platinum-doped soot produced with 10 ppm platinum in fuel. Either the platinum particles were too small to be observed (< 1.5 nm), or they were very non-uniformly distributed on the TEM grid. For the two other samples, the highly contrasting platinum points are easy to identify. The platinum particle mean diameter was found to be 4 nm for the 20 ppm Pt in fuel sample and 9 nm for the 50 ppm Pt in fuel sample. The platinum particle size increases with the platinum quantity.

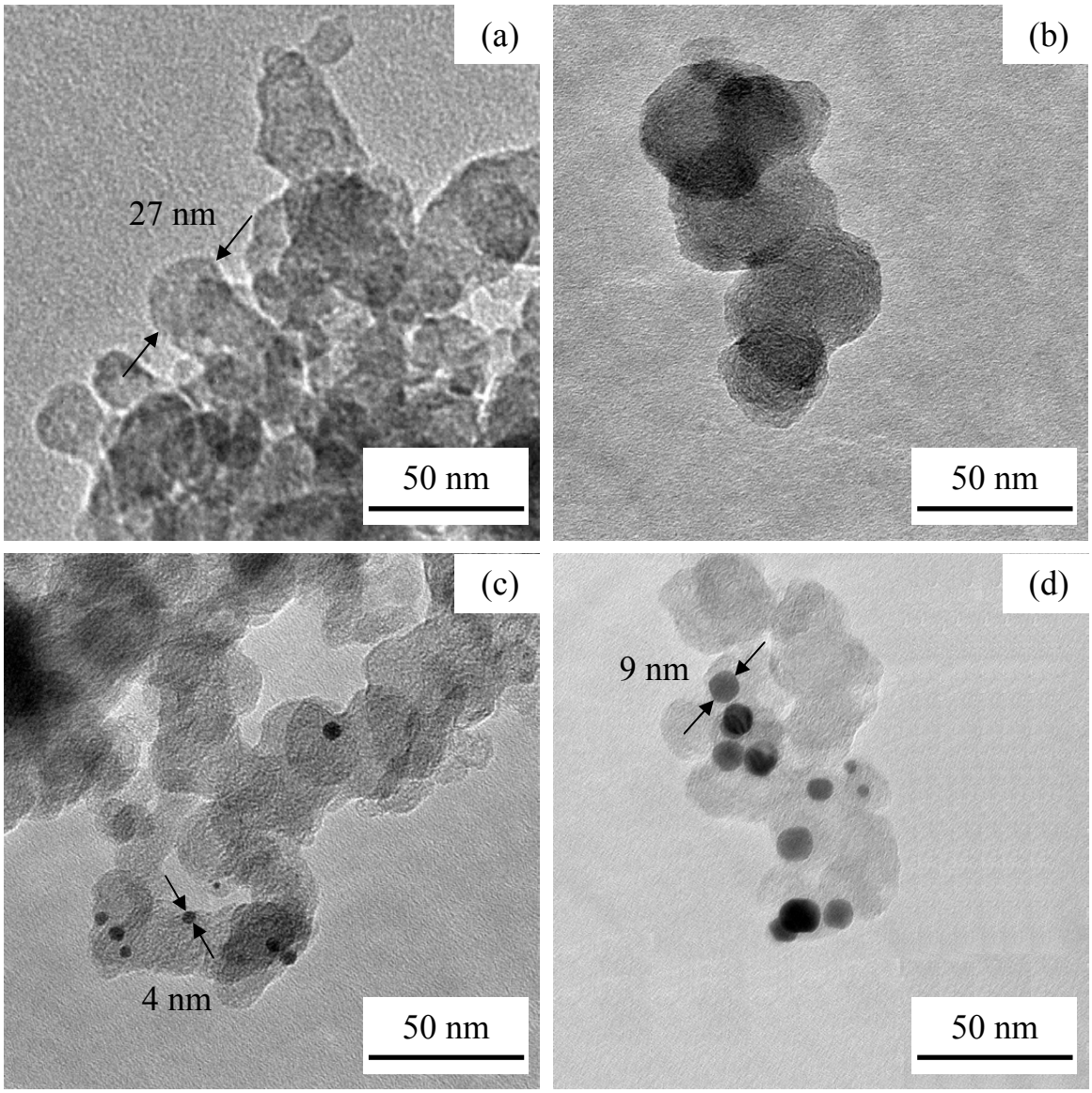

Figure 5.1: TEM image of plain LPW3 diesel soot (a), with 10 ppm additive in fuel (b), 20 ppm (c) and 50 ppm (d)

Table 5.2: Platinum particle size and surface area in the platinum-doped soot

Pt in fuel	[ppm Pt in fuel]	10	20	50
d_{TEM}	[nm]	-	4	9
σ_{TEM}	[nm]	-	1	3
$S_{TEM,total}$	[m^2 total Pt / g Pt]	-	70	31
$S_{TEM,total,soot}$	[m^2 total Pt / g soot]	-	0.21	0.22
$S_{TEM,accessible,soot}$	[m^2 accessible Pt / g soot]	-	0.13	0.15

As all the observed platinum particles on TEM micrographs had nearly circular shapes, it was assumed that the platinum was present as spherical particles. With this assumption, it is possible to calculate the total specific surface area of the platinum particles. This specific surface area can be related to the platinum mass or the soot mass. Knowing the fraction of accessible platinum, it is also possible to calculate the platinum accessible surface area related to the soot mass. These values are summarized in Table 5.2. The total and the accessible platinum surface areas are almost the same for the two samples.

5.1.2 Influence of the platinum quantity on the catalytic effect

The catalytic effect of platinum on the oxidation of LPW3 diesel soot was determined by performing ramp experiments in the TGA device. In Chapter 4, it was observed that LPW3 diesel soot contained some adsorbed species (probably hydrocarbons). To avoid complicating the analysis with the influence of the adsorbed hydrocarbons on the catalytic effect, it was decided to perform the oxidation ramp after eliminated these species during a preheating ramp in N_2 until 700°C. The experimental procedure consists thus in first heating a 10 mg sample in N_2 (60 ml/min, 10 K/min), and after cooling, performing the oxidation under a 20% O_2 in N_2 atmosphere (60 ml/min) with a ramp of 10 K/min. The conversion curves obtained for the plain LPW3 diesel soot and the three platinum-doped LPW3 diesel soot are represented in Figure 5.2.

The catalytic effect of each platinum-doped soot sample was calculated as explained in Chapter 2. The kinetic law was assumed to be governed by a pseudo reaction order model (PRO) (equations 5.1 and 5.2):

$$\frac{dX}{dt} = k'_0\, exp(-\frac{E_a}{RT})\,(1-X)^m \qquad [1/s] \qquad (5.1)$$

$$k'_0 = k_0\, {p_{O_2}}^{n_{O_2}} \qquad [1/s] \qquad (5.2)$$

The kinetic parameters m_{th}, $k'_{0,th}$ and $E_{a,th}$ of the plain LPW3 diesel soot thermal oxidation were first determined by the method of Slovak. Then, by assuming that $m_{cat} = m_{th}$ and $E_{a,cat} = E_{a,th}$, the pre-exponential factor $k'_{0,cat}$ is calculated for the catalytic oxidation of platinum-doped soot samples. The kinetic parameters are grouped in Table 5.3, and the modeled conversion in Figure 5.2.

The catalytic activity of a platinum fuel borne catalyst (FBC) was tested on an engine test bench by Jelles et al. [30]. They concluded that platinum does not present

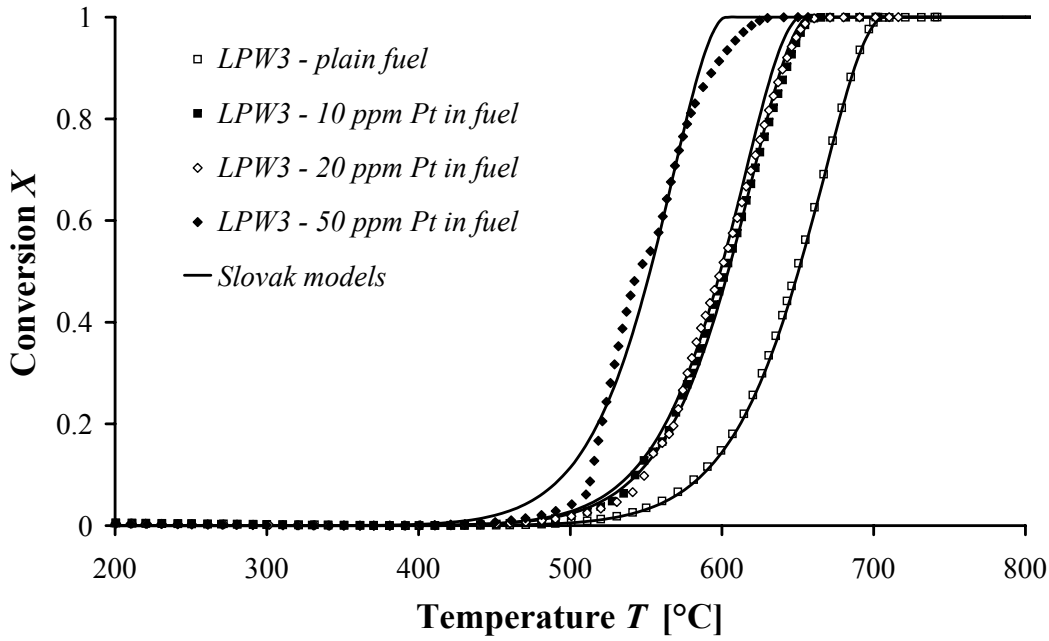

Figure 5.2: Conversion curves of the platinum-doped LPW3 diesel soot and corresponding Slovak model fits

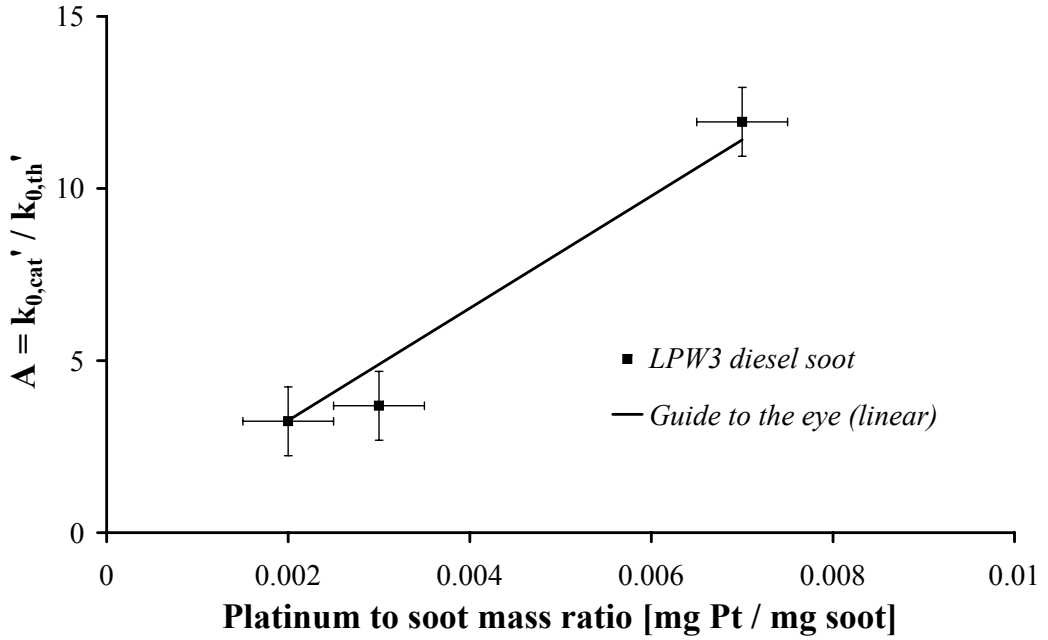

Figure 5.3: Catalytic effect $A = k'_{0,cat}/k'_{0,th}$ as a function of the platinum-to-soot mass ratio for LPW3 diesel soot

any activity on the soot oxidation. Contrary to these experiments, the platinum-doped LPW3 diesel soot studied here exhibits a catalytic effect. The influence of the total platinum quantity present in samples is shown in Figure 5.3. The catalytic effect increases with the total platinum quantity. Jelles et al. [30] performed experiments with only 2 ppm platinum in fuel. The final platinum quantity in the soot was not measured, but can be assumed to be less than 0.0005 platinum-to-soot (mg Pt / mg soot). Assuming a linear relation between the catalytic effect and the platinum quantity, this would correspond to an increase of the pre-exponential factor of about 1.2, or to a T_{50} temperature decrease of 5 K with the experimental condition used here. Jelles et al. [30] characterized the catalytic activity as the "balance point temperature". It is the lowest temperature where an equilibrium can be found between the rate of collected and oxidized soot on the filter. As the recorded temperatures by Jelles et al. have an accuracy of 5 K, it is possible that the catalytic effect was not measurable, but nevertheless present.

Table 5.3: Kinetic parameters from Slovak model for the conversion curves of platinum-doped soot

Platinum-to-soot mass ratio [mg Pt / mg soot]	m -	k'_0 [1/s]	E_a [kJ/mol]	T_{50} [°C]	$A = \frac{k'_{0,cat}}{k'_{0,th}}$ -
0	0.7	1.6×10^7	173	649	-
0.002	0.7	5.0×10^7	173	602	3.2
0.003	0.7	5.7×10^7	173	599	3.7
0.007	0.7	1.9×10^8	173	545	11.9

The increasing catalytic effect of a platinum FBC on the LPW3 diesel soot oxidation is thus demonstrated in the range of platinum-to-soot ratios between 0.002 and 0.007 in the sample. It would be interesting to determine if this trend persists also for larger platinum quantities. Furthermore, the contribution of the platinum particles located in the soot or on the soot surface could not be separated here. Indeed, this could only be determined by comparing the catalytic effect of samples containing the same total quantity of platinum but with different ratios accessible to total platinum. The influence of the platinum surface area related to the mass of soot on the catalytic effect could not be determined either. Indeed, the samples studied here exhibit too similar catalytic effect, and the determination of the platinum surface area related to the soot mass from TEM micrographs is too imprecise.

The influence of the platinum quantity over a wide range, the influence of the platinum particle location, and the influence of platinum surface area and particle size will thus be studied in more details and with additional experiments in Chapter 6.

5.2 Coated Filter

The catalytic effect of a platinum coated sintered metal filter (SMF) was investigated. In order to enhance the contact between platinum and soot particles, the platinum was not deposited directly onto the SMF, but onto an Al_2O_3 fibre which has a higher surface area than the SMF. The preparation and the characterization of the coating is presented first. Coated SMF were loaded with the reference diesel soot and oxidized in the reactor already presented in Chapter 3. As kinetic parameters could not be calculated from conversion curves obtained by these experiments (see Chapter 3), the catalytic effect was characterized as the difference of the temperature $T_{50,th}$ of the thermal diesel soot oxidation, and the temperature $T_{50,cat}$ of the catalytic diesel soot oxidation. The Al_2O_3 fibre itself was found to decrease the diesel soot oxidation temperature. Platinum only catalyzes the oxidation of adsorbed species in soot but does not decrease the soot oxidation temperature. The contact between platinum and soot particles was probably too small to enable any catalytic effect.

5.2.1 Coating preparation and characterization

To enhance the contact possibilities between platinum and soot, it was decided to use an intermediate fibre on the SMF. The fibre is commercially available by Saffil and consists of 97 wt% Al_2O_3 and 3 wt% Silica. The median fiber diameter is around 3 to 3.5 μm, and the surface area 150 to 200 m^2/g. The fibre was first dispersed in Disperal solution (commercially available by Sasol), and filtered onto the SMF with an aspirating apparatus. The concentration of fibres in the Disperal solution was adjusted to obtain 130 mg fibre on the SMF sheet. After drying (one hour at 110°C and 30 minutes at 650°C), the SMF coated with fiber was loaded with platinum. The SMF coated with fiber was simply dipped in a platinum nitrate (PN) solution for 30 seconds. The fiber was found to absorb about 5 times its weight of solution. By varying the platinum concentration in the solution, it was possible to vary the platinum loading on the fibre. The SMF was finally dried 2 hours at 110°C and calcined 30 minutes at 650°C.

Plain fibre characteristics were first investigated. Images of the Al_2O_3 fibre were performed with a scanning electron microscope (SEM) at 200 times magnification (Figure 5.4). The median fiber diameter was found to be of 5 μm, with a dispersion of 2 μm, which is a little higher as the expected fibre size of 3 μm . A surface area of 171 m^2/g was measured with the BET method. It is consistent with the data

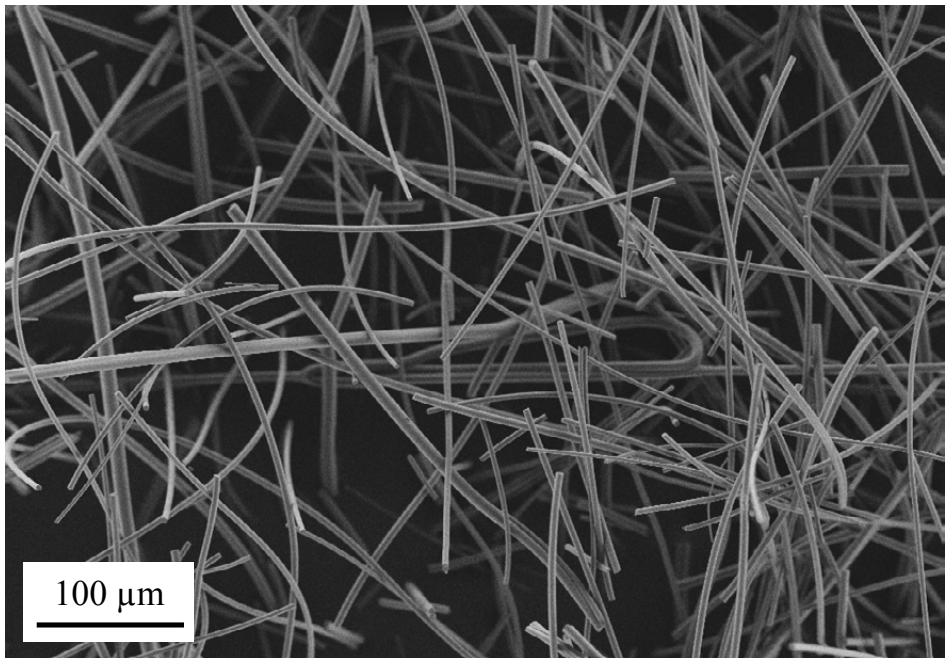

Figure 5.4: SEM image of Al_2O_3 fibre

given by the producer (150 - 200 m^2/g). The SMF also exhibits a higher surface area than the geometrical area, due to its porosity. It was measured by the BET method with Krypton (Kr), and found to be of 0.02 m^2/g. The fibre thus enhances the surface area of a plain SMF sheet up to 10^4 times.

The quantity of platinum present on the fiber was determined by elemental analysis (EA). The fibre layer was carefully scraped off the filter, and dissolved in aqua regia. After filtration, the platinum concentration in solution was determined by ICP-OES. The expected and measured platinum quantities on SMF sheets are presented in Table 5.4. The two first fibre samples (fibre-1 and fibre-2) exhibit about 40 wt% of the expected platinum on the fibre. It is possible that the platinum rest has deposited directly on the SMF, or that it remained in the solution. The last fibre sample (fibre-3) shows slightly more platinum than expected.

Table 5.4: Platinum quantities present on SMF sheets

SMF Sheet	Fibre weight [mg]	Expected Pt on fibre [mg]	Measured Pt on fibre [mg]
Fibre-1	130	130	50.8
Fibre-2	130	78	33
Fibre-3	130	15.6	17.7

The size of the platinum particles was investigated on TEM images (Figure 5.5). TEM micrograph of plain Al_2O_3 shows that the fibre surface is not perfectly smooth but presents some particles clusters, possibly composed of Al_2O_3 or SiO_2 (silica). Platinum is mostly bonded to these clusters. The platinum particle mean diameter is 9 nm with a standard dispersion of 3 nm for the three coated fibres, independently of the platinum loading.

5.2.2 Experimental results of the catalytic effect

Plain and coated SMF (with Al_2O_3 fibre and platinum) were loaded with about 2.5 g reference diesel soot / m^2 SMF, corresponds to 6.3 $\pm$ 1.2 mg reference diesel soot on the 5 $\times$ 5 cm SMF sheet. Reference diesel soot was provided by the diesel driven micro-cogenerator operated at 6 kW (characterized in Chapter 4). SEM images after one fifth loading (0.5 g soot / m^2 SMF) are shown in Figure 5.6. Closed and compact soot layers are built up on a plain SMF, which is typical for surface filtration. Coated SMF presents soot deposited on fibres with larger concentrations on fibre crossings. The fibres allow deep bed filtration with enhanced contact area between soot and fibre.

After loading, SMF sheets were oxidized in the reactor presented in Chapter 3 (4 l/min, 10% O_2 in N_2, ca. 10 K/min), with or without a preheating ramp in N_2. Conversion curves were compared with each other, but no kinetic parameters could be calculated from these curves, as explained in Chapter 3. Thus, the catalytic effect was determined by comparing the temperature $T_{50,th}$ of the thermal oxidation to the temperature $T_{50,cat}$ of the the catalytic oxidation. It has the disadvantage that the catalytic effect depends on the experimental condition used and could not be compared with experiments conducted in TGA device for example.

Conversion curves of diesel soot loaded on plain SMF and on SMF coated with fibre (but without platinum) are presented in Figure 5.7, and the corresponding temperatures T_{50} in Table 5.5. Compared to the conversion curve in TGA (Chapter 4, Figure 4.11), the temperature T_{50} of the reference diesel soot oxidation in reactor is about 45 K higher. This is due to the different O_2 concentrations used in the TGA (20%) and in the reactor (10%), and was already observed for PrintexU soot in Chapter 3.

Figure 5.7 shows that the fibre itself lowers the temperature T_{50} by about 30 K, independently of the preheating ramp. This effect is possibly be due to a change of packing density of the soot agglomerates deposited on the fibres. The deep bed fil-

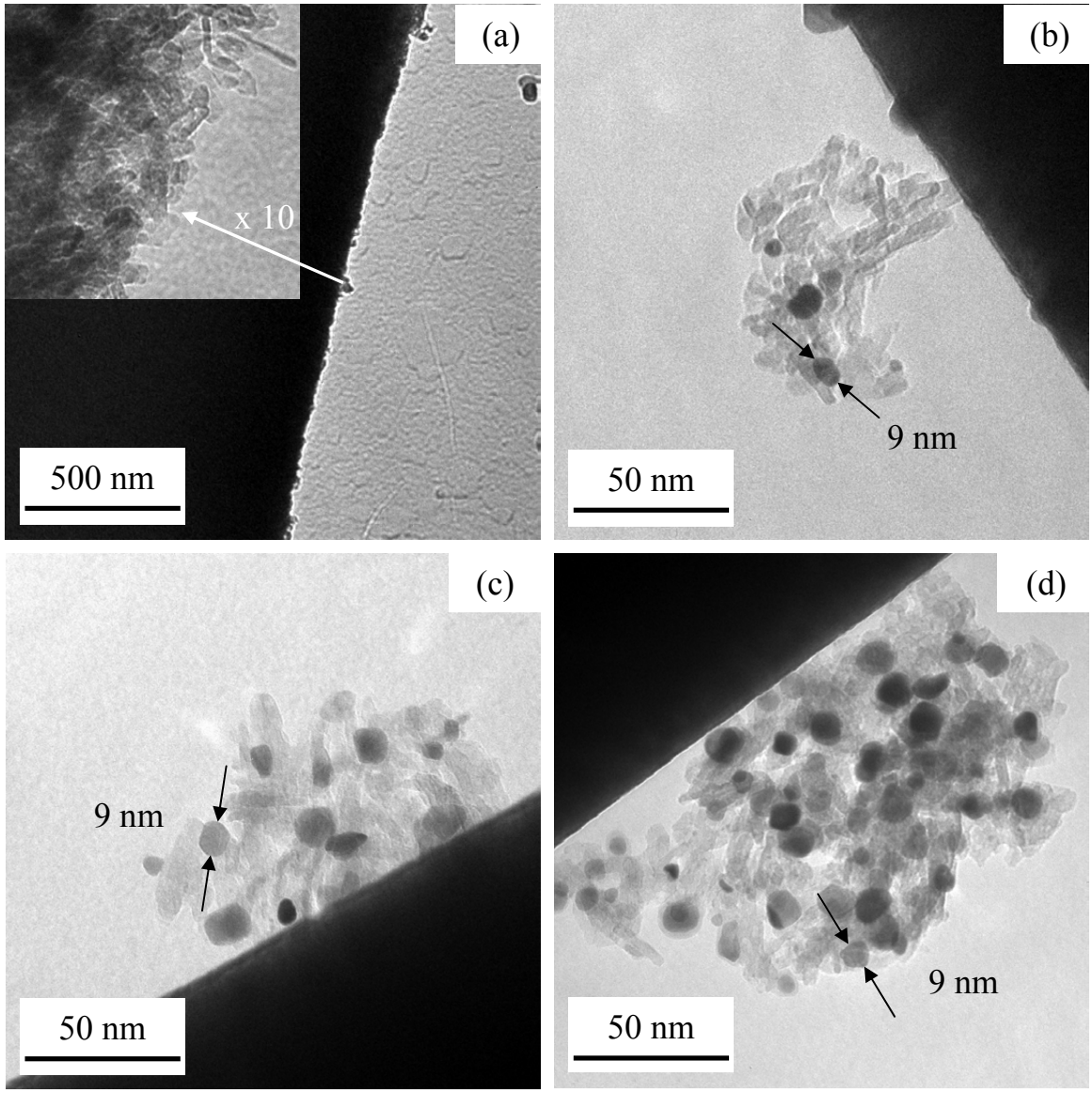

Figure 5.5: TEM image of Al_2O_3 fibre (black) loaded with platinum: plain (a), 17.7 mg Pt (b), 33 mg Pt (c) and 50.8 mg Pt (d)

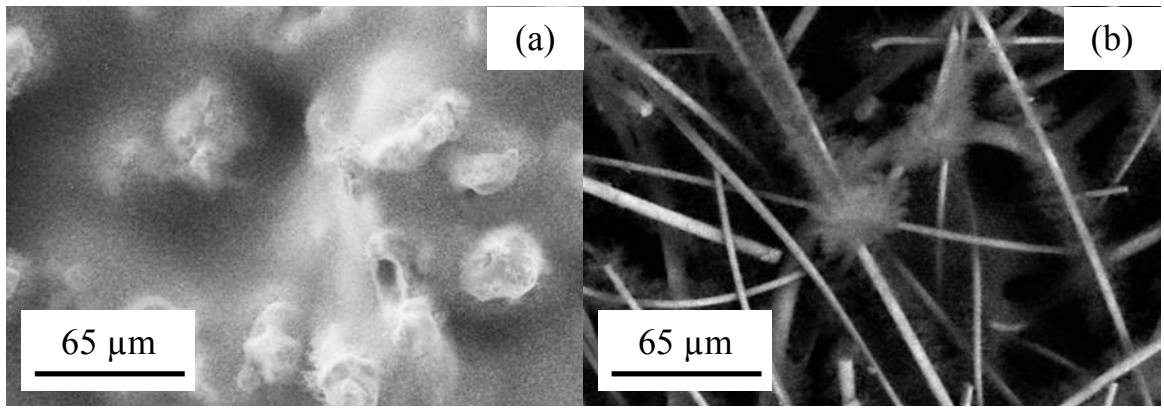

Figure 5.6: SEM images of plain (a) and fibre coated (b) SMF at 0.5 g reference diesel soot / m^2 SMF loading

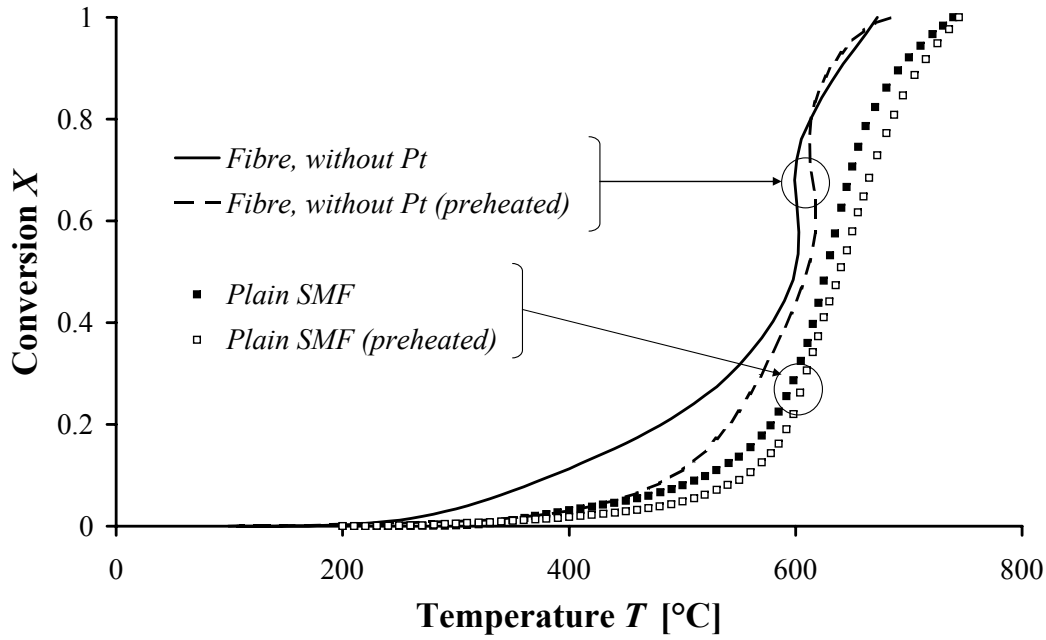

Figure 5.7: Conversion curves of the reference diesel soot oxidation (6.3 ± 1.2 mg) on plain SMF and on SMF loaded with plain fibre, with and without preheating

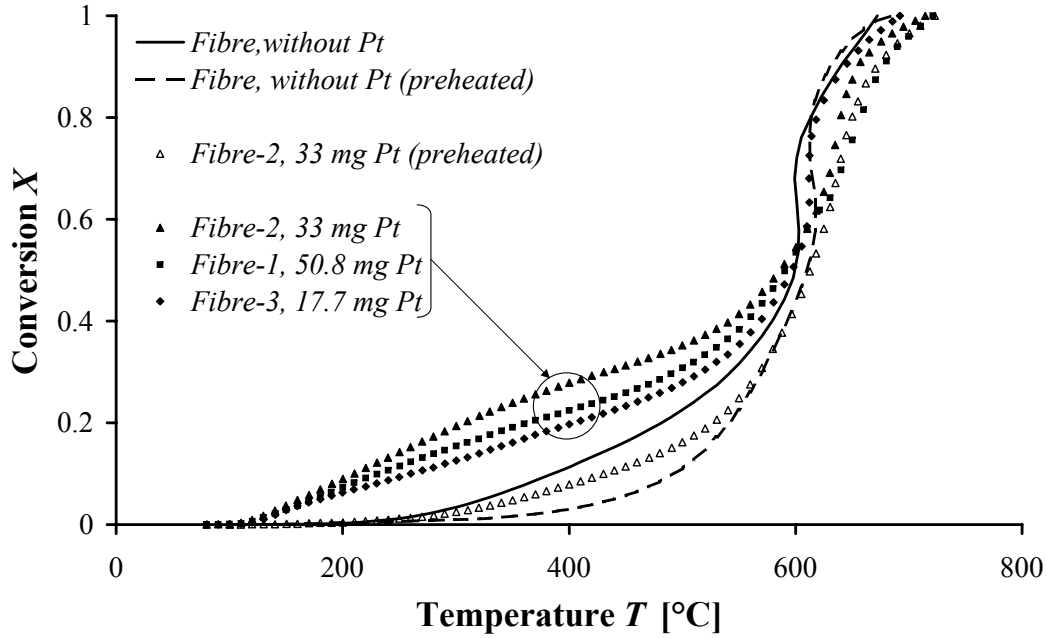

Figure 5.8: Conversion curves of the reference diesel soot oxidation (6.3 ± 1.2 mg) on SMF loaded with platinum coated fibre, with and without preheating

Table 5.5: Temperature T_{50}, platinum and soot quantities for plain, fibre coated SMF and platinum-fibre coated SMF

Name	Pt [mg]	Soot [mg]	Pt-to-soot mass ratio [mg Pt / mg soot]	T_{50} [°C]
Plain SMF	-	6.6	-	627
Plain SMF (preheated)	-	6.0	-	639
Fibre	-	5.2	-	600
Fibre (preheated)	-	7.5	-	611
Fibre-3	17.7	5.6	3.2	597
Fibre-2	33	5.7	5.8	586
Fibre-2 (preheated)	33	6.4	5.2	613
Fibre-1	50.8	6.2	8.2	591

tration occurring on fibres exhibits a loosely packing density, which is consequently more accessible to O_2, could lower the oxygen transport limitations in the soot bed and increases the soot oxidation rate. The fibre also enhances the elimination of adsorbed species: at a temperature of 500°C for example, the reference diesel soot conversion on fibre is twice higher than on plain SMF (0.2 and 0.1 respectively). For conversions higher than 0.5, the temperature-shift to lower temperatures for the two curves concerning the fibre can be explained by the great emissivity change between the soot (black) and the fibre (white). This effect was already discussed in details in Chapter 3.

Conversion curves of diesel soot loaded on SMF coated with fibre containing various platinum amount are presented in Figure 5.8, and the corresponding temperatures T_{50} in Table 5.5. Considering the curves without the preheating ramp, all the measured temperatures T_{50} are in the range 585 to 600°C. As the reproducibility of conversion curves in the reactor is $\pm$ 5 K, the variation of 15 K was mostly attributed to experimental uncertainties. Despite the high platinum-to-soot ratios on the SMF, no catalytic effect can be observed. However, at low temperatures, conversions are much higher with platinum on fibres than without platinum. Platinum acts consequently here as a catalyst for the elimination of the adsorbed species on soot.

Despite the high platinum-to-soot ratios (8.2, 5.8 and 3.2 respectively for fibre-1, -2 and -3), no catalytic effect on the soot oxidation was observed. The platinum particle size is 9 nm, which is comparable to that of FBC platinum-doped soot (9 nm for the sample produced with 50 ppm FBC in fuel). So that the platinum particle size

can not be the parameter that inhibits the catalyst effect. Moreover, the platinum is active as it was observed to catalyze the adsorbed species elimination. It can consequently only be argued that the contact between platinum and soot particles was presumably too low to enable any catalytic effect. The possibility to achieve the same catalytic effect on a coated filter as using a FBC will be investigated in more details in Chapter 7.

Chapter 6

Influence of the platinum loading using model FBC systems

This chapter focuses on the better understanding of the catalytic oxidation of platinum-doped soot samples produced using a fuel borne catalyst (FBC). Three key parameters supposed to influence the catalytic effect of platinum were investigated: the platinum quantity in the platinum-doped soot sample, the platinum particle size, and the platinum location in or/and on the soot agglomerate. In order to control these three parameters, synthetic platinum-doped soot samples were produced from different soot sources and using various preparation methods. The characterization of the platinum loading parameters is presented in the first part of this chapter. Their influence on the catalytic effect is investigated in the second part. The platinum quantity was found to be the main parameter which controls the catalytic effect and was investigated in more details in term of platinum surface area. For a determined platinum quantity, the platinum particle size also influences the catalytic soot oxidation, however to a very small degree. The platinum location was not found to have any measurable influence on the catalytic effect.

6.1 Preparation and characterization of the platinum-doped soot samples

Different synthetic soot sources were loaded with platinum nanoparticles to model platinum-doped soot produced using a FBC. The various preparation methods allow to vary the location, the quantity and the size of the platinum nanoparticles in the soot agglomerates. The resulting platinum-doped soot samples were characterized with the following methods: the platinum-to-soot mass ratio was determined by

elemental analysis (EA). The platinum size was measured by transmission electron microscopy (TEM). The platinum location was first estimated on TEM images and then determined by comparing the results of EA with or without removing the soot. Finally, the platinum surface area was also measured using CO-chemisorption.

6.1.1 Preparation methods

6.1.1.1 Platinum-doped PrintexU soot

Commercially available PrintexU soot was loaded with chemical methods to obtain different sizes of platinum at different quantities (0 to 0.1 mg Pt / mg soot). Platinum catalysts supported on carbon are commonly used for the anodic oxidation of methanol in the direct methanol fuel cells. They are two main routes for the synthesis of this catalyst: impregnation and colloidal procedures [61]. By varying the procedures it was expected to obtain PrintexU soot loaded with different platinum quantities, but also with different particle sizes [62]. Platinum was expected to be located on the PrintexU soot agglomerates surface. All chemical procedures were performed at the Fakultät Chemie - anorganische Chemie of the Technische Universität München in Germany. Procedures details are available in Appendix C.

6.1.1.2 Platinum-doped Vulcan soot

Synthetic soot loaded with different platinum quantities is commercially available for the use in the direct methanol fuel cells. Vulcan soot containing 0.05, 0.1, 0.25, 1 and 4 platinum-to-soot mass ratio (mg Pt / mg soot) was supplied by DeNora. For these products, the platinum particle size was not specified. To investigate the influence of the particle size on the catalytic effect, five additionally Vulcan soot samples were supplied by DeNora, with the following platinum loading specifications: a fixed 0.05 platinum-to-soot mass ratio, and 1.5, 2, 3, 5 and 10 nm mean platinum particle size. As in the case of PrintexU soot, platinum nanoparticles are expected to be located on the soot surface.

6.1.1.3 Platinum-doped pyrolysis soot

Platinum-doped pyrolysis soot samples generated in a pyrolysis aerosol reactor were all produced at the institute for aerosol and sensor technology (IAST) of the

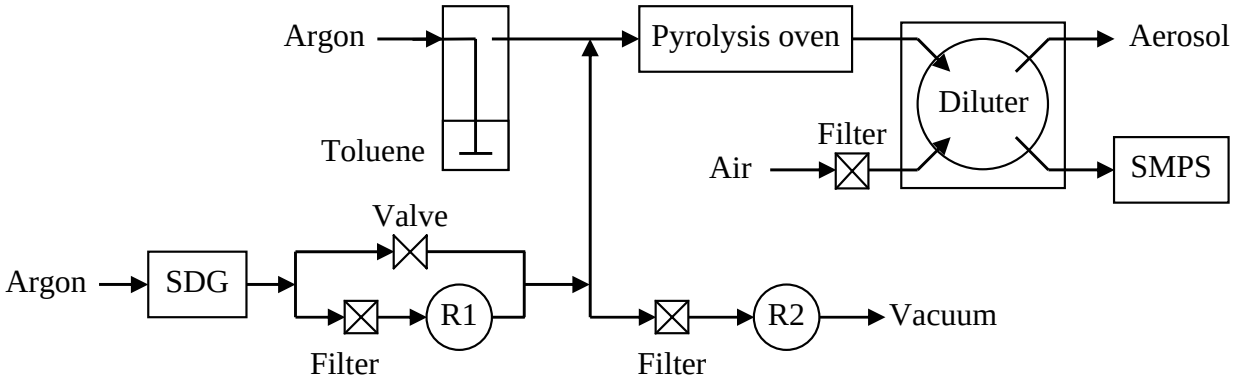

Figure 6.1: Schematic representation of the pyrolysis oven producing a Pt-soot aerosol

university of applied sciences, Aargau in northwestern Switzerland. A platinum aerosol was first produced with a spark discharge generator (SDG) in an argon flow. The platinum aerosol was mixed with a toluene droplet aerosol at the oven inlet. Pyrolysis soot is expected to grow on the platinum agglomerate inside the oven. Therefore, platinum is expected to be embedded inside the soot agglomerate. By adjusting the platinum concentration in the platinum aerosol (Figure 6.1), it was possible to vary the platinum quantity between 0.001 and 0.03 mg Pt / mg soot.

6.1.2 Characterization methods

The platinum-doped soot samples were characterized by elemental analysis (EA), transmission electron microscopy (TEM) and for some of them by CO-Chemisorption. EA allows to determine the platinum-to-soot mass ratio, and the platinum location, on the soot surface or inside the soot agglomerate. The platinum location was also verified by TEM. Platinum particle size was measured on TEM micrographs. However, some samples containing low platinum quantity or small particle size did not present any platinum particles and could not be characterized by TEM. The platinum surface area of chosen samples was measured by CO-chemisorption [39] and compared with the theoretical surface area of smooth sphere having the mean diameter measured on TEM micrographs.

6.1.2.1 Platinum-to-soot mass ratio

The total platinum quantity present in platinum-doped soot sample was measured by elemental analysis, as described in the previous chapter: soot was mixed with

nitric and sulfuric acids and oxidatively removed from the sample by heating. The residue was dispersed in aqua regia, and the platinum concentration in the solution was determined by ICP-OES. The platinum quantities are displayed as the ratio between the platinum mass and the soot mass (mg Pt / mg soot).

Elemental analysis revealed big differences between the target and the measured platinum quantities for samples produced by chemical methods. The PrintexU soot samples contained between 0.0005 and 0.05 platinum-to-soot mass ratio. For clarity reasons, the elemental analysis results for PrintexU soot are grouped in Appendix C. The efficiency of each chemical procedure is also discussed in Appendix C. The Vulcan soot samples loaded with platinum supplied by DeNora have comparable platinum quantities with the expected ones (Table 6.1). Six samples with 0.05 platinum-to-soot mass ratio but different platinum particle sizes were supplied. For these samples, the range within the platinum quantity varies for each sample is indicated in Table 6.1.

For platinum-doped soot samples produced in the pyrolysis oven, the accessible platinum quantity was measured too. The method used was already described in the previous chapter. It consists of dispersing soot in regia aqua, and removing it (and eventually the platinum particles embedded inside the soot agglomerates) by filtration. The platinum present on the soot surface dissolves in the solution and its concentration is measured by ICP-OES. Only 10 to 30% of the total expected platinum quantity (calculated from a mass balance) was found in the pyrolysis soot samples (Table 6.1). There is at this time no explanation for this fact. For the

Table 6.1: Total and accessible platinum for Vulcan and pyrolysis platinum-doped soot (details for platinum-doped PrintexU soot in Appendix C)

Soot	Expected Pt [mg Pt / mg soot]	Total Pt [mg Pt / mg soot]	Accessible Pt [mg Pt / mg soot]
PrintexU	0 - 0.1	0.0005 - 0.05	-
Vulcan	0.05	0.053 - 0.056	-
Vulcan	0.10	0.105	-
Vulcan	0.25	0.232	-
Vulcan	1	0.935	-
Vulcan	4	3.608	-
Pyrolysis	0.01	0.0011	0.0008
Pyrolysis	0.05	0.0054	<0.0001
Pyrolysis	0.10	0.033	0.0003

samples with 0.033 and 0.0054 total platinum-to-soot mass ratio, it was found that less than 2 wt% of the platinum was accessible. It means, as expected by the preparation method, that all the platinum is located inside the soot agglomerate. Soot has thus grown on the platinum during the pyrolysis. For the sample with the lower total platinum-to-soot mass ratio (0.0011), it appears that 72 wt% of the platinum is accessible. However, this result must be discussed. The quantities measured are very low and close to the resolution limit of the ICP-OES. Thus, it will be considered in the following for this sample - as for the other pyrolysis ones - that all the platinum is embedded inside the soot agglomerates.

6.1.2.2 Platinum particle size

The platinum particle size was measured on TEM micrographs. For PrintexU soot, platinum particles were only observed on two samples, containing 0.0386 and 0.0492 platinum-to-soot mass ratio. The mean platinum particle diameter d_{TEM} is 1.5 and 3 nm respectively, with a standard deviation σ_{TEM} of 0.5 and 1 nm (see in Table 6.2). On all other PrintexU soot samples containing less than 0.03 platinum-to-soot mass ratio, none platinum particles could be observed. It is possible that

Table 6.2: Platinum particle size in platinum-doped soot samples

Soot	Pt quantity [mg Pt / mg soot]	Pt d_{TEM} [nm]	Pt σ_{TEM} [nm]
PrintexU	0.0386	1.5	0.5
PrintexU	0.0492	3	1
Vulcan	0.054	3	1
Vulcan	0.105	3	1
Vulcan	0.232	3	1
Vulcan	0.935	3	1
Vulcan	3.608	3	1
Vulcan	0.053	2	1
Vulcan	0.056	2.5	1
Vulcan	0.056	3	1
Vulcan	0.053	4	1
Vulcan	0.053	7	4
Pyrolysis	0.0011	11	6
Pyrolysis	0.0054	10	4
Pyrolysis	0.033	11	4

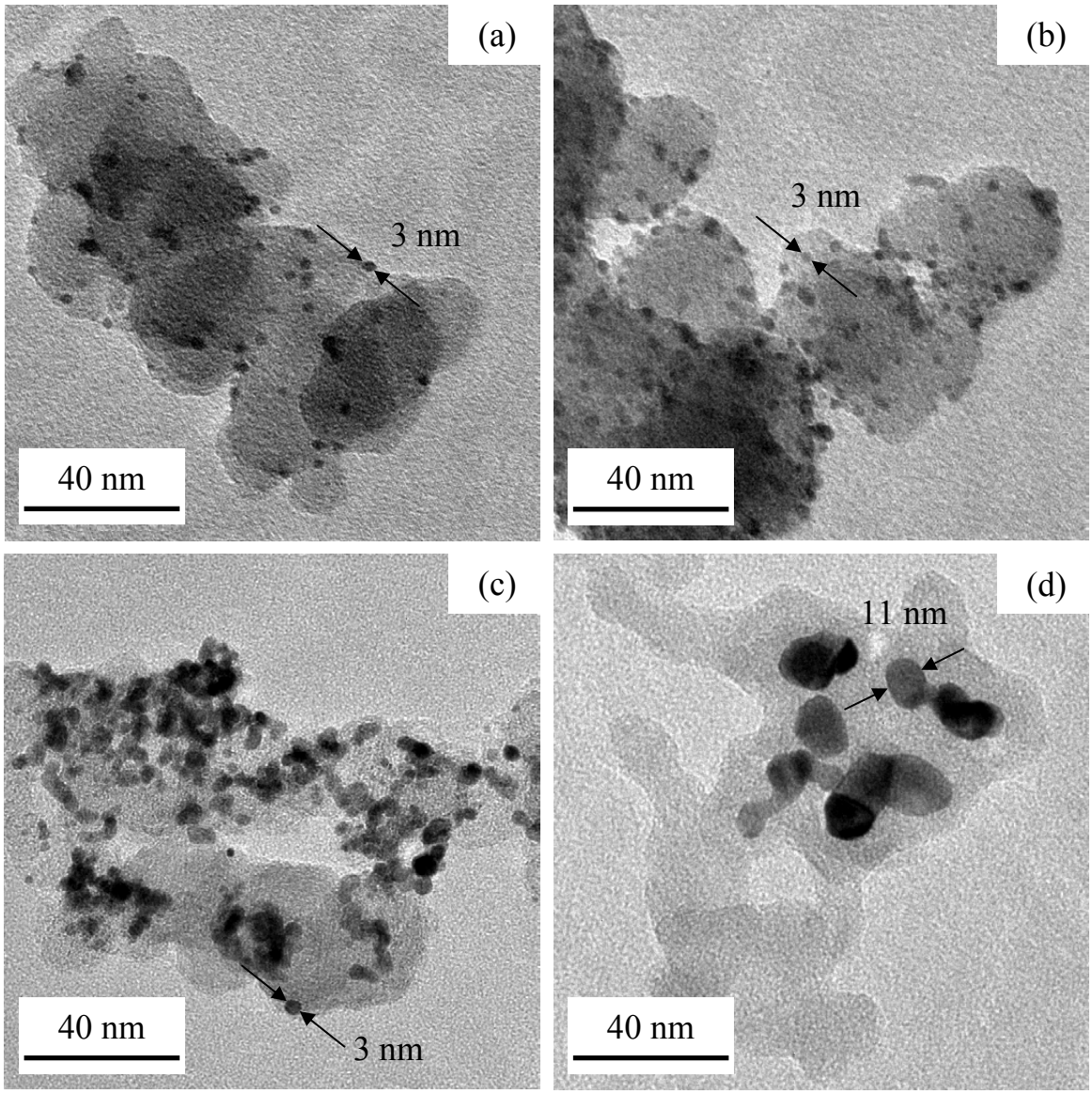

Figure 6.2: TEM micrographs: PrintexU with 0.049 mg Pt / mg soot (a), Vulcan with 0.232 mg Pt / mg soot (b), Vulcan with 0.935 mg Pt / mg soot (c) and Pyrolysis with 0.033 mg Pt / mg soot (d)

platinum is non uniformly spread on soot, making the platinum observation randomly on TEM micrographs. The platinum particles could also be too small to be observed on TEM micrographs (1 nm is the lower limit).

Platinum-doped Vulcan soot have a fixed mean platinum particle diameter of 3 nm (1 nm standard deviation), independently of the platinum quantity (Table 6.2). For the sample with a fixed 0.05 platinum-to-soot mass ratio, the mean platinum particle diameter varies from 2 to 7 nm (1 nm standard deviation). For the sample with the larger particles (7 nm), the standard deviation is however higher (4 nm).

TEM micrographs of platinum in PrintexU, Vulcan and pyrolysis soot samples are shown in Figure 6.2. The mean platinum particle diameter for platinum-doped pyrolysis soot is much higher than for all other soot samples: 10 to 11 nm with a standard deviation from 4 to 6 nm, independently of the platinum quantity present in soot (see in Table 6.2). The platinum particles were completely embedded in soot, confirming the results of the elemental analysis. These two observations can be explained by the preparation method of platinum-doped pyrolysis soot, where a platinum aerosol and a toluene droplet aerosol are simultaneously flowed through the pyrolysis reactor (1300°C). Platinum agglomerates are first expected to sinter in the reactor at low temperatures (400°C - 700°C) leading to the gradual formation of larger primary particles [63]. Soot is then expected to grow on these platinum agglomerates during pyrolysis, leading to the formation of an embedded platinum-doped soot aerosol.

6.1.2.3 Platinum surface area

From the mean platinum particle diameter d_{TEM} measured on TEM micrographs, and with the assumption that platinum particles are spherical, it is possible to calculate a theoretical platinum surface area. In addition, is was decided to measure the platinum surface area separately for some samples to determine if the spherical assumption is justified.

There are two main methods available for measuring platinum specific surface area instead of an overall surface area. One method is the electrochemical technique reported in many fuel cell related publications [64, 65]. It involves the hydrogen adsorption from solution on the platinum surface at a certain potential followed by its removal by increasing potential. However, reproducibility and precision for this method are questionable [66]. An alternative method is to bring H_2 or CO into contact with the platinum surface at a defined temperature and to follow the quantity of adsorbed H_2 or CO as a function of the gas pressure. From the adsorption, it

is possible to determine the amount per gram soot q of H_2 or CO adsorbed in a monolayer. Knowing q and the surface density of platinum atom s, it is possible to calculate the platinum specific surface area S (Equation 6.1).

$$S = \frac{q\,N}{f\,s} \tag{6.1}$$

N is the Avogadro number. The stoichiometric factor f depends on the adsorption nature. CO can form two types of adsorption on platinum: a "linear" adsorption (CO:Pt = 1:1, f = 1) or a "bridged" adsorption (CO:Pt = 1:2, f = 0.5) [39]. H_2 always adsorbed dissociatively on platinum (H:Pt =1:1, f =1) [39], there is thus no uncertainty by using H_2 concerning the adsorption model. However, it is possible that H_2 already present on the platinum surface can lower the effective amount of adsorbed H_2, and consequently the calculated surface area. It was thus decided to use CO as adsorbent. As it was not possible to quantify the contribution of the two adsorption models, it was decided to perform the calculations with the bridge model. The absolute values of surface areas can thus be overestimated, but it does not effect the comparison of surface areas with each other.

The results of the CO-chemisorption analysis are presented in Table 6.3. Eleven samples (PrintexU and Vulcan Pt-soot) with varying platinum quantities were studied. The measured platinum specific surface areas are already converted in platinum surface areas related to the soot mass for clarity reason.

Table 6.3: Comparison of platinum-to-soot surface areas measured by CO-chemisorption and calculated from particle diameter d_{TEM} obtained by TEM

Soot	Pt quantity [mg Pt / mg soot]	Pt d_{TEM} [nm]	S_{TEM} [m^2 Pt / g soot]	S (CO-chemisorption) [m^2 Pt / g soot]
PrintexU	0.0022	-	-	0.04
PrintexU	0.0031	-	-	0.06
PrintexU	0.0049	-	-	0.04
PrintexU	0.0061	-	-	0.06
PrintexU	0.0190	-	-	0.81
PrintexU	0.0294	-	-	0.27
Vulcan	0.054	3	5.1	4.3
Vulcan	0.105	3	9.8	12.8
Vulcan	0.232	3	21.6	20.9
Vulcan	0.935	3	87.2	25.7
Vulcan	3.608	3	336.4	53.6

The platinum surface area corresponding to spherical particles with the mean diameter determined on TEM images was also calculated. For high platinum quantities (> 0.9 mg Pt / mg soot), the measured platinum surface area related to the soot mass is lower than the calculated one. This difference is certainly due to the fact that at high platinum quantities, the soot surface gets saturated with platinum. Platinum particles agglomerate and thus loose surface area (see in Figure 6.2).

The platinum surface area related to the soot mass measured by CO-chemisorption is plotted as function of the platinum-to-soot mass ratio in Figure 6.3 for samples with platinum quantities lower than 0.25 mg Pt / mg soot. The slope of the linear regression corresponding to spherical particles of 3 nm mean diameter is also added. As explained, for high platinum quantities (> 0.9 mg Pt / mg soot) some saturation effect happens and the corresponding points are not represented. For low platinum quantities (< 0.25 mg Pt / mg soot), the platinum surface area increases linearly with the platinum-to-soot mass ratio. Assuming spherical platinum particles, this would signify that the mean diameter of platinum particles remains almost constant for all the studied samples, confirming the TEM analysis. The difference to this trend at very low platinum quantities for PrintexU samples can be due to measurement uncertainties.

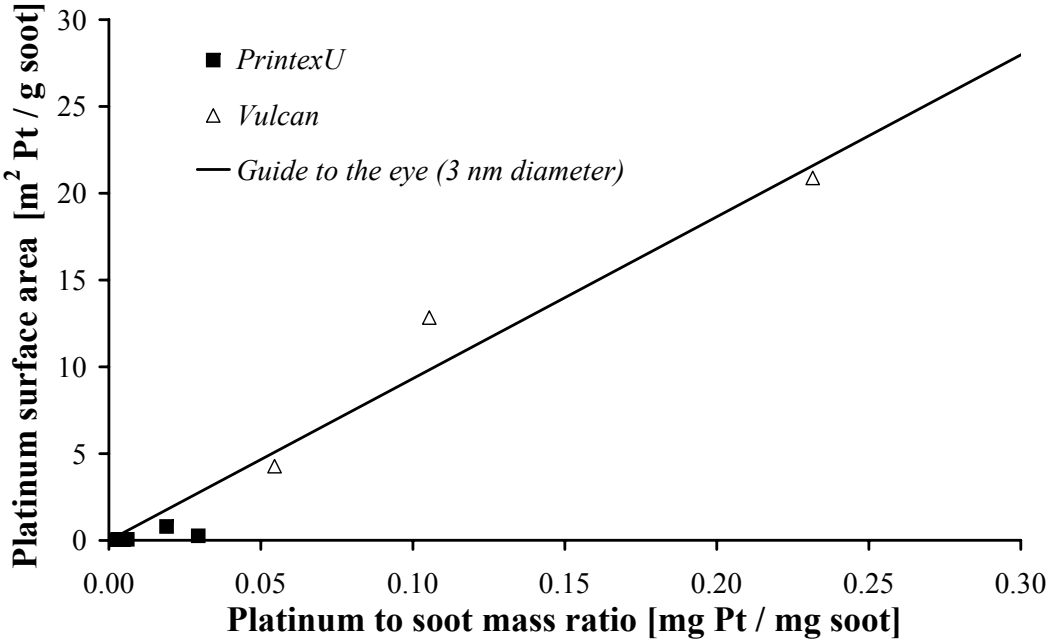

Figure 6.3: Variation of the platinum surface area measured by CO-chemisorption as function of the platinum-to-soot mass ratio for PrintexU and Vulcan soot samples

6.2 Influence of the platinum loading

The catalytic oxidation of the loaded soot samples was studied in the TGA device. Temperature ramp experiments (10 K/min) were performed with 20% O_2 in N_2 (60 ml/min). The catalytic effect was determined as the pre-exponential factor ratio $A = k'_{0,cat} / k'_{0,th}$ between the catalytic and the thermal oxidation, with the other kinetic parameters kept constant (as explained in Chapter 3). The catalytic effect varies linearly with the platinum quantity, and for all studied samples with a fixed platinum particle size, with the initial platinum surface area. The platinum particles were observed to sinter with each other during the oxidation but as the soot was itself consumed, this did not influence the platinum surface area related to the soot mass. For a fixed platinum quantity, the platinum particle size exhibits an optimum at about 3 nm. Finally, the platinum location, either on the soot surface or embedded in soot agglomerate, did not influence the catalytic effect.

6.2.1 Influence of platinum quantity on the catalytic effect

The influence of the platinum quantity on the catalytic effect was investigated for PrintexU and Vulcan soot samples, which characteristics (platinum-to-soot mass ratio, platinum particle size and platinum surface area) are summed-up in Tables 6.1, 6.2 and 6.3. For these two soot sources, platinum is only present on the surface of the soot agglomerates. Vulcan soot samples with 0.05 platinum-to-soot mass ratio but various platinum particle sizes (see in Table 6.2) were investigated separately in Section 6.2.3.

Platinum-doped soot samples were oxidized in the TGA. The catalytic effect $A = k'_{0,cat} / k'_{0,th}$ was determined as explained in Chapter 3, so that it is independent of the soot type used. Thus the variation of the catalytic effect A with the platinum quantity for both PrintexU and Vulcan soot can be plotted in Figure 6.4. The slope of the linear regression on the log-log diagram is 1.1, indicating that the catalytic effect exhibits an almost linear dependence with the platinum quantity. For soot containing less than 0.0005 platinum-to-soot mass ratio (500 ppm), no catalytic effect could be measured.

It was decided to check this trend for the catalytic effect A as a function of the initial platinum surface area. The platinum surface area was measured with CO-chemisorption for some samples, as explained in the previous part. Figure 6.5 shows the variation of the catalytic effect as a function of the initial platinum surface area in a log-log scale. The slope of the linear regression is 0.9, indicating

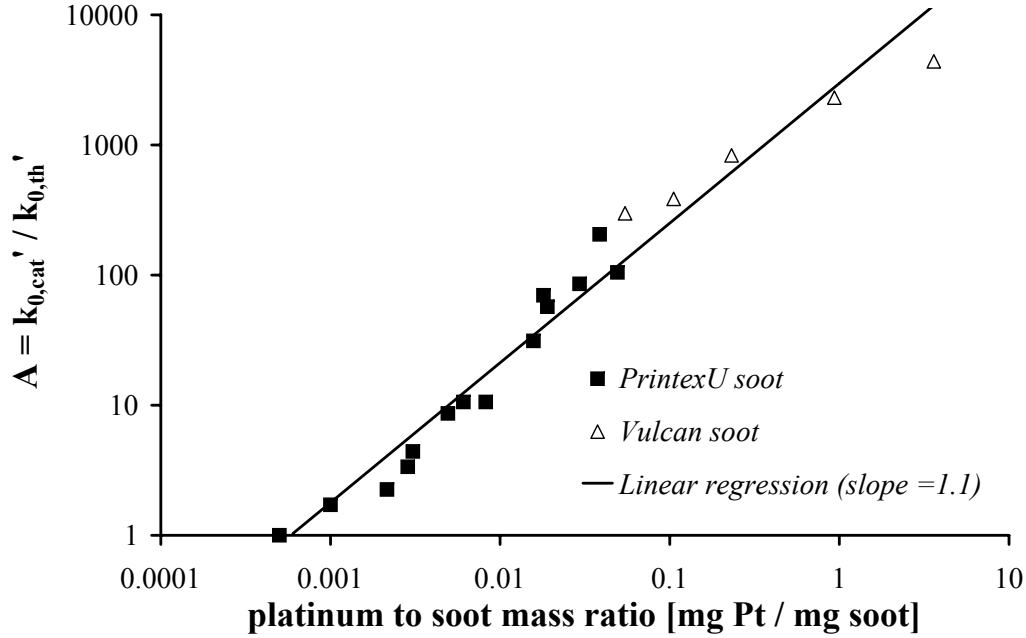

Figure 6.4: Influence of the platinum-to-soot mass ratio on the catalytic effect

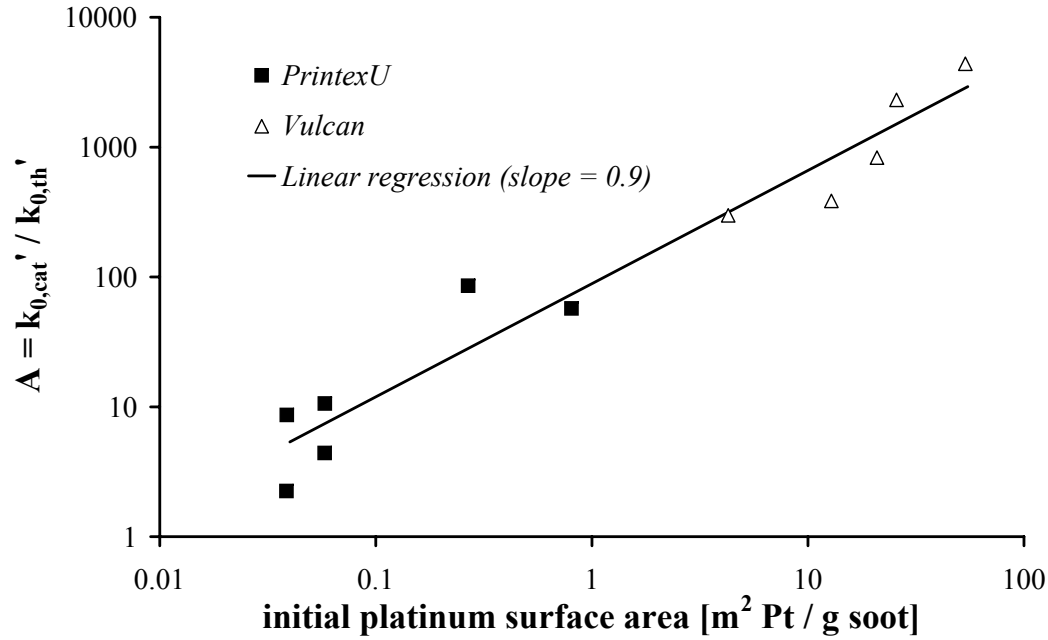

Figure 6.5: Influence of the initial platinum surface area on the catalytic effect

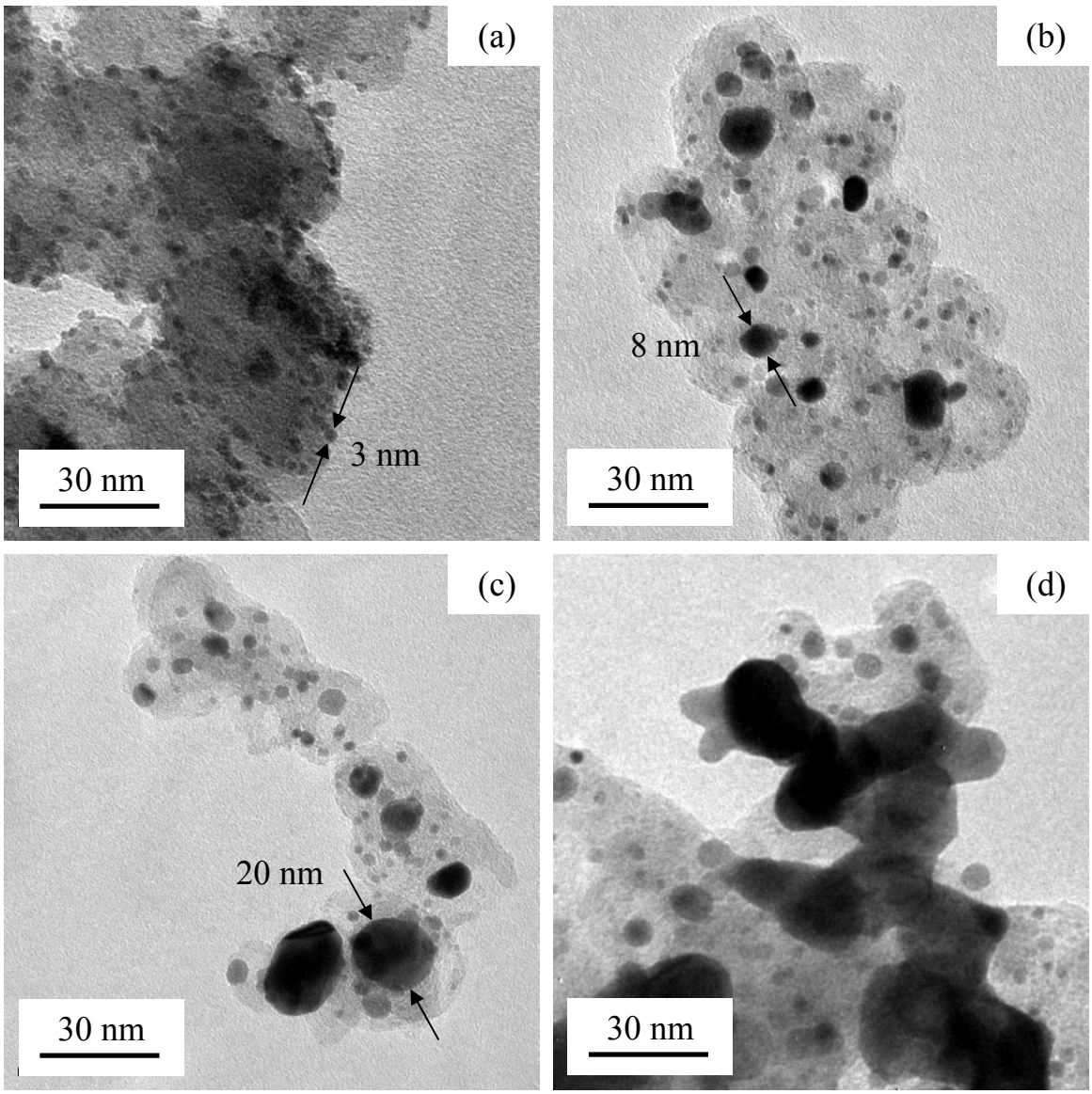

Figure 6.6: Evolution of the platinum sintering with conversion (temperature) for Vulcan soot with 0.232 mg Pt / mg soot: X = 0 (a), X = 0.25 (b), X = 0.5 (c), X = 0.75 (d)

Table 6.4: Evolution of the platinum particle size and surface area related to the soot mass for Vulcan soot with 0.232 mg Pt / mg soot

X -	T [°C]	Pt d_{TEM} [nm]	Pt σ_{TEM} [nm]	Soot mass [g]	Pt mass [g]	resulting S [m^2 Pt / g soot]
0	-	3	1	10	2.32	21.6
0.25	400	3.5	3	7.5	2.32	24.7
0.5	420	5	5	5	2.32	25.9
0.75	440	11	8	2.5	2.32	23.6

again an almost linear dependence of the catalytic effect with the initial platinum surface area. Assuming the oxygen transfer model as the preponderant mechanism governing the catalytic soot oxidation, it is expected that the platinum acts as an oxygen donor. Consequently, the catalytic effect is expected to vary linearly with the number of active sites of platinum, and with the surface area of platinum. The relation between the platinum surface area and the platinum quantity depends on the particle size and shape. For all samples measured with CO-chemisorption (Table 6.3), particle size was found to be about 3 nm, leading to a linear dependence between platinum surface area and quantity (Figure 6.3). The catalytic effect varies thus linearly with the platinum-to-soot mass ratio too. However, a saturation effect in the platinum surface area as a function of the platinum quantity was measured by CO-chemisorption for high platinum quantities (> 0.90 mg Pt / mg soot). This may explain the slight discrepancy of the last point in Figure 6.4.

To conclude, the catalytic effect varies linearly with the platinum quantity, for soot containing more than 0.0005 platinum-to-soot mass ratio (500 ppm). For all studied samples with a fixed platinum particle size, the catalytic effect varies linearly with the initial platinum surface area too, in accordance with the oxygen transfer model.

6.2.2 Effect of platinum particle sintering

The evolution of the platinum particle size during the soot oxidation was studied for one platinum-doped soot sample (Vulcan soot containing 0.232 platinum-to-soot mass ratio). Temperature ramps were performed in the TGA device (10 K/min, 60 ml/min, 20% O_2 in N_2) until temperatures of 400, 420 and 440°C. For this sample, this corresponds to oxidize the soot until the conversion reaches X = 0.25, 0.5 and 0.75, respectively. The remaining sample in the TGA crucible was analyzed with TEM. TEM images for an unoxidized sample, and oxidized samples until X = 0.25, 0.5 and 0.75 are presented in Figure 6.6.

The mean diameters calculated from TEM images are presented in Table 6.4. It is obvious that the platinum particle size increases with the conversion. This can be explained by platinum sintering during the oxidation. Indeed platinum nanoparticles in an aerosol were already observed to sinter at temperatures between 300°C and 700°C [63]. Platinum sintering leads to a loss of the platinum specific surface area during the soot oxidation. But at the same time, the mass of soot decreases due to the soot oxidation. The resulting surface area of the platinum related to the mass of soot remains consequently almost constant during the soot oxidation (see in Table 6.4).

6.2.3 Influence of platinum particle size on the catalytic effect

The influence of the initial platinum particle size on the catalytic effect was studied for a defined platinum quantity. Vulcan soot samples containing about 0.05 (0.053 to 0.056) platinum-to-soot mass ratio and platinum particles with a mean diameter between 2.5 and 7 nm were oxidized in the TGA device. The experimental conditions were kept constant: 10 mg soot, 10 K/min, 60 ml/min and 20% O_2 in N_2. The catalytic effect was calculated as already explained in Chapter 2. The catalytic effect $A = k'_{0,cat} / k'_{0,th}$ is plotted in Figure 6.7 as function of the platinum particle size. Two series of experiments were performed to confirm the results obtained.

For a fixed platinum quantity, the platinum surface area decreases with increasing platinum particle size. As the catalytic effect was previously found to increase with the platinum surface area, it was expected that it decreases with the platinum particle size. However, a particle size optimum was found at about 3 nm particle mean diameter. This optimum seems to results from two contradictory effects. Beside the effect mentioned above, there must be another mechanism increasing the catalytic effect with increasing particle size. This second mechanisms seems to be predominant for small platinum particle sizes.

Such size effects were already observed while studying catalytic oxidation on platinum [63] and on other catalytic systems. For example, quantum effects were

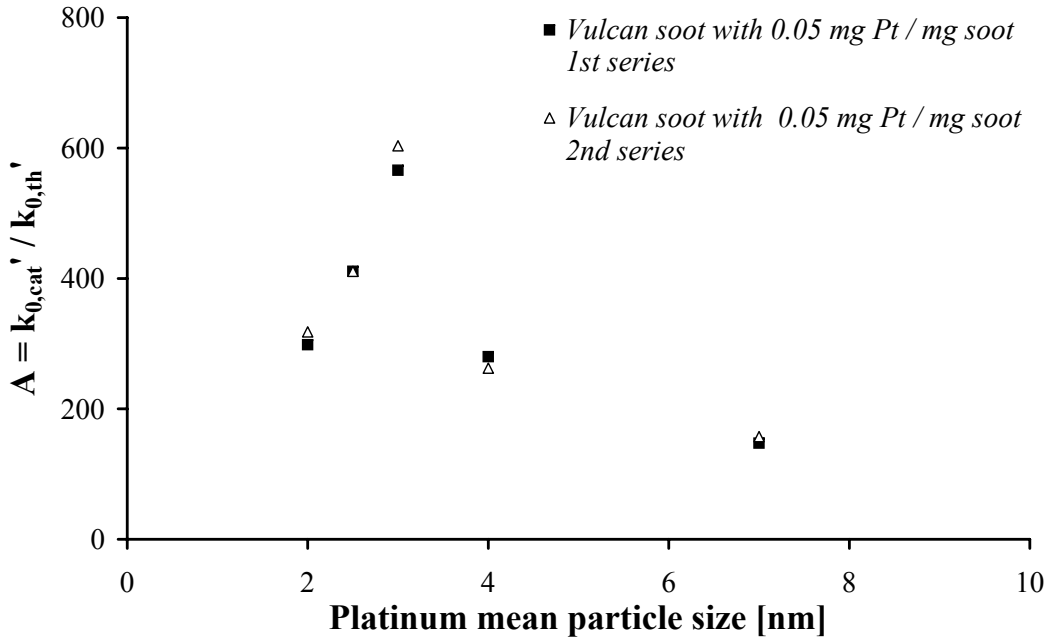

Figure 6.7: Influence of the platinum mean particle size on the catalytic effect

invoked to explain an optimum in the CO oxidation activity on gold nanoparticles [67]. But recently, the observed differences in reactivity of gold nanoparticles were proposed to arise from the presence of highly uncoordinated gold atoms [68]. In comparison with the influence of the platinum quantity, this effect is however secondary.

6.2.4 Influence of platinum location on the catalytic effect

The influence of the platinum location on the catalytic effect was investigated by comparing the catalytic oxidation of platinum-doped pyrolysis soot, with the one of PrintexU and Vulcan soot samples already mentioned in Section 6.2.1. All the oxidation experiments with pyrolysis soot were performed after a ramp in N_2 to avoid the influence of the adsorbed species (see in Chapter 4). As determined on TEM-micrographs and with elemental analysis, the platinum particles are completely embedded in the pyrolysis soot agglomerates. For PrintexU and Vulcan soot, platinum particles were observed to be only present on the soot agglomerate surface. The influence of the platinum quantity on the catalytic effect for PrintexU and Vulcan soot is plotted in Figure 6.8. The linear dependence for these two soot types was also plotted as a guide to the eye (slope = 0.9). The catalytic effect obtained with pyrolysis soot was added in Figure 6.8. Pyrolysis soot with platinum embed-

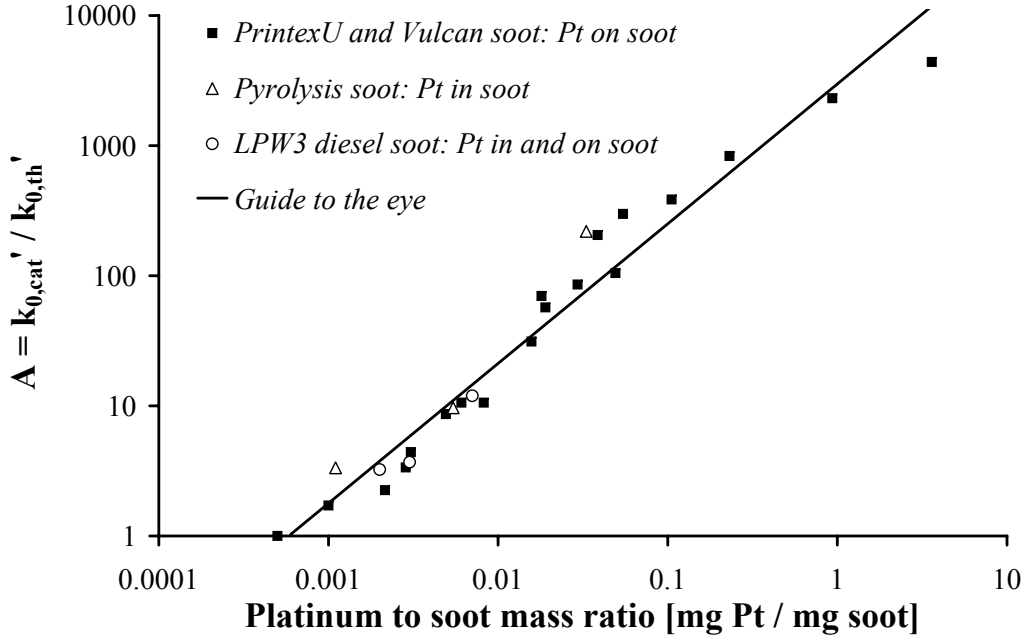

Figure 6.8: Influence of the platinum location on the catalytic effect

ded in soot apparently does not exhibit any measurable catalytic effect difference with PrintexU and Vulcan soot.

To confirm this result, the catalytic activity of the platinum-doped LPW3 diesel soot samples obtained using a platinum fuel borne catalyst (FBC) were also added in Figure 6.8. As determined in Chapter 5, platinum-doped LPW3 diesel soot samples present between 40 and 70% of the platinum particles on the surface of the soot agglomerate. The rest is embedded inside the soot agglomerates. It was previously found that the catalytic effect of these samples vary almost linearly with the platinum quantity between 0.002 and 0.008 platinum-to-soot mass ratio (Chapter 5). These samples were also added in Figure 6.8, where they do not exhibit any measurable catalytic effect difference with PrintexU and Vulcan soot. It is thus confirmed that the soot location does not have any influence on the catalytic effect.

CO-chemisorption was performed on plain pyrolysis soot (without platinum) and on pyrolysis soot with 0.033 platinum-to-soot mass ratio. It was observed that platinum particles embedded in soot agglomerate were always completely accessible to CO. A platinum surface area of 0.09 m^2 Pt / g soot was measured for the platinum-doped soot sample. The reference sample without platinum does not exhibit any adsorption surface for CO. Apparently, as CO, O_2 can also diffuse through the soot to the platinum particles embedded in the soot agglomerate, explaining the fact that the platinum location does not play any role on the catalytic effect.

Chapter 7

Effect of the platinum-soot contact on coated filters

The aim of this chapter is to determine if it is possible to achieve the same catalytic effect on a platinum coated filter as using a platinum fuel borne catalyst (FBC). For this purpose, three different platinum-soot contact scenarios were investigated, modeling the use of a FBC soot aerosol (platinum-doped soot aerosol filtration), a conventional coated filter (consecutive filtration of platinum and soot aerosols), and approximating on a filter the contact obtained with a FBC (simultaneous filtration of platinum and soot aerosols). The loaded sintered metal filter (SMF) sheets were oxidized in the reactor described in Chapter 3. The catalytic effect of the platinum for each configuration was determined by comparing the temperature $T_{50,th}$ of the thermal oxidation to the temperature $T_{50,cat}$ of the the catalytic oxidation. The simultaneous filtration exhibits a high catalytic effect, comparable with the one of the platinum-doped soot filtration, and increasing with the platinum quantity. Only a very low catalytic effect was observed for the consecutive filtration, enhanced when the soot aerosol was filtered before the platinum aerosol. These results suggest that it is possible to enhance the catalytic activity of coated filters by increasing uniformly the platinum particle density in the soot cake.

7.1 Generation of three platinum-soot contact configurations

Two different soot aerosols were used to generate three configurations of platinum-soot contact on SMF. The pyrolysis soot aerosol was produced by pyrolyzing a toluene aerosol, and a spark discharge generator (SDG) was used to produce the

SDG soot aerosol (Chapter 4). For the two soot sources, the generation of three contact configurations was performed. The first configuration represents the contact obtained using FBC, which is known to be effective. For this purpose an aerosol of platinum-doped soot agglomerates is generated and then filtered onto the SMF. In the second configuration, platinum and soot aerosols are generated in parallel and filtered simultaneously onto the SMF. Assuming that both types of particles are uniformly distributed in the filter cake, this second type of contact may approximate that of the FBC. The third configuration represents the typical contact obtained on conventional diesel particle filters. It is achieved by first filtering a platinum aerosol onto the SMF surface to create a layer of catalyst, followed by the formation of a soot cake on top of the catalyst layer (or vice-versa).

7.1.1 Pyrolysis soot

Three configurations of platinum-soot contact on SMF were generated with pyrolysis soot. All samples were produced on a test bench at the institute for aerosol and sensor technology (IAST) of the university of applied sciences, Aargau in northwestern Switzerland (Figure 7.2).

The configuration modeling the contact obtained using a FBC was generated by filtering a platinum-doped pyrolysis soot aerosol. A toluene aerosol (0.07 l/min) was mixed with a platinum aerosol (2.54 l/min) and guided through the pyrolysis oven (1300°C). The platinum aerosol was initially produced by a SDG with a flow

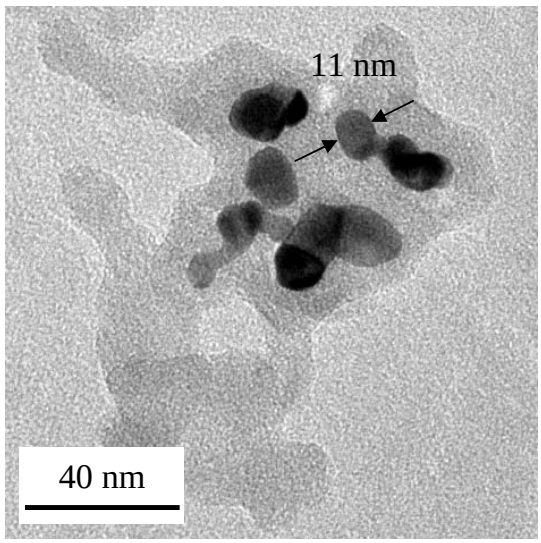

Figure 7.1: TEM-micrograph of a platinum-doped pyrolysis soot agglomerate

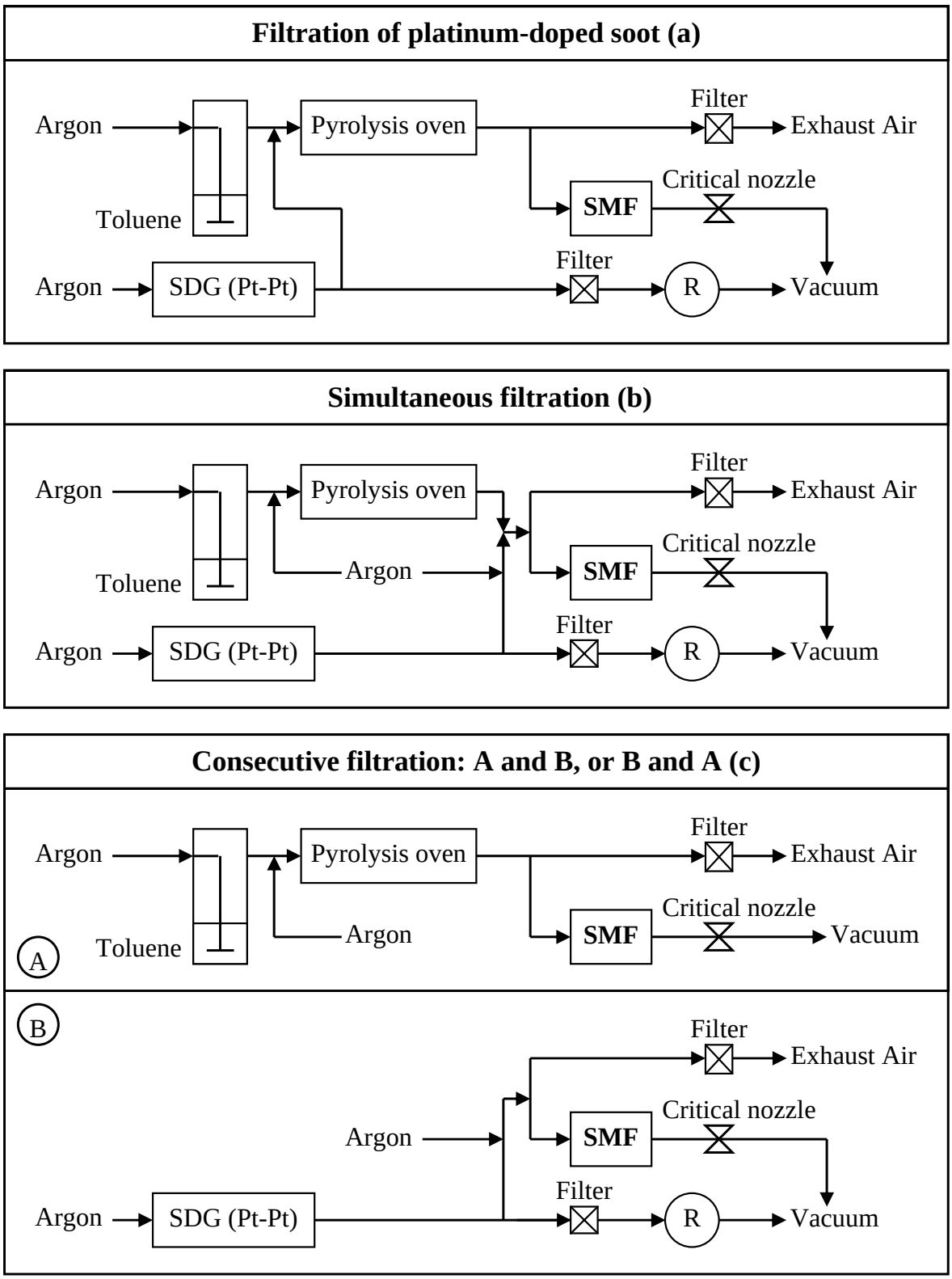

Figure 7.2: Generation of three platinum-soot contact configurations with pyrolysis soot: platinum-doped soot filtration (a), simultaneous filtration (b) and consecutive filtration (c)

rate of 4 l/min but adjusted to 2.54 l/min before entering in the oven. The resulting platinum-doped soot aerosol was already characterized in Chapter 6. It was here decided to work with the maximal platinum quantity of 0.033 mg Pt / mg soot (determined by elemental analysis). The platinum particle mean diameter is of 11 $\pm$ 4 nm (see in Figure 7.1), and all the platinum is embedded in the soot agglomerate (see in Chapter 6). The production rate of the platinum-doped soot aerosol was about 10 mg/h pyrolysis soot.

For the two other configurations, a pyrolysis soot aerosol and a platinum aerosol were produced separately. The pyrolysis soot aerosol was produced by flowing a toluene aerosol (0.07 l/min) diluted in argon (2.54 l/min) through the pyrolysis oven. The platinum aerosol was produced by a SDG. Its flow rate was first adjusted to 2.54 l/min, and then diluted with argon (0.07 l/min). Contrary to the platinum-doped pyrolysis soot aerosol, the platinum mean diameter is of 3 $\pm$ 1 nm (measured on TEM micrographs). This difference was already discussed in Chapter 6.

The second configuration was generated by filtering simultaneously the platinum and the pyrolysis soot aerosol. The conventional coated filter model was generated by filtering consecutively the platinum and the pyrolysis soot aerosol for the same time. SMF samples with first filtered soot and then filtered platinum, and vice-versa, were both collected. A soot quantity of 10 mg on the SMF and a platinum quantity of 0.033 mg Pt / mg soot was used as reference for the three configurations. So that all SMF sheets were loaded with 10 mg soot and 0.33 mg platinum.

7.1.2 SDG soot

The three configurations of platinum-soot contact on SMF were also generated with SDG soot. All samples were produced at the Institut für Mechanische Verfahrenstechnik und Mechanik (IMVM) - Universität Karlsruhe, in Germany (Figure 7.4).

The configuration modeling the contact obtained using a FBC was generated by operating the SDG with one platinum and one carbon electrode (Figure 7.3). The following experimental conditions were applied: a capacity of 50 nF, a distance of ca. 3 mm between the electrodes, a capacitor charge current of 2 mA and a nitrogen flow rate of 10 l/min. The resulting aerosol contains about 0.88 mg Pt / mg soot with all the platinum being present on the soot surface (determined by elemental analysis). The mean particle diameter was determined on TEM micrograph (Figure 7.5) and found to be 3 $\pm$ 1 nm. The platinum-doped SDG soot aerosol was filtered through the SMF sheet with a production rate of about 4 mg/h .

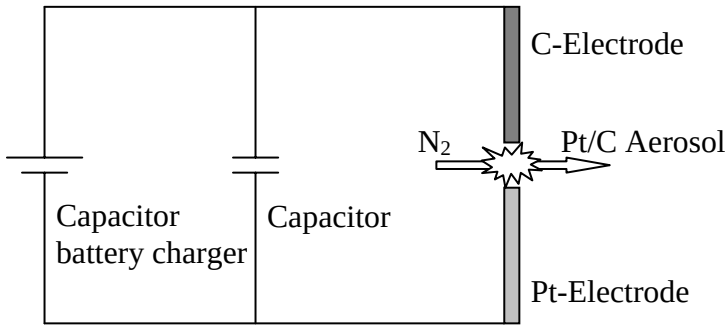

Figure 7.3: Pt-doped soot aerosol produced by a spark discharge generator (SDG)

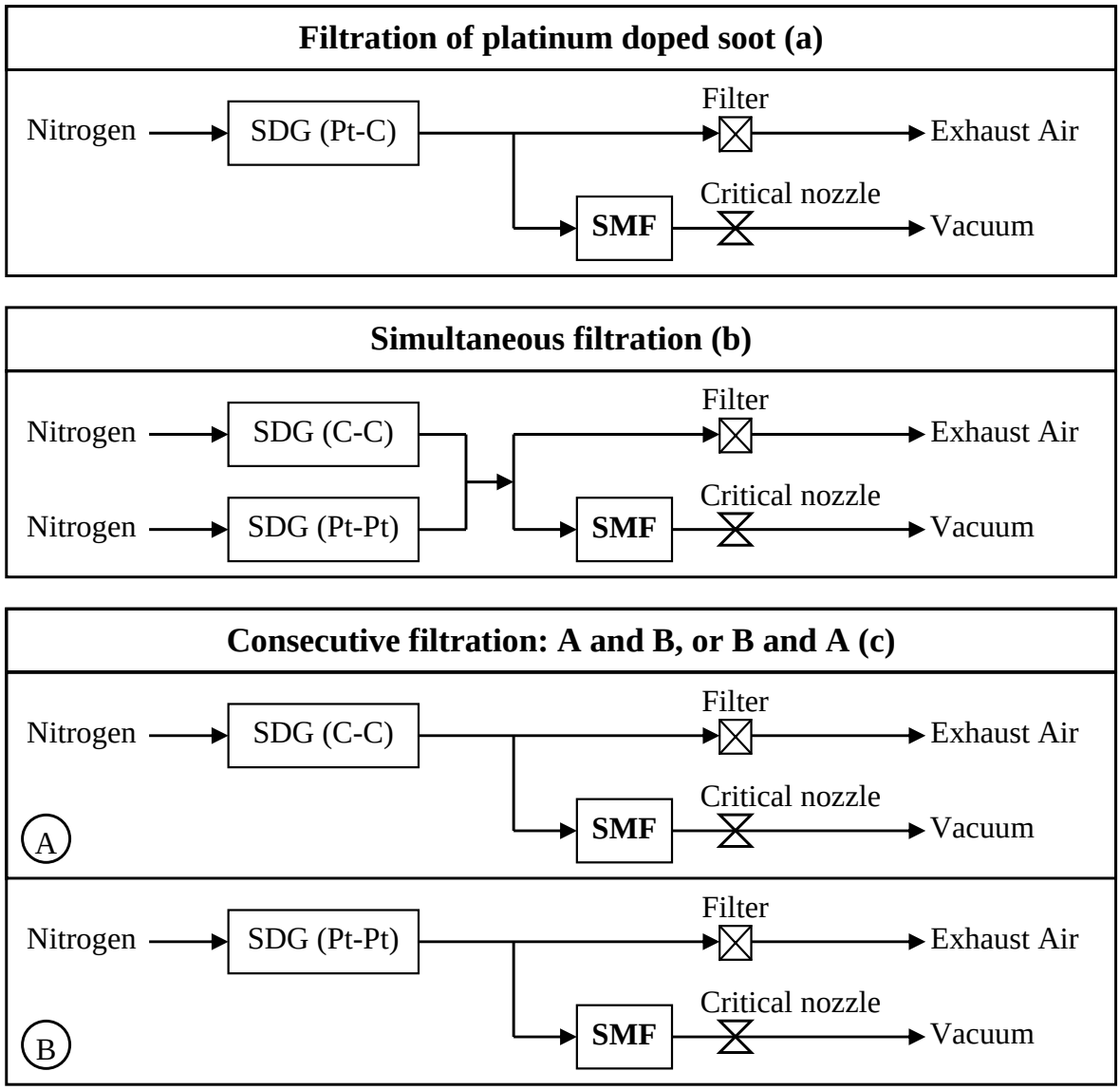

Figure 7.4: Generation of three platinum-soot contact configurations with SDG soot: platinum-doped soot filtration (a), simultaneous filtration (b) and consecutive filtration (c)

For the two other configurations, a soot aerosol and a platinum aerosol were produced separately. Both aerosols were produced by a SDG operating with two carbons or with two platinum electrodes. The same experimental conditions as for the platinum-doped SDG soot aerosol were used: a capacity of 50 nF, a distance of ca. 3 mm between the electrodes, a capacitor charge current of 2 mA and a nitrogen flow rate of 10 l/min. The platinum particle mean diameter of 3 nm in the platinum aerosol (determined by TEM) is the same as in the platinum-doped soot SDG aerosol.

The second configuration was generated by filtering simultaneously the SDG soot aerosol and the platinum aerosol. The conventional coated filter model was generated by the consecutive filtration of the SDG soot and the platinum aerosol for the same time. SMF samples with first filtered soot and then filtered platinum, and vice-versa, were both collected. To avoid long sampling times, a soot quantity of 5 mg on the SMF was collected on the filter, for the three configurations. The platinum quantity of 0.88 mg Pt / mg soot was used as reference. So that for all configurations, 5 mg soot and 5 mg platinum were collected on the SMF sheets.

Furthermore, the influence of the platinum quantity was also studied in the range of 0.03 to 0.88 mg Pt / mg soot for the simultaneous filtration configuration. To vary the platinum quantity, just a part of the platinum aerosol, or of the platinum aerosol previously diluted in nitrogen was mixed to the soot aerosol. The sampling time was adjusted to collect 5 mg soot on the filter. SMF samples with 0.88, 0.59, 0.06 and 0.03 mg Pt / mg soot were thus produced.

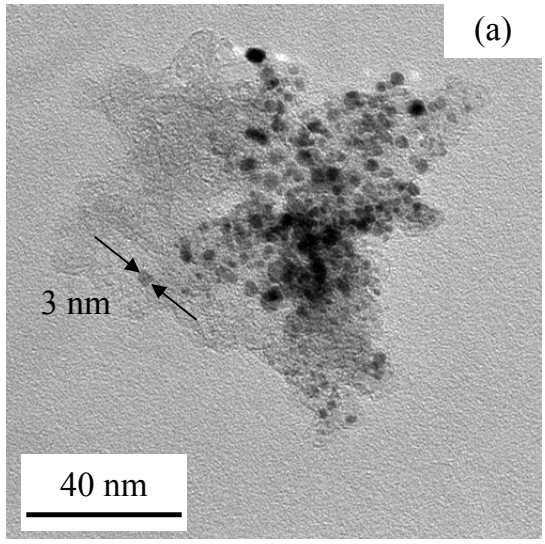

Figure 7.5: TEM-micrograph of a platinum-doped soot agglomerate from the SDG

7.2 Influence of the contact configuration on the catalytic effect

The catalytic effect of the three contact configurations was investigated in the reactor described in Chapter 3. SMF sheets were oxidized with a 10% O_2 in N_2 atmosphere, a flow rate of 4 l/min and a temperature ramp of 10 K/min. Since no kinetic parameters can be calculated from the resulting conversion curves (see in Chapter 3), the catalytic effect was determined as the temperature difference ΔT_{50} between the thermal and the catalytic oxidation. For each soot source, ΔT_{50} is proportional to the logarithm of A, the catalytic effect defined in Chapter 2. ΔT_{50} is consequently dependant on the experimental conditions, and also on the soot source. Results of the oxidation experiments for pyrolysis soot and SDG soot were thus presented first separately, and then compared with each other.

7.2.1 Pyrolysis soot

Conversion curves for the three platinum-pyrolysis soot contact configurations and for the thermal pyrolysis soot oxidation are plotted in Figure 7.6. The corresponding temperatures T_{50} are grouped in Table 7.1. All the samples contained about 0.33 mg Pt / mg soot and were loaded with about 10 mg soot.

In the consecutive filtration case, a the temperature difference ΔT_{50} of 32 K was found when platinum was deposited over the pyrolysis soot. As the reproducibility of the conversion curves in the reactor is $\pm$ 5 K, this difference can be attributed to a very low catalytic effect. However the temperature difference was negligible when soot was filtered after the platinum (ΔT_{50} = 13 K). For the simultaneously fil-

Table 7.1: Catalytic effect of the three contact configurations for pyrolysis soot on SMF (0.033 mg Pt / mg soot)

Configuration	T_{50} [°C]	ΔT_{50} [K]
Plain soot	614	-
Consecutive filtration (Pt and soot)	601	13
Consecutive filtration (soot and Pt)	582	32
Simultaneous filtration	475	139
Platinum-doped soot filtration	479	135

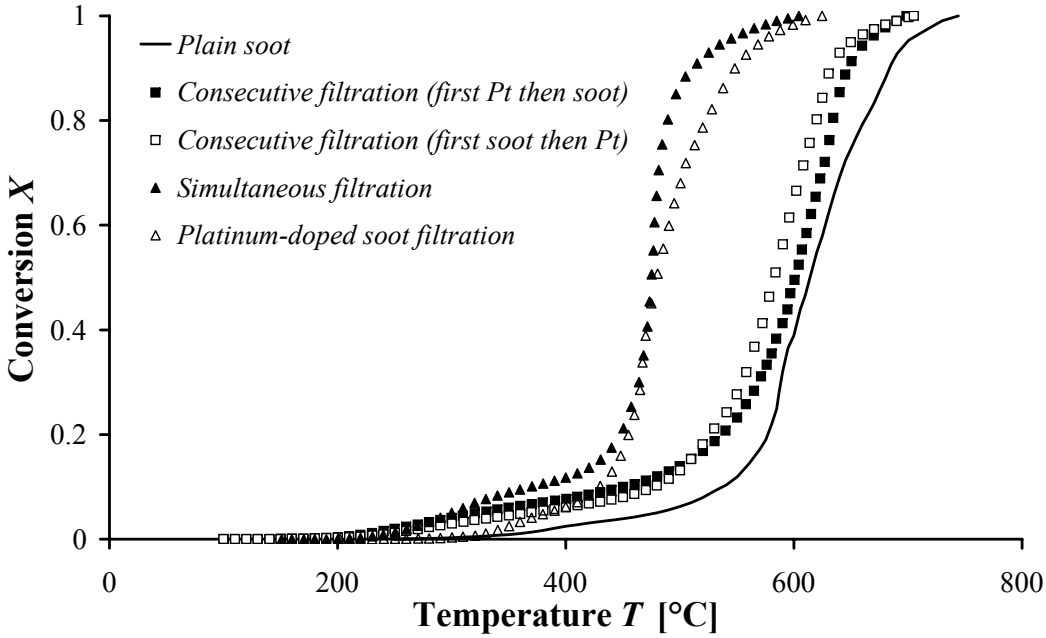

Figure 7.6: Conversion curves of the three contact configurations for pyrolysis soot on SMF (0.033 mg Pt / mg soot)

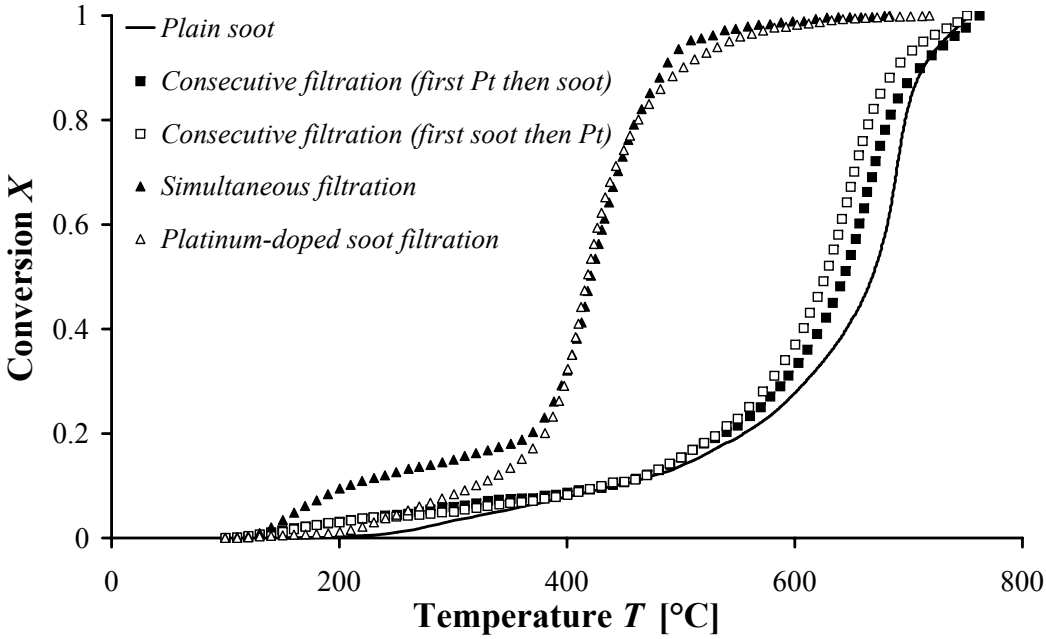

Figure 7.7: Conversion curves of the three contact configurations for SDG soot on SMF (0.88 mg Pt / mg soot)

tration and the filtration of the platinum-doped pyrolysis soot, both exhibit a strong catalytic effect, characterized by the temperature differences ΔT_{50} of 139 K and 135 K, respectively.

7.2.2 SDG soot

Conversion curves for the three platinum-SDG soot contact configurations and for the thermal SDG soot oxidation are plotted in Figure 7.7. The corresponding temperatures T_{50} are grouped in Table 7.2. All the samples contained about 0.88 mg Pt / mg soot and were loaded with about 5 mg soot.

The temperature difference ΔT_{50} was found to be 26 K for the consecutive filtration of the platinum aerosol before the soot aerosol. Given a reproducibility of the conversion curves of $\pm$ 5 K, this difference can be attributed to a very low catalytic effect. By inverting the filtration order on the SMF (soot filtered before platinum), the temperature difference increases to 42 K but still remains rather low. The simultaneous filtration and the platinum-doped soot filtration both exhibit a strong catalytic activity, characterized by almost identical temperature differences ΔT_{50} of about 248 K and 251 K, respectively. The two conversion curves are exactly superposed.

The influence of platinum quantity on the catalytic effect was additionally investigated for the case of the simultaneous filtration with SDG soot. 5 mg soot were deposited simultaneously with platinum amounts between 0.15 mg to 5 mg. This corresponds to effective platinum-to-soot mass ratio varying between 0.88 and 0.03 mg Pt / mg soot in the sample.

Conversion curves are plotted in Figure 7.8. The corresponding temperatures T_{50}

Table 7.2: Catalytic effect of the three contact configurations for SDG soot on SMF (0.88 mg Pt / mg soot)

Configuration	T_{50} [°C]	ΔT_{50} [K]
Plain soot	669	-
Consecutive filtration (Pt and soot)	643	26
Consecutive filtration (soot and Pt)	627	42
Simultaneous filtration	421	248
Platinum-doped soot filtration	418	251

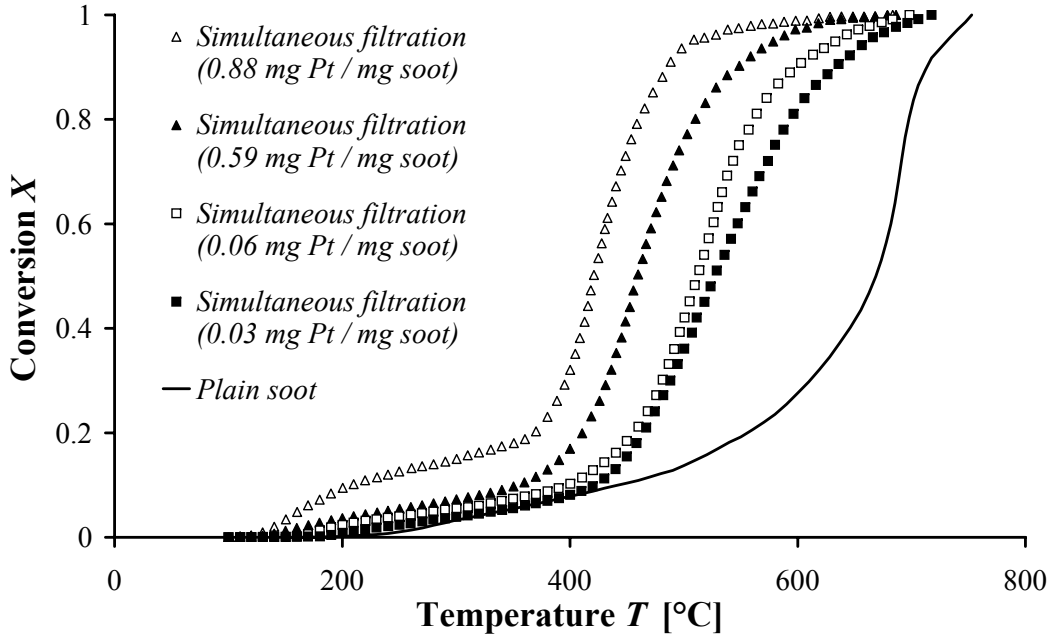

Figure 7.8: Conversion curves of the simultaneous filtration configuration with various platinum quantities on SMF (SDG soot)

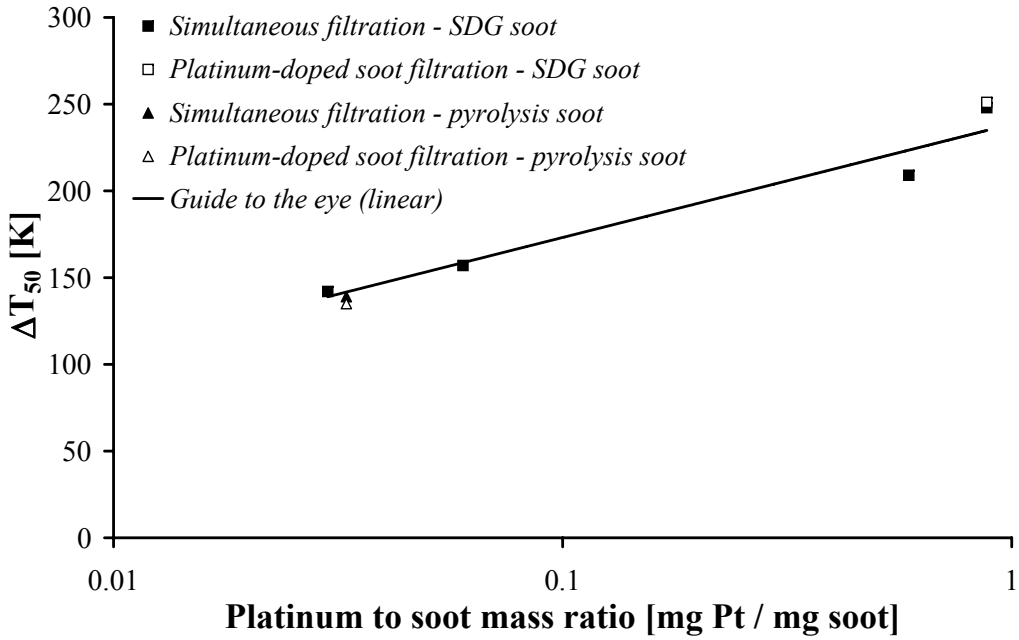

Figure 7.9: Temperature difference ΔT_{50} in function of the platinum quantity for both pyrolysis and SDG soot, for the simultaneous filtration and the platinum-doped soot filtration

and the temperature shifts ΔT_{50} show an increase of the catalytic effect with increasing platinum quantity (Table 7.3). In Figure 7.9 these temperature shifts are compared with those obtained for pyrolysis soot, for both the simultaneous filtration and the platinum-doped soot filtration configurations. The temperature shift for the platinum-doped SDG soot configuration was also added. As already observed previously, the temperature shifts for the simultaneous filtration and the platinum-doped soot filtration configurations are nearly indistinguishable. It is also interesting to note that very similar temperature shifts were observed for the simultaneous filtration with about 0.03 platinum-to-soot mass ratio, independently of the soot used (pyrolysis or SDG).

On a first glance, it was found that ΔT_{50} varies linearly with logarithm of platinum-to-soot mass ratio on the studied quantity range. As ΔT_{50} is proportional to the logarithm of the catalytic effect A, this would signify that the logarithm of the catalytic effect varies linearly with the logarithm of the platinum-to-soot mass ratio. However, as the proportional factor between ΔT_{50} and A remains unknown, it is not possible to identify the slope of the linear regression as 1. In Chapter 6, it was shown that for the platinum-doped soot samples (FBC model), the catalytic effect varies linearly with the platinum quantity. The simultaneous filtration exhibits thus a similar behavior as the platinum-doped soot filtration.

Table 7.3: Catalytic effect of the simultaneous filtration configuration with various platinum quantities (SDG soot)

Pt quantity [mg Pt / mg soot]	T_{50} [°C]	ΔT_{50} [K]
0	669	-
0.03	527	142
0.06	512	157
0.59	460	209
0.88	421	248

7.2.3 Discussion of the results

For both types of soot aerosols (generated by spark discharge or by pyrolysis of toluene), the same trends in catalytic effect were observed for the three contact configurations. The simultaneous filtration exhibits a high catalytic effect, comparable with the one of the platinum-doped soot filtration, and increasing with the

platinum quantity, as it was also observed in Chapter 6 for the platinum-doped soot (even with a linear dependence). The catalytic effect for the consecutive filtration of soot and platinum was marginal, but slightly enhanced when the platinum aerosol was filtered onto the soot cake.

From these results, it can be concluded that the catalytic effect increases with the platinum particle density in the cake. This is consistent with the oxygen transfer mechanism, where platinum is considered as a renewable activated oxygen donor, which then has to be transported to the soot particles within a given lifetime. One can thus expect the reactive oxygen to reach only those soot particles located in the close vicinity of a catalyst particle. This scenario is fulfilled both by filtering a platinum-doped soot aerosol, and by simultaneously depositing a platinum and a soot aerosol onto a filter. As the platinum location does not have any influence on the catalytic effect (Chapter 6), the slight catalytic effect decreases of the platinum-doped soot filtration compared to the simultaneous filtration (in the case of pyrolysis soot) can be attributed to a lower platinum surface area (due to the bigger platinum particle size). Concerning the consecutive filtration of a platinum and a soot aerosol, the density of platinum particles in the soot cake is certainly more or less zero. The slight enhancement when platinum was deposited on the soot cake might be explained by a diffusion of platinum agglomerates into the soot cake (for platinum deposited onto soot) and/or some losses of platinum inside the filter structure when platinum was deposited first.

To conclude, it is possible to enhance the catalytic effect of coated filters by increasing uniformly the platinum particle density in the soot cake. There is consequently still potential in research field concerning the production of new coatings with deep filtration structure (e.g. honeycomb structures) allowing a better dispersion of soot inside the coated filter.

Chapter 8

Discussion and conclusion

8.1 Procedure to answer the objectives

This work was focused on the catalytic soot oxidation by platinum on sintered metal filters. From the literature review it appears that, if the catalytic effect of platinum under physical contact conditions was proven, its application as fuel borne catalyst (FBC) or as coated filter remains unclear. The objectives of this work were first to identify the key parameters which influence the catalytic effect, such as the platinum-to-soot mass ratio, the platinum particle size and the platinum location, in the case of a FBC system. The second objective was to determine if it is possible to achieve the same catalytic effect on a coated sintered metal filter (SMF) than the one obtained using a FBC.

The first requirement to answer the objectives was to characterize the catalytic effect of the platinum. The first step was to determine the kinetic parameters of the thermal soot oxidation from the temperature ramp experiments performed, thanks to the Slovak method [50]. Isothermal experiments of thermal and catalytic soot oxidation indicated that the activation energies of both reactions are the same. Conversion curves obtained from ramp experiments of the catalytic soot oxidation were thus fitted with the same activation energy as for thermal soot oxidation, but with the pre-exponential factor as the free parameter. The catalytic effect was thus defined as A, the pre-exponential factor ratio between the catalytic and the thermal soot oxidation, with the other kinetic parameters being kept constant.

Temperature ramp oxidation experiments were performed with thermogravimetric analysis (TGA) for platinum doped-soot powder samples. During this thesis, a reactor was designed and constructed to investigate the catalytic soot oxidation on sinter metal filters. The soot temperature was measured by an infrared camera and

the reaction conversion was calculated from the reaction product concentrations (CO and CO_2) measured at the outlet of the reactor. As the emissivity of filter does not remain constant during an entire experiment (depending on the presence of soot or not), a temperature shift was observed for conversion superior to 0.5 by comparing conversion curves obtained in TGA device and in the reactor. No kinetic parameters could be calculated from conversion curves obtained in the reactor. Thus the catalytic effect was related in this case as the temperature difference between thermal and catalytic soot oxidation at a conversion of 0.5, which is proportional to the logarithm of the catalytic effect A. However, this definition does not allow to compare the catalytic effect obtained for different soot sources with each other.

The kinetic parameters of the thermal soot oxidation were first studied in the TGA device. The catalytic effect achieved using established diesel particle filter (DPF) technologies with fuel borne catalyst and coated filter was then investigated. After that, platinum-doped soot samples (modeling the one obtained using a FBC) with varying platinum-to-soot mass ratio, varying platinum particle size and varying platinum location were produced. The sample characterization was performed with elemental analysis (EA), transmission electron microscopy (TEM) and CO-chemisorption. The influence of the three key parameters on the catalytic soot oxidation was investigated in the thermogravimetric analysis device. Finally, the catalytic soot oxidation by platinum on a sintered metal filter with three different contact configurations was investigated in the designed reactor, to determine if it is possible to achieve the same catalytic effect on a platinum-coated filter as using a platinum FBC.

8.2 Results discussion

8.2.1 Thermal soot oxidation

The thermal soot oxidation was performed to determine the kinetic parameters of six different soot sources. It was observed that some soot sources release adsorbed species during a preheating ramp in N_2. These adsorbed species were supposed to be adsorbed hydrocarbons, or due to the oxidation of carbon bonded to the oxygen contained in soot. The kinetic parameters were calculated from conversion curves obtained after the preheating ramp.

The activation energy of PrintexU soot (160 kJ/mol) and Vulcan soot (191 kJ/mol),

which both does not contain any adsorbed species, were comparable with literature for these types of soot [15, 50]. Soot obtained by pyrolyzing toluene and LPW3 diesel soot both contain adsorbed hydrocarbons. Their activation energies after a desorption ramp (159 kJ/mol and 173 kJ/mol, respectively) were comparable with activation energies reported in literature for various soot types [15]. Soot from a spark discharge generator (SDG) and diesel soot provided by a micro-cogenerator were both assumed to contain oxygen bonded to carbon. The activation energy of SDG soot after a preheating ramp (78 kJ/mol) was lower than the one already observed for such soot sources [56]. The activation energy of diesel soot after a preheating ramp (206 kJ/mol) was found to be a little high in comparison with activation energies reported in literature for general soot sources [15]. The validity of the use of the Slovak method for these two soot sources was questionable.

Diesel soot provided by a micro-cogenerator was chosen as reference for diesel soot. By comparing the shapes of the conversion curves, it was found that pyrolysis soot models the reference diesel soot the best. Pyrolysis soot also exhibits structure and composition closest to diesel soot. The differences between the structure, composition and oxidation of both diesel soot (issued from a LPW3 engine or from the micro-cogenerator) underline the relativity of this result, and the fact that the future results obtained studying all synthetic soot sources can be further applied on diesel soot.

8.2.2 Catalytic soot oxidation by platinum using established DPF technologies

The catalytic effect of platinum using two established diesel particle filter technologies (a platinum fuel borne catalyst and a platinum-coated sintered metal filter) was studied. The catalytic effect of the platinum FBC was investigated by thermogravimetric analysis, and observed to increase with the platinum quantity in the soot (0.002 - 0.007 mg Pt / mg soot). The catalytic effect of the platinum-coated SMF was investigated in the reactor test bench. An intermediate fibre supporting the platinum catalyst was applied onto the SMF. The fibre itself lowers the soot oxidation temperature, but the platinum did not exhibit any catalytic effect, even with very high platinum quantities (3.2 - 8.2 mg Pt / mg soot). The contact between platinum and soot particles was presumably to low.

The dependence of the catalytic effect on the platinum quantity, and the influence of the platinum particle size and location has to be investigated in more details in the case of the FBC technology. Furthermore, the possibility of the contact

enhancement between platinum and soot on a coated SMF to achieve the same catalytic effect than the one obtained using a FBC has to be investigated too.

8.2.3 Influence of the platinum loading using model FBC systems

The catalytic effect A was observed to linearly increase with the platinum-to-soot mass ratio, for a fixed platinum particle size, and for more than 0.0005 mg Pt / mg soot. This was confirmed by plotting the catalytic effect as a function of the initial platinum surface area. Assuming the oxygen transfer mechanisms [18, 19], it was expected that the catalytic effect was linearly dependent on the platinum surface area. Platinum nano-particulate agglomerates can sinter together between 300°C and 700°C [63]. The influence of the platinum particle sintering during the oxidation was investigated. Platinum particle size increases with progressing conversion, but the platinum surface area related to the mass of soot remains constant.

The influence of the initial platinum particle size on the catalytic effect at a constant platinum-to-soot mass ratio was investigated too. As previously determined, it was expected that the catalytic effect increases with a decreasing platinum particle size (increasing platinum surface area). However, a size optimum was found at a mean platinum particle diameter of 3 nm. This optimum can be explained by the superposition of two contrarily trends: the expected trend, and a decrease of the catalytic effect with decreasing platinum particle size for very small particles. Size optimum was already observed in other systems such as the CO oxidation on gold nanoparticles. Quantum size effects as well as geometric size effects have been advanced to explain it [67, 68]. This trend is however secondary in comparison with the influence of the platinum-to-soot mass ratio.

The catalytic effect is independent of the platinum location, embedded inside the soot agglomerate, or present on the soot surface. Oxygen is supposed to diffuse through the soot to the embedded platinum particles. This result was confirmed by studying the catalytic effect of platinum-doped soot obtained using a FBC. Platinum-doped soot issued from a FBC exhibit the same catalytic effect as synthetic platinum-doped soot samples, increasing linearly with the platinum-to-soot mass ratio. This result is not in contradiction with the results obtained in literature using FBC, were platinum was found to be inactive [30]. Indeed, the FBC quantities used in literature probably lead to lower platinum quantity than the 0.0005 mg Pt / mg soot found here as the minimum to detect any catalytic effect.

8.2.4 Effect of the platinum-soot contact on coated filters

The catalytic effect of a platinum-coated SMF with a presumably enhanced contact area between platinum and soot was previously investigated with the intermediate fibre. However, no catalytic effect was detected. At the present research state, platinum-coated filter does not exhibit a sufficient contact between platinum and soot to achieve the same catalytic effect as using a FBC.

The catalytic effect of three configurations modeling three contact possibilities on SMF was investigated. The contact obtained using a FBC was modeled by the filtration of a platinum-doped soot aerosol. The conventional coated filter configuration was produced by the consecutive filtration of a platinum and a soot aerosol. And finally, the contact obtained with a FBC was approximated on a filter by the simultaneous filtration of a platinum and a soot aerosols. These three configurations were produced for two different soot sources and lead to the same results, independently of the soot source. The simultaneous filtration exhibits a high catalytic effect, comparable with the one of the platinum-doped soot filtration, and increasing with the platinum quantity. Only a very low catalytic effect was observed for the consecutive filtration, enhanced when the soot aerosol was filtered before the platinum aerosol. These results suggest that it is possible to enhance the catalytic activity of coated filters by increasing uniformly the platinum particle density in the soot cake.

8.3 Outlook for future research work

The great challenge of the next years concerning the emission control for diesel engines is to develop diesel particle filters with catalytic regeneration systems. The use of an organometallic compound of transition metal oxides (FBC) allows today to lower the soot oxidation temperature from 600°C to 450°C. This is not sufficient for continuously regenerating the DPF, and FBC remains as ashes on the filter. This solution had therefore low potential for a lifetime concept. An alternative system with catalyst directly attached on the surface of the filter (coated DPF) is now in research field. The results obtained in this work for a platinum catalyst are now discussed to outlook the potential of the two methods and the future research work directions.

Platinum-doped soot obtained by using a platinum FBC exhibits platinum particles partially embedded in the soot agglomerate and partially present on the soot

surface. The location of the platinum does not play any role on the catalytic effect, both particles can catalyze the soot oxidation. The catalytic effect increases linearly with the platinum-to-soot mass ratio. Thus high amounts of platinum are needed to load each soot agglomerate with the platinum quantity wished. From an economical point of view, it is a serious disadvantage in the use of this system. The only development possibilities to improve the performances of the FBC (however only with a low influence on the catalytic effect) is to lower the platinum particle size in the platinum-doped soot obtained. If the FBC is a well established system, its development possibilities with platinum catalyst seem to be reduced.

Concerning a platinum-coated filter, the main challenge is to enhance the contact between platinum and soot particles. Today, this contact is not sufficient to establish a catalytic effect. But it has be shown that, if platinum particles are uniformly distributed in the soot cake (as obtained with the simultaneously filtration of a platinum and a soot aerosol), the catalytic effect is the same than for a platinum FBC. On a coated filter, the platinum particles are present at the best on the soot surface, but could never be embedded in the soot agglomerate. However, it is not a disadvantage, as the platinum location does not influence the catalytic effect. The main advantage of using a coating that could allow an uniformly platinum dispersion in the soot cake, is that the platinum particles can not sinter together if they are sufficiently dispersed on the coating. In this case, a fixed amount of platinum can be used on the filter to catalyze all the filtered soot agglomerates. Much lower platinum quantities are thus necessary to achieve the same catalytic effect as the FBC.

To conclude, by applying the results obtained with platinum on the two actual catalytic systems, it seems that the well established FBC systems have few development possibilities. Otherwise, if it is possible to enhance the platinum density in the soot cake on a coated filter, the concept would have promising development possibilities. However, it should be kept in mind that the results obtained with platinum as a catalyst of the noble metal family could be very different for catalysts from the metal oxide family.

Appendix A

Radiation model code developed with EES Software

The radiation model code developed with the EES Software is presented. All statement in italic are program comments. The user should give a value for T_{cam} in K, the temperature recorded by the camera, T_r in K, the reactor chamber temperature measured by a thermocouple and ϵ_f, the emissivity of the filter surface (0.93 for soot or 0.81 for plain filter). The program returns the corrected filter surface temperature T_f in K.

Intrinsic wavelength used by the camera (in m):
λ_{av} = 4.5 $\times$ 10^{-6}
$\delta\lambda$ = 3 $\times$ 10^{-6}

Constant of the Planck's law (in W.m^2 and m.K respectively):
c_1 = 3.7418 $\times$ 10^{-16}
c_2 = 1.4388 $\times$ 10^{-2}

Transmissivity of the window (without unit):
τ_w = 0.81

Assumption: "window temperature = reactor chamber temperature":
$T_w = T_r$

Calculation of the incident radiation measured by the camera (in W/m^2):

$$\Phi_{cam} = \frac{c_1\,\delta\lambda}{{\lambda_{av}}^5\,(exp(\frac{c_2}{\lambda_{av}\,T_{cam}})-1)}$$

Calculation of the radiation emitted by the reactor chamber (in W/m^2):

$$\Phi_r = \frac{c_1\,\delta\lambda}{{\lambda_{av}}^5\,(exp(\frac{c_2}{\lambda_{av}\,T_r})-1)}$$

Calculation of the radiation emitted by the window (in W/m^2):

$$\Phi_w = \frac{c_1\,\delta\lambda}{{\lambda_{av}}^5\,(exp(\frac{c_2}{\lambda_{av}\,T_w})-1)}$$

Calculation of the radiation emitted by the filter surface, using the radiation model (in W/m^2):

$$\Phi_f = \frac{1}{\epsilon_f}\,(\frac{\Phi_{cam}-(1-\tau_w)\,\Phi_w}{\tau_w} - (1-\epsilon_f)\,\Phi_r)$$

Calculation of the filter surface temperature (in K):

$$T_f = \frac{c_2}{\lambda_{av}\,ln(1+\frac{c_1\,\delta\lambda}{\lambda^5\,\Phi_f})}$$

Appendix B

Thermodynamic tables

Standard free enthalpy of formation $\Delta_f G^0$ of CO_2, CO and O_2 are presented in the following Table. The standard free enthalpy of reaction $\Delta_r G^0$ was also calculated for the CO oxidation reaction.

Temperature [K]	$\Delta_f G^0(CO_2)$ [kcal/mol]	$\Delta_f G^0(CO)$ [kcal/mol]	$\Delta_f G^0(O_2)$ [kcal/mol]	$\Delta_r G^0$ [kcal/mol]
0	-93.965	-27.200	0	133.53
100	-94.100	-28.471	0	131.258
200	-94.191	-30.718	0	126.946
298	-94.265	-32.783	0	122.964
300	-94.267	-32.823	0	122.888
400	-94.335	-34.975	0	118.72
500	-94.399	-37.144	0	114.51
600	-94.458	-39.311	0	110.294
700	-94.510	-41.468	0	106.084
800	-94.556	-43.612	0	101.888
900	-94.596	-45.744	0	97.704
1000	-94.628	-47.859	0	93.538
1100	-94.658	-49.962	0	89.392
1200	-94.681	-52.049	0	85.264

Appendix C

Chemical methods

The chemical methods used to load platinum nanoparticles onto PrintexU soot are first explained. The efficiency of each methods comparing the target and the measured platinum-to-soot mass ratio is then discussed.

Impregnation procedure

The impregnation involves an adsorption and a subsequent reduction step. The adsorption step determines the quantity of platinum that can be loaded onto the soot. The adsorption of a platinum precursor is controlled by the surface area of the soot, and by its chemical surface composition (presence of oxygen surface groups). Moreover, the chemical surface composition controls also the resistance to the platinum sintering behavior during the reduction step, which determines the final size dispersion of platinum [69]. In the following, two impregnation procedures will be performed: the typical precipitation method on plain soot with various precursors and solvents, and the adsorption method on previous oxidized soot.

For the precipitation procedure, a soot slurry was prepared by mixing vigorously PrintexU soot with distilled water. The platinum precursor was slowly added to the slurry. Two typical precursors were used [70]: An aqueous solution of tetraamine platinum nitrate $(NH_3)_4Pt(NO_3)_2$ (TAPN) was used as a first precursor. A chloroplatinic acid (CPA) solution was prepared by dissolving CPA (H_2PtCl_6) into distilled water and used as an alternative precursor. The slurry was heated up to the desired temperature around 80°C, and the pH was adjusted to the basic around pH = 8 using a 10 wt% sodium hydroxide (NaOH) solution. A reducing agent (hydrazine or formaldehyde) was then introduced into the slurry for in situ liquid-phase reduction (the slurry temperature was remained at 80°C for 30 minutes). The platinum-soot slurry was washed 3 times by centrifugation and dried under vacuum.

The precipitation was also conducted in ethylene glycol (EG) following the method of Xin [71, 72]. PrintexU soot were suspended in an EG solution. A CPA-EG solution (7.4 mg Pt/mL) was slowly added to the solution. The pH was measured in the basic range (pH = 13). The solution was kept for 3 hours at 140°C in an oil bath to ensure that platinum was completely reduced. Refluxing conditions were used to keep water in the synthesis system. The washing and drying procedures are the same as for the precipitation in water as described above.

Concerning the adsorption procedure, PrintexU soot was first submitted to an oxidation treatment to increase the oxygen surface content. The soot was mixed with a solution of potassium persulfate ($K_2S_2O_8$) at room temperature under constant stirring for 24 hours [73]. The soot was then filtered, washed 3 times by centrifugation and dried over night at 130°C. The fraction of oxygen in oxidized PrintexU soot was measured with elemental analysis. Thus 9 wt% O was achieved towards 2.4 wt% O in plain PrintexU soot. Plain and oxidized soot were mixed with distilled water and the pH was adjusted to pH = 10 using ammoniac. The platinum precursor $(NH_3)_4Pt(NO_3)_2$ (TAPN) was added to the slurry, and it was stirred over night. Soot was then filtered with an ammoniac solution or washed by centrifugation, dried under vacuum, and finally reduced under a nitrogen flow at 200°C for 2 hours.

For the different impregnation procedures, precursor quantities were adjusted to obtain various platinum-doped soot samples containing between 0.005 and 0.10 mg Pt / mg soot.

Colloidal procedure

Colloidal procedure are used to control the platinum particle size dispersion. They are especially used at high platinum loadings where sintering is difficult to avoid if impregnation procedures are used [61]. Platinum particle size can be controlled during the colloid synthesis by varying the amount and type of reducing agent or the acidity of the solution, or after the synthesis by selective separation [74]. There are various routes to synthesize and depose platinum colloids on soot [75–77]. The method of Reetz [78] originally described for palladium colloids was applied here for platinum.

A platinum precursor was first obtained by diluting platinum nitrate $Pt(NO_3)_2$ (PN) in tetrahydrofuran (THF). An excess of $(n\text{-}C_8H_17)_4N^+(CH3CO_2{}^-)$ (tetraoctylammonium acetate) was added to the precursor, and the solution was heated 4 hours at

66°C under reflux in argon atmosphere. PrintexU soot was added and stirred to the resulting platinum colloid suspension for 60 hours. THF was removed by filtration or by evaporation. The platinum soot samples were finally dried under vacuum.

For the colloidal procedure, precursor quantities were adjusted to obtain various platinum-doped soot samples containing between 0.005 and 0.05 mg Pt / mg soot.

Total platinum quantity

The target platinum quantities and the measured platinum quantities for samples obtained by chemical methods are presented in Table 8.1. For each method, the influence of the solvent, the precursor, the reduction and the washing on the loading were studied. The efficiency was defined as the measured quantity to the target quantity ratio. Concerning the precipitation method, all loadings performed with the tetraamine platinum nitrate (TAPN) precursor show efficiencies less than 20% (except the first sample with a very few target quantity). Loadings performed with

Table 8.1: Target and measured platinum quantities (mg Pt / mg soot), depending on the chemical procedure

Procedure	Soot-Solvent	Precursor	Reduction-Washing	Target	Measured	Efficiency
Precipitation	plain-H_2O	TAPN	hydrazine-centrifuge	0.005	0.0031	62%
Precipitation	plain-H_2O	TAPN	hydrazine-centrifuge	0.05	0.0082	16%
Precipitation	plain-H_2O	TAPN	hydrazine-centrifuge	0.10	0.0157	16%
Precipitation	plain-H_2O	TAPN	formaldehyde-centrifuge	0.005	0.001	20%
Precipitation	plain-H_2O	TAPN	formaldehyde-centrifuge	0.05	0.0033	7%
Precipitation	plain-H_2O	TAPN	formaldehyde-centrifuge	0.10	0.0061	6%
Precipitation	plain-H_2O	CPA	formaldehyde-centrifuge	0.05	0.0386	77%
Precipitation	plain-EG	CPA	heating-centrifuge	0.05	0.0492	92%
Adsorption	plain-H_2O	TAPN	heating after filtration	0.03	0.0049	16%
Adsorption	plain-H_2O	TAPN	heating after centrifuge	0.03	0.0061	20%
Adsorption	oxidized-H_2O	TAPN	heating after filtration	0.03	0.0180	60%
Adsorption	oxidized-H_2O	TAPN	heating after centrifuge	0.03	0.0190	63%
Colloid	plain-THF	PN	filtration	0.005	0.0005	10%
Colloid	plain-THF	PN	filtration	0.05	0.0022	4%
Colloid	plain-THF	PN	evaporation	0.005	0.0029	58%
Colloid	plain-THF	PN	evaporation	0.05	0.0294	59%

formaldehyde exhibit a smaller efficiency compared to hydrazine. Replacing the TAPN precursor by the CPA (chloroplatinic acid) allows to reach an higher efficiency, up to 77%. An efficiency of about 92% was obtained by performing the precipitation in ethylene glycol (EG) as solvent. The adsorption procedure on oxidized soot allows to load about 3 times more platinum than on plain soot, with an efficiency of about 60%. Some platinum is lost during the filtration step. The colloidal procedure shows a small efficiency if THF (tetrahydrofuran) is retried through filtration, but about 60% efficiency when retried with evaporation. The method with the highest efficiency is thus the precipitation in EG developed by Xin [71, 72].

Bibliography

[1] DARMON O., *Oui aux voitures propres*, Hoebeke, Paris, 2001.

[2] EASTWOOD P., *Critical Topics in Exhaust Gas Aftertreatment*, Engineering Design Series, Research Studies Press Ltd., Baldock, 2000.

[3] DINMAN B., Basic physiology of carbon monoxide, *SAE Technical Paper*, (710300), 1971.

[4] BATTIGELLI M., Biological significance of nitrogen oxides, *SAE Technical Paper*, (710298), 1971.

[5] WICHMANN H., PETERS A., Epidemiological evidence of the effects of ultrafine particles exposure, *Philosophical Transactions of the Royal Society of London Series A*, vol. 358: pp. 2751–2768, 2000.

[6] SOMERS C.M., MCQUERRY B.E., MALEK F., QUINN J., Reduction of particulate air pollution lowers the risk of heritable mutation in mice, *Science*, vol. 304: pp. 1008–1010, 2004.

[7] OBERDÖRSTER G., SHARP Z., ATUDOREI V., ELDER A., GELEIN R., KREYLING W., COX C., Translocation of inhaled ultrafine particles to the brain, *Inhalation Toxicology*, vol. 16: pp. 437–445, 2004.

[8] MERKER G., STIESCH G., *Technische Verbrennung, Motorische Verbrennung*, Teubner, Stuttgart - Leipzig, 1999.

[9] DIESELNET, Emissions Standards, *www.DieselNet.com*, 2005.

[10] DIESELNET, Technology Guide, *www.DieselNet.com*, 2005.

[11] SCHALLER J., Schadstoffminderung beim Dieselmotor, in: ROBERT BOSCH GMBH, editor, *Kraftfahrtechnisches Taschenbuch*, pp. 596–601, Vieweg und Sohn, Stuttgart, 2002.

[12] DELISLE M., New emission limit philosophy based on total number of solid particles in the size range of 200-300 nm, in: *7th ETH Conference on combustion generated nanoparticles*, Zurich, 2003.

[13] ADAMS K., CAVATAIO J., SALE T., RIMKUS W., HAMMERLE R., Laboratory screening of diesel oxidation catalyst and validation with vehicle testing: the importance of hydrocarbon storage, *SAE Technical Paper*, (962049), 1996.

[14] HENN J., LÜDERS H., Dieselpartikelfilter- Potential und Chancen moderner Filtermaterialien für zukünftige Abgasnachbehandlungskonzepte, in: *7. Aachener Kolloquium Fahrzeug und Motorentechnik*, pp. 1061–1074, Aachen, 1998.

[15] STANMORE B., BRILHAC J., GILOT P., The oxidation of soot: a review of experiments, mechanisms and models, *Carbon*, vol. 39: pp. 2247–2268, 2001.

[16] MOULIJN J., KAPTEIJN F., Towards a unified theory of reactions of carbons with oxygen-containing molecules, *Carbon*, vol. 33(8): pp. 1155–1165, 1995.

[17] LONG F., SYKES K., The catalysis of the oxidation of carbon, *Journal de Chimie Physique et de Physico-Chimie Biologique*, vol. 47: pp. 361–378, 1950.

[18] AMARIGLIO H., DUVAL X., Etude de la combustion catalytique du graphite, *Carbon*, vol. 4: pp. 323–332, 1966.

[19] MCKEE D., *The catalyzed gasification reactions of carbon*, Chemistry and Physics of Carbon, Dekker, M., New York, 1981.

[20] MARSH H., KUO K., Kinetics and catalysis of carbon gasification, in: MARSH H., editor, *Introduction to Carbon Science*, pp. 107–151, Butterworths, London, 1989.

[21] BAKER R., Factors controlling the mode by which a catalyst operates in the graphite-oxygen reaction, *Carbon*, vol. 24(6): pp. 715–717, 1986.

[22] BAKER R., Metal catalyzed gasification of graphite, in: FIGUEIREDO J., MOULIJN J., editors, *Carbon and Coal Gasification*, pp. 231–268, Proc. NATO Advanced Science Institute, Alvar, Portugal, 1986.

[23] VAN SETTEN B., MAKKEE M., MOULIJN J., Science and technology of catalytic diesel particulate filters, *Catalysis Reviews*, vol. 43(4): pp. 489–564, 2001.

[24] KHOOBIAR S., Particle to particle migration of hydrogen atoms on platinum-alumina catalysts from particle to neighboring particles, *Journal of Physical Chemistry*, vol. 68(2): pp. 411–412, 1964.

[25] NERI G., BONACCORSI L., DONATO A., MILONE C., MUSOLINO M., VISCO A., Catalytic combustion of diesel soot over metal oxide catalysts, *Applied Catalysis B: Environmental*, vol. 11: pp. 217–231, 1997.

[26] GOLODETS G., *Heterogeneous catalytic reactions involving molecular oxygen*, Studies in surface science and catalysis, Elsevier Science Publisher B.V., Amesterdam - Oxford - New York, 1983.

[27] OI-UCHISAWA J., OBUCHI A., ZHAO Z., KUSHIYAMA S., Carbon oxidation with platinium supported catalysts, *Applied Catalysis B: Environmental*, vol. 18: pp. L183–L187, 1998.

[28] WEBER A., SEIPENBUSCH M., DAVOODI P., SCHALOW T., KASPER G., Quality of contact between platinium and carbon nanoparticles: influence on the carbon oxidation, in: *European Aerosol Conference*, Madrid, 2003.

[29] SEIPENBUSCH M., VAN ERVEN J., SCHALOW T., WEBER A., VAN LANGEVELD A., MARIJNISSEN J., FRIEDLANDER S., Catalytic soot oxidation in microscale experiments, *Applied Catalysis B: Environmental*, vol. 55(1): pp. 31–37, 2005.

[30] JELLES S., MAKKEE M., MOULIJN J., Ultra low dosage of platinium and cerium fuel additives in diesel particulate control, *Topics in Catalysis*, vol. 16/17(1-4): pp. 269–273, 2001.

[31] NEEFT J., VAN PRUISSEN O., MAKKEE M., MOULIJN J., Catalysts for the oxidation of soot from diesel exhaust gases II. Contact between soot and catalyst under practical conditions, *Applied Catalysis B: Environmental*, vol. 12: pp. 21–31, 1997.

[32] VAN SETTEN B., SCHOUTEN J., MAKKEE M., MOULIJN J., Realistic contact for soot with an oxidation catalyst for laboratory study, *Applied Catalysis B: Environmental*, vol. 28: pp. 253–257, 2000.

[33] OI-UCHISAWA J., OBUCHI A., OGATA A., ENOMOTO R., KUSHIYAMA S., Effect of feed gas composition on the rate of carbon oxidation with Pt/SiO_2 and the oxidation mechanism, *Applied Catalysis B: Environmental*, vol. 21: pp. 9–17, 1999.

[34] OI-UCHISAWA J., OBUCHI A., ENOMOTO R., LIU S., NANBA T., KUSHIYAMA S., Catalytic performance of Pt supported on various metal oxides in the oxidation of carbon black, *Applied Catalysis B: Environmental*, vol. 26: pp. 17–24, 2000.

[35] OI-UCHISAWA J., WANG S., NANBA T., OHI A., OBUCHI A., Improvement of Pt catalyst for soot oxidation using mixed oxide as a support, *Applied Catalysis B: Environmental*, vol. 44: pp. 207–215, 2003.

[36] SETIABUDI A., VAN SETTEN B., MAKKEE M., MOULIJN J., The influence of NOx on soot oxidation rate: molten salt versus platinum, *Applied Catalysis B: Environmental*, vol. 35: pp. 159–166, 2002.

[37] MATSUOKA K., ORIKASA H., ITOH Y., CHAMBRION P., TOMITA A., Reaction of NO with soot over Pt-loaded catalyst in the presence of oxygen, *Applied Catalysis B: Environmental*, vol. 26: pp. 89–99, 2000.

[38] SEIPENBUSCH M., FRIEDLANDER S., Catalytic soot oxidation in microscale experiments: Simulation of interactions between co-deposited graphitic nanoparticle agglomerates and platinum nanoparticles, *Journal of Nanoparticle Research*, vol. 6: pp. 605–611, 2004.

[39] SCACCHI G., BOUCHY M., FOUCAUT J., ZAHRAA O., *Cinétique et catalyse*, Tec et Doc Lavoisier, Paris, 1996.

[40] BARRET P., *Cinétique hétérogène*, Gauhier-Villars, Paris, 1973.

[41] BROWN M., *Introduction to thermal analysis: techniques and applications*, Hot topics in thermal analysis and calorimetry, Kluwer Academic Publisher, Dordrecht - Boston - London, brown, m.e. edn., 2001.

[42] NEEFT J.P.A., HOORNAERT F., MAKKEE M., MOULIJN J.A., The effects of heat and mass transfer in thermogravimetrical analysis. A case study towards the catalytic oxidation of soot, *Thermochimica Acta*, vol. 287: pp. 261–278, 1996.

[43] DERNAIKA B., UNER D., A simplified approach to determine the activation energies of uncatalyzed and catalyzed combustion of soot, *Applied Catalysis B: Environmental*, vol. 40: pp. 219–229, 2003.

[44] JELLES S., KRUL R., MAKKEE M., MOULIJN J., The influence of NOx on the oxidation of metal activated diesel soot, *Catalysis Today*, vol. 53: pp. 623–630, 1999.

[45] NEEFT J., NIJHUIS T., SMAKMAN E., MAKKEE M., MOULIJN J., Kinetics of the oxidation of diesel soot, *Fuel*, vol. 76(12): pp. 1129–1136, 1997.

[46] CIAMBELLI P., CORBO P., GAMBINO M., PALMA V., VACCARO S., Catalytic combustion of carbon particulate, *Catalysis Today*, vol. 27(1-2): pp. 99–106, 1996.

[47] DE SOETE G., Catalysis of soot combustion by metal oxides, in: *Western states section meeting*, pp. 1–44, The combustion Institute, Salt Lake City, 1988.

[48] GILOT P., BONNEFOY F., MARCUCCILLI F., PRADO G., Determination of kinetic data for soot oxidation. Modeling of competition between oxygen diffusion and reaction during thermogravimetric analysis, *Combustion and Flame*, vol. 95: pp. 87–100, 1993.

[49] CRIADO J., ORTEGA A., GOTOR F., Correlation between the shape of controlled rate thermal analysis curves and the kinetics of solid-state reactions, *Thermochimica Acta*, vol. 157: pp. 171–179, 1990.

[50] SLOVÀK V., Determination of kinetic parameters by direct non-linear regression from TG curves, *Thermochimica Acta*, vol. 372: pp. 175–182, 2001.

[51] RODANTE F., VECCHIO S., SLOVÀK V., Application of direct nonlinear regression from single TG curve to compounds undergoing simple and complex thermal decompositions, *International Journal of Chemical Kinetics*, vol. 35: pp. 611–622, 2003.

[52] SIEGEL R., HOWELL J., *Thermal radiation heat transfer*, Series in thermal and fluid engineering, Hemisphere, Washington DC, 2nd edn., 1981.

[53] INFRATEC GMBH, Einführung in Theorie und Praxis der Infrarot-Thermografie, 2003.

[54] MARCUCILLI F., GILOT P., STANMORE P., PRADO G., Experimental and theoritical study of diesel soot reactivity, in: *Twenty-fifth international symposium on combustion*, pp. 619–626, 1994.

[55] SU D., JENTOFT R., MÜLLER J.O., ROTHE D., JACOB E., SIMPSON C., TOMOVIC Z., MÜLLEN K., MESSERER A., PÖSCHL U., NIESSER R., SCHLÖGL R., Microstructure and oxidation behaviour of Euro IV diesel engine soot: a comparative study with synthetic model soot substances, *Catalysis Today*, vol. 90: pp. 127–132, 2004.

[56] MÜLLER J.O., SU D., JENTOFT R., KRÖHNERT J., JENTOFT F., SCHLÖGL R., Morphology-controlled reactivity of carbonaceous materials towards oxidation, *Catalysis Today*, vol. 102-103: pp. 259–265, 2005.

[57] FRIDEMAN H., New methods for evaluating kinetic parameters from thermal analysis data, *Polymer Letters*, vol. 7: pp. 41–46, 1969.

[58] VANDER WAL R., TOMASEK A., Soot oxidation: dependence upon initial nanostructure, *Combustion and Flame*, vol. 134: pp. 1–9, 2003.

[59] CATON J., RUEMMELE W., KELSO D., EPPERLY W., Performance and fuel consumption of a single-cylinder, direct-injection diesel engine using a platinum fuel additive, *SAE Technical Paper*, (910229), 1991.

[60] RICARDO, Investigation into the effect of a platinum fuel additive on the performance and emissions of a heavy duty diesel engine with a particulate trap, *Report Ricardo Consulting Engines DP92/1230*, 1992.

[61] ARICO A., SRINIVASAN S., ANTONUCCI V., DMFCs: from fundamental aspects to technology development, *Fuel Cells*, vol. 1(2): pp. 133–161, 2001.

[62] NEERGAT M., LEVERATTO D., STIMMING U., Catalysts for direct methanol fuel cells, *Fuel Cells*, vol. 2(1): pp. 25–30, 2002.

[63] SEIPENBUSCH M., *Katalytische und photoelektrische Aktivität gasgetragener Nanopartikel-Agglomerate*, Ph.D. thesis, Universität Karlsruhe (TH), 2003.

[64] GIORDANO N., PASSALACQUA E., PINO L., ARICO A., ANTONUCCI V., VIVALDI M., KINOSHITA K., Analysis of platinum particle size and oxygen reduction in phosphoric acid, *Electrochimica Acta*, vol. 36(13): pp. 1979–1984, 1991.

[65] WATANABE M., SAEGUSA S., STONEHART P., High platinum electrocatalyst utilizations for direct methanol oxidation, *Journal of Electroanalytical Chemistry*, vol. 271(1-2): pp. 213–220, 1989.

[66] TRASATTI S., PETRII O., Real surface area measurements in electrochemistry, *Pure and Applied Chemistry*, vol. 63(5): pp. 711–734, 1991.

[67] VALDEN M., LAI X., GOODMAN D., Onset of catalytic activity of gold clusters on titania with the appearence of nonmetallic properties, *Science*, vol. 281: pp. 1647–1650, 1998.

[68] LEMIRE C., MEYER R., SHAIKHUTDINOV S., FREUND F., Do quantum size effects control CO adsorption on gold nanoparticles?, *Angewandte Chemie International Edition*, vol. 43: pp. 118–121, 2004.

[69] RODRIGUEZ-REINOSO F., The role of carbon materials in heterogeneous catalysis, *Carbon*, vol. 36(3): pp. 159–175, 1997.

[70] KECK L., BUCHANAN J., HARDS G., Catalyst material, *US Patent*, (5.068.161), 1991.

[71] LI W., LIANG C., ZHOU W., QIU J., ZHOU Z., SUN G., XIN Q., Preparation and characterization of multiwalled carbon nanotube-supported platinum for cathode catalysts of direct methanol fuel cells, *Journal of physical Chemistry B*, vol. 107: pp. 6292–6299, 2003.

[72] ZHOU Z.H., WANG S., ZHOU W., WANG G., JIANG L., LI W., SONG S., LIU J., SUN G., XIN Q., Novel synthesis of highly active Pt/C cathode electrocatalyst for direct methanol fuel cell, *Chemical Communications*, vol. 2003(3): pp. 394–395, 2003.

[73] PAPIRER E., LACROIX R., DONNET J., Chemical modifications and surface properties of carbon blacks, *Carbon*, vol. 34(12): pp. 1521–1529, 1996.

[74] BÖNNEMANN H., RICHARDS R.M., Nanoscopic metal particles - synthetic methods and potential applications, *European Journal of Inorganic chemistry*, vol. 2001(10): pp. 2455–2480, 2001.

[75] PETROW H., ALLEN R., Finely particulated colloidal platinum compound and sol for producing the same, and method of preparation of fuell cell electrodes and the like employing the same, *US Patent*, (4.044.193), 1977.

[76] LEE S., PARK K., KWON B., SUNG Y., Method of preparing platinum alloy electrode catalyst for direct methanol fuel cell using anhydrous metal chloride, *US Patent*, (6.506.228), 2003.

[77] BÖNNEMANN H., BRAUN G., BRIJOUX W., BRINKMANN R., SCHULZE TILLIMG A., SEEVOGEL K., SIEPEN K., Nanoscale colloid metals and alloys stabilized by solvents and surfactants, Preparation and use as catalyst precursors, *Journal of Oranometallic Chemistry*, vol. 520(1-2): pp. 143–162, 1996.

[78] REETZ M., MAASE M., Redox-controlled size-selective fabrication of Nanostructured transition metal colloids, *Advanced Materials*, vol. 11(9): pp. 773–777, 1999.

Universität Karlsruhe (TH)
Institut für Mechanische Verfahrenstechnik und Mechanik (IMVM)

BOSCH
Technik fürs Leben

ISBN: 978-3-86644-103-3

www.uvka.de